CHALMERS
UNIVERSITY OF TECHNOLOGY

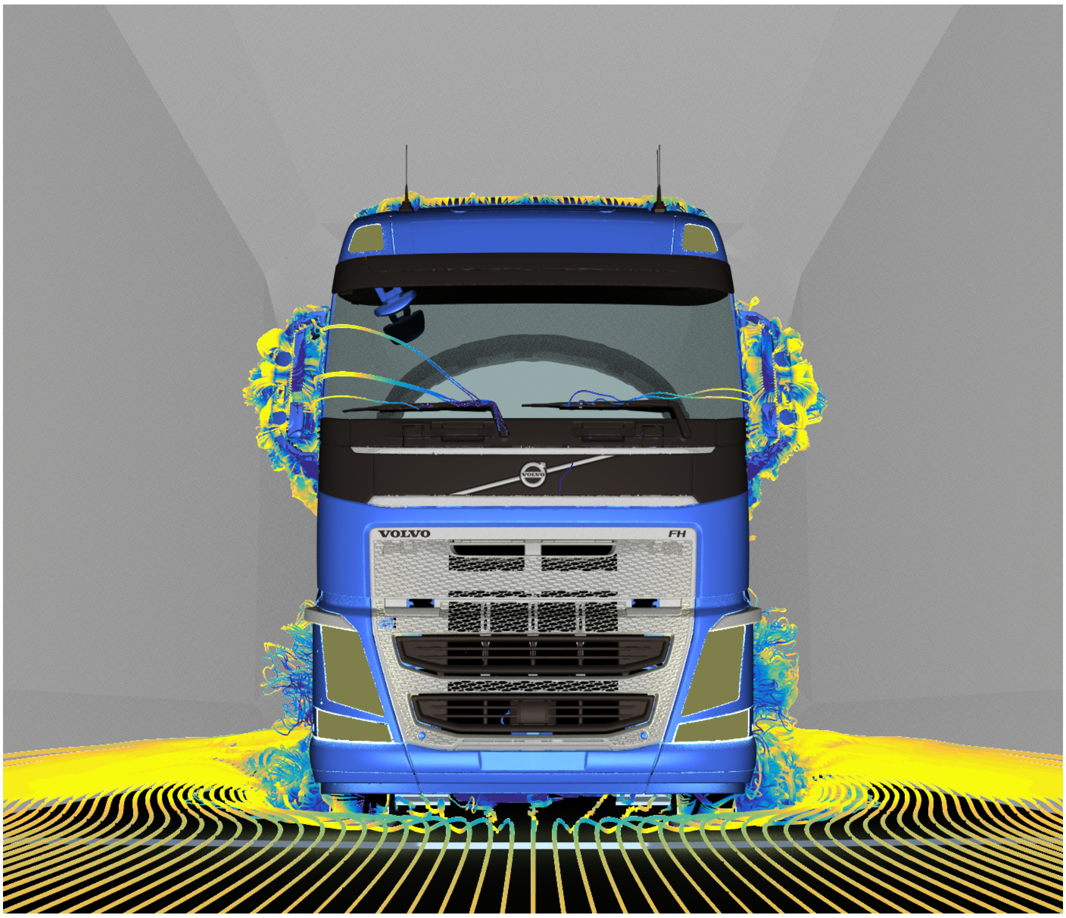

Improving Accuracy and Efficiency of Aerodynamic Simulations for Heavy Vehicles

Master's thesis in Engineering Mathematics and Computational Science

Simon Johansson

Department of Mechanics and Maritime Sciences
CHALMERS UNIVERSITY OF TECHNOLOGY
Göteborg, Sweden 2020

MASTER'S THESIS 2020:48

Improving Accuracy and Efficiency of Aerodynamic Simulations for Heavy Vehicles

Simon Johansson

CHALMERS
UNIVERSITY OF TECHNOLOGY

Department of Mechanics and Maritime Sciences
Division of Fluid Dynamics
CHALMERS UNIVERSITY OF TECHNOLOGY
Göteborg, Sweden 2020

Improving Accuracy and Efficiency of Aerodynamic Simulations for Heavy Vehicles
SIMON JOHANSSON

Master's Thesis 2020:48
Department of Mechanics and Maritime Sciences
Division of Fluid Dynamics
Chalmers University of Technology
SE-412 96 Göteborg
Sweden
Telephone +46 (0)31 772 10 00

Cover:
Velocity streamlines over a virtual Volvo FH Globetrotter 4x2 tractor.

Chalmers Reproservice
Göteborg, Sweden 2020

Improving Accuracy and Efficiency of Aerodynamic Simulations for Heavy Vehicles
Master's thesis in Engineering Mathematics and Computational Science
SIMON JOHANSSON
Department of Mechanics and Maritime Sciences
Division of Fluid Dynamics
Chalmers University of Technology

Abstract

Heavy-duty vehicles are a necessity in the current society but they answer to 6% of the total CO_2 emissions in Europe. Therefore new regulations are set by the European Union to limit those emissions. These limits make the losses of the vehicles an important factor and especially aerodynamic drag. Reducing the aerodynamic drag calls for good developing methods and accurate predictions. This means that validations and limitations of the methods are needed.

This thesis will investigate a CFD method by creating a base case simulation and validate this against wind tunnel test. The method will use unsteady simulations to capture transient behaviour in the flow. A statistical confidence intervals for the averaged values as well as a starting point for the averaging will be presented. Further, the spatial mesh will be studied and the effects of the number of inner iterations will be presented. The validation of the base case will be stated as differences in the coefficients C_d , C_s , and C_p to understand advantages and disadvantages of the method. The frequency content from the time-resolved coefficients will also be studied. When a well-defined base setup has been validated the temporal resolution will be investigated to see how it affects the results. This will be done for increased time steps as well as a significantly reduced time step. The significantly reduced time step ensures the CFL number to be less than unity in the entire domain.

The validation of the base case shows that there is an error in C_d of 45 ± 7 drag counts for the base case and that the error in pressure on the rear end of the truck is yaw angle dependent. The error in C_d is almost fully explained by the error in pressure on the rear end of the truck. The result from the simulations with different time steps show that for a fully resolved flow very fine time steps are needed to keep the CFL number less than unity in the majority of the domain, but if global force coefficients are of primary interest the time step can be increased moderately without significant changes. It is also found that the force coefficients alone are not a good estimators of how the method performs since errors can cancel each other. This means that a coarser mesh or a longer time step can generate a smaller error compared to wind tunnel tests but this is not reflecting the actual accuracy of the method.

Keywords: Heavy-duty vehicles, Aerodynamics, CFD, Wind tunnel correlation, Absolute accuracy, Temporal resolution.

Preface

This thesis was written during extraordinary circumstances in the world. The COVID-19 pandemic made the second half of this project very special and limited. I am grateful that there were many people to support me during this time.

I would like to thank my supervisors Anders Tenstam and Anton Lundberg at Volvo GTT. Thank you for your patience, motivation, and constructive feedback throughout the thesis. I would also like to thank my examiner, Prof. Lars Davidson, from Chalmers for the support through the project. I am also grateful to the coworkers at Volvo GTT in the CAST group as well as the Cab Analysis group for a pleasant time at the office. Finally, I would like to thank my friends from Chalmers helping me through my studies and this final project.

Thanks

Simon Johansson, Göteborg, 2020

Nomenclature

Abbreviations

CFD	Computational Fluid Dynamics
CFL	Courant Friedrichs Lewy
dc	Drag Counts
DDES	Delayed Detached Eddy Simulation
DES	Detached Eddy Simulation
DNS	Direct Numerical Simulation
ES	Enhanced Stability
EU	European Union
FVM	Finite Volume Method
GTT	(Volvo) Group Truck Technology
IDDES	Improved Delayed Detached Eddy Simulation
LES	Large Eddy Simulation
NRC	National Research Council Canada
PSD	Power Spectral Density
R	Recommended
RR	Repeat Reference (method)
SDR	Specific Dissipation Rate
Sim	Simulation
URANS	Unsteady Reynolds Averaged Navier-Stokes
URF	Under Relaxation Factor
WT	Wind Tunnel
YWA	Yaw Weighted Average

Symbols

ϵ	Uncertainty error	$[-]$
$\hat{\Phi}$	Averaged quantity	$[\Phi]$
μ	Mean	$[-]$
$\overline{\Phi}$	Time averaged quantity	$[\Phi]$
Φ_∞	Free stream value of quantity	$[\Phi]$
ρ	Density	$[kg/m^3]$
σ	Variance	$[-]$
A	Vehicle frontal area	$[m^2]$
C_d	Drag coefficient	$[-]$
C_p	Pressure coefficient	$[-]$
C_s	Side force coefficient	$[-]$
L_{int}	Turbulent integral-length scale	$[m]$

P	Pressure	$[N/m^2]$
s	Standard deviation	$[-]$
v_i	Velocity component in i direction	$[m/s]$
x_i	Spatial coordinate in i direction	$[m]$

Contents

List of Figures

List of Tables

1
Introduction

This chapter includes four sections. Firstly it will introduce the thesis by describing the background of the project. The following section will state the purpose of the thesis. Later the third section will state the limitations of the thesis. Finally, the outline of the report will be presented.

1.1 Background

One of the most concerning issues in society today is global warming and the following climate impacts generated from humanity. This topic has forced higher authorities to limit the climate impact from society by different means, thus e.g. the Paris Agreement was established [1]. One of the European Union (EU)'s regulations issued to achieve this agreement is to limit emissions from heavy-duty vehicles. Heavy-duty vehicles including, lorries, buses, and coaches, generate approximately 6% of EU's total CO_2 emissions [2]. The regulation contains two goals at 2025 and 2030, where the emissions should have been reduced by 15% and 30% respectively. This reduction is compared to the average emissions from all truck OEM's, from summer 2019 to summer 2020 [2].

Diesel heavy-duty vehicles are not something that can be removed or replaced by zero-emission alternatives today. Therefore, improving the vehicles ability to follow regulations by reducing the emission of CO_2 from diesel will remain the top priority in the current situation. There are many ways to improve the performance of the vehicles, such as reducing the resistance of moving the vehicle. Reducing the moving resistance makes the vehicle consume less energy, and thus have a longer mission range. The reduced energy consumption lowers the CO_2 emissions which benefits the vehicles used today. The increased range is more beneficial for the electric vehicles that do not produce any CO_2 themselves but instead have issues with mission range. The four major forces that act on the vehicle and contribute to the moving resistance are the following, air resistance, rolling resistance, climbing resistance, and acceleration resistance according to Hucho [3]. Considering driving at a constant speed on a flat road simplifies to the two previously mentioned resistances, the air and rolling resistance. The rolling resistance is considered to be linearly depending on the speed of the vehicle while the air resistance depends on the velocity square. This gives a breaking point so that when the vehicle reaches about 80km/h the air resistance becomes the dominant source of losses according to Hucho [3]. Since air resistance/drag force of the vehicle is the most dominant loss for heavy-duty vehicles travelling at a constant speed of 80km/h, as they usually spend more of their mission profiles on high ways, this loss is worth looking into. The drag force, F_d, depends on the following parameters; the velocity square, V^2, the frontal area, A, the drag coefficient, C_d , and the air density, ρ. C_d and A are the parameters of most interest. A is often given by the size of the cargo, but C_d depends on the shape of the vehicle and can be reduced by different means. The most efficient and obvious method is to make the bodies streamlined and by doing so, it can reduce the pressure difference of the front and rear of the object since the wake creates a significant portion of the force for bluff bodies, such as heavy-duty vehicles [3]. Making the bodies streamlined is a limited option in reality, so instead, aerodynamic devices usually are created to guide the flow around the vehicle in a more efficient way. Two critical questions arise in the development of these aerodynamic devices: "How the devices should be designed?" and "Do they perform as expected?".

The answers to these questions can be achieved by computational fluid dynamics (CFD) and wind tunnel tests. CFD is a powerful tool when it comes to designing aerodynamic devices. It is powerful since different concepts and solutions can be tested without building prototypes and testing them in reality. Moreover, it is cheaper and more convenient when it comes to an industrial environment. However, CFD also includes multiple uncertain parameters such as the temporal resolution, spatial resolution, numerical errors, etc. Thus, the simulated environment must be verified to ensure that the results from the simulations agree with what is observed in reality. This correlation can be done using some different approaches, wind tunnel testing and on-road testing for example. Testing on road with the conditions of reality includes various new factors that can not be simulated in a controlled way, for example the accurate wind conditions of the testing day. This makes wind tunnel tests advantageous for validation. In a wind tunnel, many of the conditions can be replicated in the simulations and the method can be compared to the actual test data. The simulation method validated in the wind tunnel can then be used to simulate the real-world conditions.

Previous research was done by Josefsson [4] at Volvo GTT regarding wind tunnel modelling. Josefsson developed a virtual copy of the wind tunnel environment of the National Research Council (NRC) in Canada. This model will be further used in this thesis as new validation studies are performed on the CFD methodology at Volvo GTT to ensure accuracy and quality.

1.2 Purpose

The purpose of the Master's thesis is to investigate different means to improve the current CFD methodology at Volvo GTT, mainly by increasing the absolute and relative accuracy. There will be two main parts covering this, and they will be subsequently presented.

The absolute accuracy of the simulations will be compared to wind tunnel tests, where multiple error sources will be discussed and identified. The error will be measured in terms of normalized coefficients.

The relative accuracy of the simulations will focus on the temporal and spatial resolution of the transient simulations. This part will treat different temporal time steps as well as refined regions in the spatial mesh.

The CFD simulations will be done by using transient simulations to predict the force coefficients and flow properties on and around the truck in a wind tunnel environment. The error from averaging transient results will be statistically determined.

1.3 Limitations

This thesis is limited by 60 ECTS which equals 40 weeks. The computations have been limited by the use of Volvo GTT's in-house computational cluster which necessitates the computations to be industrially applicable. The only solver used was StarCCM+. There has only been one geometric model and one turbulence model tested thoroughly in the CFD method. The tests and analyses have only been conducted in a wind tunnel environment. Also the supervised time at Volvo GTT was limited during the project due to the short-time layoffs caused by the COVID-19 outbreak.

1.4 Thesis Outline

The outline of the thesis will be divided into 6 main chapters. The different chapters will be briefly described below.

Chapter 1 (Introduction) introduces the thesis background as well as its purpose and limitations.

Chapter 2 (Theory) states fundamental facts necessary in the computational calculations to support the thesis in the theoretical aspect.

Chapter 3 (Method) presents several methods that each will be used to understand what sources contribute to an error in the predictions. Each part will have the method used to determine the error from the specific source and functions to find the errors in the CFD simulations evaluated.

Chapter 4 (Result) will show all the results of the thesis. The results from each part, namely the methods used, the absolute accuracy validated with wind tunnel data and the change in temporal resolution, will be stated separately.

Chapter 5 (Discussion) raises important aspects of both the methods as well as the results for absolute accuracy and temporal resolution. Further development is also suggested.

Chapter 6 (Conclusion) will summarise the essence of the thesis, present the essential parts, and results of the thesis.

2
Theory

When simulating flow fields using CFD, the theory is based on the governing equations for fluid dynamics and discretization methods of the domain in space and time. Because of the complex properties of fluid turbulence and the prohibiting cost of resolving all scales of turbulence, turbulence modelling is also included. The theoretical models used in this work will be presented together with the assumptions made.

2.1 Governing Equations

The governing equations for the flow physics are the Navier-Stokes equations stated in isothermal form in Eq. (2.1). The first one is the continuity equation and the latter one is the momentum equation. The equations are presented using Einstein's notation. The variables in the equations are as follows, v is the velocity, t is time, x is the position, P is the pressure, ρ is the air density, and ν is the kinematic viscosity. The index, i, represent the direction in 3-dimensional space such that $i \in \{1, 2, 3\}$.

$$
\begin{aligned}
\frac{\partial v_i}{\partial x_i} &= 0 \\
\frac{\partial v_i}{\partial t} + \frac{\partial v_i v_j}{\partial x_j} &= -\frac{1}{\rho}\frac{\partial P}{\partial x_i} + \nu \frac{\partial^2 v_i}{\partial x_j \partial x_j}
\end{aligned}
\tag{2.1}
$$

There are some assumptions made in the flow properties. The first assumption is incompressible and isothermal flow i.e. that the air density and temperature does not change in time or space. The viscosity of the air is also assumed to be constant. The air is also assumed to be Newtonian, meaning that the shear stresses are proportional to the time-rate-of-strain according to Wendt [5].

A general solution to the Navier-Stokes has not been presented in the literature except for some simple cases, which requires the equations to be solved numerically. The Finite Volume Method (FVM), is the most commonly used method in CFD for commercial software to solve the equations according to Versteeg and Malalasekera [6], and this is also the method being employed in this thesis. To solve those equations unmodified is called Direct Numerical Simulations (DNS). This is rarely done because of the computational cost for the very high spatial and temporal resolution needed to capture the behaviour of the flow at all scales in space and time. The computational cost scales with the Reynolds number and is thus extremely high for a full scale vehicle model and it is unnecessary in most engineering applications according to Versteeg and Malalasekera [6].

2.2 Turbulence Modelling

To solve the Navier-Stokes equations at a much lower computational cost, the modelling of turbulent structures is adopted. The turbulence models average the instantaneous properties in time and space and model the smallest scales rather than resolving them. The turbulence model used in this work is the Shear Stress Transport (SST) $k-\omega$ Improved Delayed Detached Eddy Simulation (IDDES) model. This model is a combination of turbulence models. These models will be presented in the following sections.

URANS

Unsteady Reynolds Averaged Navier-Stokes (URANS) averages the instantaneous quantities in time. Doing this in a discretized time-domain essentially means that the averaging in time done by URANS are of a much smaller time scale than the discrete time steps. The instantaneous values are decomposed according to Eq. (2.2).

$$\Phi = \overline{\Phi} + \Phi' \tag{2.2}$$

Here the quantity Φ is divided into a mean, $\overline{\Phi}$ and a fluctuating component, Φ'. Then Eq. (2.2) is substituted into Eq. (2.1) to create the URANS equation, Eq. (2.3).

$$\begin{gathered}\frac{\partial \bar{v}_i}{\partial x_i} = 0 \\ \frac{\partial \bar{v}_i}{\partial t} + \frac{\partial \bar{v}_i \bar{v}_j}{\partial x_j} = -\frac{1}{\rho}\frac{\partial \overline{P}}{\partial x_i} + \nu \frac{\partial^2 \overline{v_i}}{\partial x_j \partial x_j} - \frac{\partial \overline{v_i' v_j'}}{\partial x_j}\end{gathered} \tag{2.3}$$

When the fluctuating parts are introduced as independent variables, the system of equations is no longer closed. Therefore additional equations must be added to describe the system. This can be done by different modelling methods suggested by different researchers. In this thesis the SST $k-\omega$ model has been used. The SST model uses two different settings. One for regions close to walls and another one for regions far away from the walls. This is to combine valuable properties from different models in different regions. The first region, close to the walls, is modelled with a $k-\omega$ model. The SST $k-\omega$ model uses the Boussinesq assumption that model the Reynolds stresses in Eq. (2.3) according to Eq. (2.4) where ν_t is the turbulent kinematic viscosity and δ_{ij} is the Kronecker Delta.

$$-\overline{v_i' v_j'} = \nu_t \left(\frac{\partial \bar{v}_i}{\partial x_j} + \frac{\partial \bar{v}_j}{\partial x_i} \right) + \frac{1}{3}\delta_{ij} k \tag{2.4}$$

The set of equations added to close the system of equations is the transport equations for turbulent kinetic energy, k, and Specific Dissipation Rate, (SDR), ω, those equations are presented as Eq. (2.5) according to Menter [7].

$$
\begin{aligned}
\frac{\partial k}{\partial t} + \frac{\partial}{\partial x_j}(\bar{v}_j k) &= \frac{\partial}{\partial x_j}\left[\left(\nu + \frac{\nu_t}{\sigma_k}\right)\frac{\partial k}{\partial x_j}\right] + P^k - \beta^* k\omega \\
\frac{\partial \omega}{\partial t} + \frac{\partial}{\partial x_j}(\bar{v}_j \omega) &= \frac{\partial}{\partial x_j}\left[\left(\nu + \frac{\nu_t}{\sigma_\omega}\right)\frac{\partial \omega}{\partial x_j}\right] + \alpha\frac{P^k}{\nu_t} - \beta\omega^2 \\
&+ 2(1-F_1)\sigma_{\omega 2}\frac{1}{\omega}\frac{\partial k}{\partial x_i}\frac{\partial \omega}{\partial x_i} \\
F_1 &= tanh(\xi^4), \xi = min\left[max\left\{\frac{\sqrt{k}}{\beta^*\omega d}, \frac{500\nu}{d^2\omega}\right\}\frac{4\sigma_{\omega_{k-\varepsilon}} k}{CD_\omega d^2}\right] \\
CD_\omega &= max\left\{2\sigma_{\omega_{k-\varepsilon}}\frac{1}{\omega}\frac{\partial k}{\partial x_i}\frac{\partial \omega}{\partial x_i}, 10^{-10}\right\} \\
\nu_t &= \frac{a_1 k}{max(a_1\omega, |\bar{s}|F_2)} \\
F_2 &= tanh(\eta^2), \eta = max\left\{\frac{2\sqrt{k}}{\beta^*\omega d}, \frac{500\nu}{d^2\omega}\right\}
\end{aligned}
\tag{2.5}
$$

d is the distance to the wall and the constants in Eq. (2.5) are as follows, $\beta^* = 0.09$, $a_1 = 0.3$, $\alpha_{k-\omega} = 5/9$, $\beta_{k-\omega} = 3/40$, $\sigma_{k,k-\omega} = 0.85$, $\sigma_{\omega,k-\omega} = 0.5$, $\alpha_{k-\varepsilon} = 0.44$, $\beta_{k-\varepsilon} = 0.0828$, $\sigma_{k,k-\varepsilon} = 1$, and $\sigma_{\varepsilon,k-\varepsilon} = 0.856$.

These equations then use the $k-\omega$ model close to the wall and transfer to the $k-\varepsilon$ model in the far away from the wall regions according to Eq. (2.6).

$$\Phi = F_1\Phi_{k-\omega} + (1-F_1)\Phi_{k-\varepsilon} \tag{2.6}$$

The SST model uses the combination of the benefits from the $k-\omega$ model in the close wall region and the $k-\varepsilon$ model in the regions far away from the wall.

LES

Large Eddy Simulation (LES) is a method that resolves more of the turbulence than the URANS model. This is done by volume filtering instead of time filtering. The corresponding decomposition to Eq. (2.2) for LES is Eq. (2.7), where $\overline{\Phi}$ again is the average and Φ'' is the fluctuating part, but now for a spatial system.

$$\Phi = \overline{\Phi} + \Phi'' \tag{2.7}$$

Using Eq. (2.7) and substituting it into Eq. (2.1) yields the LES Eq. (2.8), where τ_{ij} is the Sub-Grid Stresses (SGS).

$$
\begin{aligned}
\frac{\partial \bar{v}_i}{\partial x_i} &= 0 \\
\frac{\partial \bar{v}_i}{\partial t} + \frac{\partial \bar{v}_i \bar{v}_j}{\partial x_j} &= -\frac{1}{\rho}\frac{\partial \overline{P}}{\partial x_i} + \nu \frac{\partial^2 \overline{v_i}}{\partial x_j \partial x_j} - \frac{\partial \tau_{ij}}{\partial x_j} \\
\tau_{ij} &= \overline{v_i' v_j'} - \bar{v}_i{}' \bar{v}_j{}'
\end{aligned}
\tag{2.8}
$$

In LES the SGS are modelled as for the Reynolds stresses in URANS. LES is numerically cheaper than DNS but for the region close to walls a very fine grid is needed to accurately predict the flow and therefore LES is still very expensive according to Davidson [8].

DES, DDES and IDDES

Detached Eddy Simulations (DES) is a way to combine LES with URANS to harvest the accuracy of LES but keep the computational cost down. This is done by modelling the turbulence according to URANS in the boundary layers near the walls and then switch to LES away from the wall where the turbulent length and time-scales are longer and can be described by the computational grid. This is done by using the $k-\omega$ model and modify it such that instead of transforming to use the $k-\varepsilon$ model away from the walls it uses LES. This is done by substituting the dissipation term according to Eq. (2.9).

$$
\begin{aligned}
&\beta^* k\omega \rightarrow \beta^* k\omega F_{DES} \\
&F_{DES} = max\left(\frac{L_t}{C_{DES}\Delta}, 1\right) \\
&\Delta = max(\Delta_i) \\
&L_t = \frac{\sqrt{k}}{\beta^* \omega}
\end{aligned}
\tag{2.9}
$$

The model constant $C_{DES} = 0.61$. This method may suffer from stability issues in the switching as it switches only depending on the grid size. This creates a risk of switching to LES too early when there are small turbulent length scales present and thus predict the flow poorly in that region, as described by Davidson [8]. Improvements were done to the model to address this issue and the Delayed Detached Eddy Simulations (DDES) was introduced by Menter and Kuntz [9]. Their model used the modification of the switching factor according to Eq. (2.10).

$$
F_{DDES} = max\left(\frac{L_t}{C_{DES}\Delta}(1 - F_2), 1\right) \tag{2.10}
$$

This switch utilizes the function F_2 from Eq. (2.5). Further improvements have been made on this model and the IDDES model was introduced by Shur, Spalart, Strelets and Travin [10]. The idea of the IDDES model was to create a model that includes one set of equations that can handle the flow over a complex geometry as well as in the rest of the domain. Their work highlights how the DES model does not handle the match in the close wall regions very well and there is a difference in the skin-friction predicted by the RANS and LES regions where they should align. This mis-match in DES follows directly into DDES and occurs in the log-layer of the wall modelling for the two models.

IDDES is, as LES, very dependent on the mesh sizes near the wall. LES performs very poorly on a coarse grid since the relatively simple subgrid turbulence model will then assume isotropic turbulence on a length and time scale which is clearly anisotropic, especially where interacting with solid walls. The IDDES model takes into consideration the actual wall distance and not only the grid size as DES model. There are two blending functions in IDDES that handle the switching between URANS and LES mode, f_B and f_e. Function f_B makes sure that the transition from URANS to LES is rapid with minimum delay and f_e has two functions, firstly to let LES be used in the boundary layer if the grid is fine enough and secondly to not allow the LES solution to corrupt the RANS solution if the RANS is well predicted, often referred to as "shielding".

Eq. (2.11) describes how the IDDES model is formulated according to Siemens [11], where κ is the von Karman constant, d is the distance to the wall and Δ is the largest distance between the cell center under consideration and the cell centers of the neighboring cells. The constants are $C_{DES,k-\omega} = 0.78$, $C_{DES,k-\varepsilon} = 0.61$, $C_{dt} = 20$, $C_l = 5$ and $C_t = 1.87$.

$$
\begin{aligned}
\tilde{\omega} &= \frac{\sqrt{k}}{l_{HYBRID} f_{\beta^*} \beta^*} \\
l_{HYBRID} &= \tilde{f}_d(1+f_e) l_{RANS} + (1-\tilde{f}_d) C_{DES} \Delta_{IDDES} \\
f_B &= min\Big[2exp(-9\alpha^2), 1\Big] \\
\alpha &= 0.25 - \frac{d}{\Delta} \\
f_e &= max\Big[(f_{e1}-1), 0\Big] \psi f_{e2} \\
f_{e1} &= \begin{cases} 2exp(-11.09\alpha^2), & \text{if } \alpha \geq 0 \\ 2exp(-9\alpha^2), & \text{if } \alpha < 0 \end{cases} \\
f_{e2} &= 1 - max(f_t, f_l) \\
f_t &= tanh\Big[(C_t^2 r_{dt})^3\Big] \\
f_l &= tanh\Big[(C_l^2 r_{dl})^{10}\Big] \\
r_{dt} &= \frac{\nu_t}{\sqrt{\nabla \mathbf{v} : \nabla \mathbf{v}^T} \kappa^2 d^2} \\
r_{dl} &= \frac{\nu}{\sqrt{\nabla \mathbf{v} : \nabla \mathbf{v}^T} \kappa^2 d^2} \\
\tilde{f}_d &= max((1-f_{dt}), f_B) \\
f_{dt} &= 1 - tanh\Big[(C_{dt} r_{dt})^3\Big] \\
\Delta_{IDDES} &= min(max(0.15d, 0.15\Delta, \Delta_{min}), \Delta)
\end{aligned}
\tag{2.11}
$$

2.3 Implicit solver

Using an implicit solver for a time-dependent problems means that the parameter to be calculated depends not just on former time steps, as in an explicit formulation, but also on the current time step. This requires an iterative method to be used at each time step. In contrast, with the explicit solver, there is no need to know the parameter at the new time step but the solution can instead march forward in time and calculate the new step directly. The upside with the implicit solver is that there is no numerical limit on how large time-steps can be taken, the solution is unconditionally stable as stated by Versteeg and Malalasekera [6]. This does not guarantee that the solution is physically meaningful at large time steps but there is no numerical limitation in the equations to be solved. The requirement in the explicit solvers is derived from the CFL condition presented by Courant, Friedrichs, and Lewy [12]. The CFL number relates the spatial grid, velocity and temporal resolution together as Eq. (2.12). For the solution to be stable the CFL number should be less than unity. This is a criterion for having a stable numerical process for the partial differential equations.

$$C = u\frac{\Delta t}{\Delta x} \tag{2.12}$$

As the CFL criterion is not required to be less then unity for implicit solvers one can increase the time steps. By increasing the time step and letting the CFL number exceed unity, information may be lost in the temporal resolution as well as ensuring a converging numerical process. The temporal resolution in the simulations is crucial in the sense that all the relevant time scales appearing in the flow should be resolved. Reynolds suggests that a sufficient time scale is when a fluid particle does not travel further than one mesh cell in one time step [13], which is equivalent with the CFL criterion. This time step would then capture the smallest eddies in the flow that is spatially resolved by the given mesh. By adhering to this guideline, it could be seen as maximum use is made of the constructed computational mesh. This guideline can, however, result in very small time steps.

Mocket [14] investigated the influence of an increased time step in DES on flow over a cylinder simulation. The time step was increased by a factor of 5/3 such that the CFL number exceeded unity in some regions of the domain, especially in the the onset region of the shear layer. The results that could be observed from this increase is that the instantaneous vortical structures in the shear layer disappeared for the bigger time step because of the excessive time averaging occurring. It was also visible that the re-circulation region was extended behind the cylinder for the bigger time step. This also gives a strong under-prediction in drag because of the change in the pressure field. This analysis showed that a big difference in the flow prediction was experienced when changing the time step, although this was for a very simple and sensitive geometry setup according to Mocket [14].

2.4 Non-dimensionalized and Statistical Quantities

When comparing simulations, a convenient way is to use non-dimensionalized quantities. The following section will list some of those used in this thesis as well as some statistical properties.

The two force coefficients, C_d and C_s describe in the longitudinal and transverse direction the aerodynamic forces for an object. The coefficients refer to drag and side force respectively. The coefficients are defined as Eq. (2.13) and Eq. (2.14). They are derived from the force in the drag, F_d, or side, F_s, direction as well as the air density, ρ, free stream velocity, V_∞, and reference area of the object, A. The reference area is taken to be the projected frontal area for this thesis, and for ground vehicle aerodynamics in general.

$$C_d = \frac{F_d}{\frac{1}{2}\rho V_\infty^2 A} \tag{2.13}$$

$$C_s = \frac{F_s}{\frac{1}{2}\rho V_\infty^2 A} \tag{2.14}$$

The pressure coefficient, C_p , is calculated according to Eq. (2.15), where the index, i, corresponds to each position evaluated. C_p depends on the pressure, p_i, free stream pressure, p_∞, free stream velocity and air density.

$$C_{p_i} = \frac{p_i - p_\infty}{\frac{1}{2}\rho V_\infty^2} \tag{2.15}$$

Bernoulli's equation, Eq. (2.16), is a one-dimensional simplification of the momentum equation in Navier-Stokes equation, Eq. (2.1). Eq. (2.16) state a relation between pressure, velocity and density. These parameters are constant in a flow when no dissipation or friction is present, the constant is the total pressure.

$$p + \frac{1}{2}\rho v^2 = \text{Total Pressure} \tag{2.16}$$

Using Eq. (2.15) and Eq. (2.16) the stagnation pressure, p_0, can be written as Eq. (2.17).

$$p_0 = p_\infty + \frac{1}{2}\rho V_\infty^2 \tag{2.17}$$

The non-dimensionalized time, T^*, is used to describe the physical time in relation to flow passages. T^* is defined according to Eq. (2.18) were t is time, L is the length of the vehicle, and V_∞ is the free stream velocity. This parameter can substitute the time when analysing time dependent parameters. T^* relates how many times the flow from the free stream can pass over the vehicle analysed in a given physical time t.

$$T^* = t \cdot \frac{V_\infty}{L} \tag{2.18}$$

This work will compare different values for ΔC_d , ΔC_s and ΔC_p . The absolute differences are often in the order of 10^{-3} and therefore it is common practice to use the notations of counts. Drag Counts (dc), side counts and pressure counts are defined according to Eq. (2.19) for convenience in the report.

$$\begin{aligned} 1 \text{ drag count} &:= 0.001 C_d \\ 1 \text{ side count} &:= 0.001 C_s \\ 1 \text{ pressure count} &:= 0.001 C_p \end{aligned} \tag{2.19}$$

The standard deviation of a data set describes the probability for a new value taken from the same data set to lie within certain limits. The estimated standard deviation, s, for Independent and Identically Distributed (IID) random variables is defined as Eq. (2.20) according to Sagitov [15]. N is the number of IID samples in the data set and $\bar{x}$ is the mean value of the data set.

$$s = \sqrt{\frac{1}{N-1}\sum_{i=1}^{N}(x_i - \bar{x})^2} \tag{2.20}$$

Assuming the data to be normally distributed and IID one can use the standard deviation to predict confidence intervals for the parameter analysed. The confidence interval for mean value, $\bar{x}$, is given by Eq. (2.21) according to Sagitov [15].

$$s_{\bar{x}} = \frac{s}{\sqrt{N}} \tag{2.21}$$

To test if two mean values are different from each other the two-sided t-test can be applied. This assumes that the variance is equal for the two means. The test statistic, t, is then calculated as Eq. (2.22) according to Sagitov [15] and test $H_0 : \bar{x} = \bar{y}$. The test statistic is then compared to the null distribution of the test statistic, $T \sim t_{n+m-2}$, where n and m is number of IID samples for each mean value.

$$t = \frac{\bar{x} + \bar{y}}{\sqrt{s_{\bar{x}}^2 + s_{\bar{y}}^2}} \tag{2.22}$$

2.5 Spectral analysis

Transient simulations generates discrete time series that can be analysed with spectral analysis to understand the signals better. The following chapter will state some theoretical aspects for analysing time series.

Time series can be considered a summation of cyclic functions. Shumway and Stoffer [16] mention a periodic process as Eq. (2.23).

$$x_t = A \cdot \cos(2\pi\omega t + \phi) \tag{2.23}$$

Where A is the amplitude, t is time, ω is the frequency and ϕ is the phase. If the process would be considered random, with random amplitude and phase, Eq. (2.23) can be re-written as Eq. (2.24).

$$x_t = U_1 \cdot \cos(2\pi\omega t) + U_2 \cdot \sin(2\pi\omega t), \tag{2.24}$$

where U_1 and U_2 is normally distributed random variables and with amplitude $A = \sqrt{U_1^2 + U_2^2}$ and phase $\phi = tan^{-1}(-U_2/U_1)$. When discrete data is analysed at least two points are needed to describe a cycle. This gives a limitation of the highest frequency described which would be $1/2\Delta t$, where Δt is the time step. This frequency is called the folding frequency. Having defined one periodic process as Eq. (2.24) this can be generalised to Eq. (2.25).

$$x_t = \sum_{k=1}^{q} U_{k1} \cdot \cos(2\pi\omega_k t) + U_{k2} \cdot \sin(2\pi\omega_k t) \tag{2.25}$$

Eq. (2.25) can be used to describe a signal that includes different signals of different frequencies and different amplitudes. Conversely, when a signal is given in reverse, this concept can be used to distinguish what frequencies are dominating in terms of amplitude in a signal. An efficient way to do this is to use fast Fourier transform, FFT. According to The Mathworks [17] the FFT transformation is done according to Eq. (2.26) where ω is one of the n complex roots and $i = \sqrt{-1}$.

$$\begin{aligned} y_{k+1} &= \sum_{j=0}^{n-1} \omega^{jk} x_{j+1} \\ \omega &= e^{-2\pi i/n} \end{aligned} \tag{2.26}$$

As stated by National Instruments [18] the data used in the FFT is finite, meaning the cyclic process is cut arbitrarily to have a start and ending point. This is not considered in the FFT by construction, the FFT assumes the data is exactly one period long repetitive signal. This would mean that the two end-points could be connected. If this is not the case and the data cannot be sampled in exact periods there will be high-frequency signals appearing in the frequency domain. These come from the discontinuity caused by truncation and does not exist in the original time series. This phenomenon is called spectral leakage. To address this issue a method called windowing can be applied. This method is based upon the idea to connect the endpoints and reduce the spectral leakage in the frequency domain. Applying a window to a signal is essential to multiply the time series with a window function. There are different windowing functions but the shape is based on a smooth shape that diminishes smoothly towards zero at the boundaries of the window. One window function is the Hann window which is satisfactory in 95% of the cases according to National Instruments [18].

3
Method

This chapter will cover different methods to determine the errors of the simulations. The different methods will consider the wind tunnel, convergence, initial transient, mesh analysis, frequency content, inner iterations and finally list all simulations used in the thesis.

The main objective of this thesis is to estimate the error for simulations. To do this the method used should be validated to make sure it agrees with reality. Oberkampf and Trucano [19] presented how the validation of a model of a complex process can be made. They discussed how one can do a validation of the complex process in a controlled environment by comparing real tests in this environment and compare it to results from the model of the same environment. The difference between those can then be used to do inference to see at what degree the model can be trusted in a setup that has not yet been validated. One way of doing this for truck aerodynamics is to measure them in a wind tunnel and then simulate the wind tunnel environment and compare the physical properties that can be measured and are of interest. When nature is compared with the model the difference, or error, can be stated as Eq. (3.1) according to Oberkampf and Trucano.

$$E = E1 + E2 + E3 \tag{3.1}$$

In Eq. (3.1), $E_1 = u_{\text{nature}} - u_{\text{experiment}}$, $E_2 = u_{\text{experiment}} - u_{\text{exact}}$, and $E_3 = u_{\text{exact}} - u_{\text{discrete}}$ and thus $E = u_{\text{nature}} - u_{\text{discrete}}$. Explaining this in words, E_1 is the error from the wind tunnel test compared to nature. E_2 is the error between the wind tunnel data and the exact solution to the governing equations. E_3 is the error between the exact solution and the discretized numerical solution.

The objective is to estimate the size of the error and reduce it. This is not possible for all the terms in Eq. (3.1). The first term, E_1, is the error from the wind tunnel test and is therefore under limited control by Volvo GTT. The second error, E_2, is not possible to estimate or reduce for the geometries simulated. The geometries are too complex and the domain is not possible to simulate with an exact solver. Therefore the error of interest is the combination of E_2 and E_3. There are many components of E_3 and only some of them will be analysed in this work. The errors this work will focus on are those caused by temporal resolution, spatial resolution and convergence uncertainties. These all contribute to the error, $E_2 + E_3$, in Eq. (3.1), which is the error observed in the validation of a CFD method against an actual wind tunnel test. Examples of sources of errors that are not going to be treated in this work include the turbulence model and the solvers.

3.1 Wind Tunnel

The validation done in this work will be conducted with the data from a wind tunnel test campaign in 2019. This campaign was performed in the 9x9 low-speed wind tunnel in Canada operated by the National Research Council (NRC). Some of the data from this test was used to validate the current CFD method and see how well it corresponds with reality. To make sure the validation process is conducted in a correct way the simulation environment should be as close to the real test case as possible. This was investigated at the beginning of the project as all of the analysis will be made in the wind tunnel environment.

The NRC wind tunnel test section is 9.1 times 9.1 m in cross-section and 24 m long [20]. The truck model used in the test is a truck used for testing aerodynamic performance. The truck is a Volvo FH Globetrotter 4x2 tractor with a short trailer to fit the wind tunnel environment. The truck's frontal area is about 10.5 m^2 resulting in a blockage ratio of 13%. The air speed used for testing is 90 km/h. The wheels are non-rotating and there is a turntable that makes it possible to do a yaw sweep. The yaw sweep for the tests is -10 to +10 degrees. From the tunnel tests, a document with relevant data was provided, including drag and side forces and relevant coefficients. This test campaign also included pressure measurements at 71 locations on the truck. Those 71 pressure probes were taped flat against the surface of the truck. The test setup is similar to the one described in the work by Steen et al. [21].

In the wind tunnel, the static and total pressure is measured in probes on the wall about ten meters in front of the truck. This is positioned at the very end of the converging part of the tunnel. To make up for the remaining convergence of the tunnel those values are corrected with a factor to match with the actual test section in the tunnel. This factor is calculated by testing a velocity sweep in an empty tunnel with a measuring probe 2 m above the turntable center. The difference is further used to calibrate this correction factor. This information was acquired from discussions with the NRC engineers by Forsgren and Tenstam [22]. In this work, the reference dynamic pressure and static pressure from those probes will be referred to in the form of velocity and pressure as velocity, V_{ref}, and reference pressure, P_{ref}, respectively. This is because of convenience and is valid because of the assumption of incompressible flow in the tests.

Wind Tunnel Simulation Setup

The virtual wind tunnel geometry model used in this work has been developed at Volvo GTT. An important aspect of this model is that it is not created from manufacturing specifications since those are proprietary to the NRC. The tunnel geometry is constructed from limited measurements during testing and sources by Forsgren and Tenstam [22] and Josefsson [4]. The inlet of the tunnel is assumed to be a velocity inlet with velocity perpendicular to the inlet surface and the outlet is a pressure outlet. In the test section of the wind tunnel, where the truck is, the walls are modeled with a no-slip condition. Far upstream and downstream in the wind tunnel the walls are modeled with a slip condition. The test section of the tunnel together with the truck in -10 degree yaw setting, is shown from above in Fig. 3.1. This figure illustrates how the coordinate system is set up and how the rotation is made. The coordinate system is based on having the z-axis pointing upwards and the x-axis pointing backwards in the direction of the truck. θ is the rotation angle around the z-axis. The rotation refers to rotating the wind tunnel environment and not the truck around the z-axis. It follows that for negative yaw angles the tunnel, and thus the airflow, is rotated such that it hits the passenger/right hand side of the truck. Rotating the wind tunnel environment makes the post-processing convenient as the truck will remain in the same coordinates and the same planes and positions can be used for different yaw angles. The truck is placed with the front of the truck at x = 2, y = 0 in the middle of the truck and z = -0.6 on the floor.

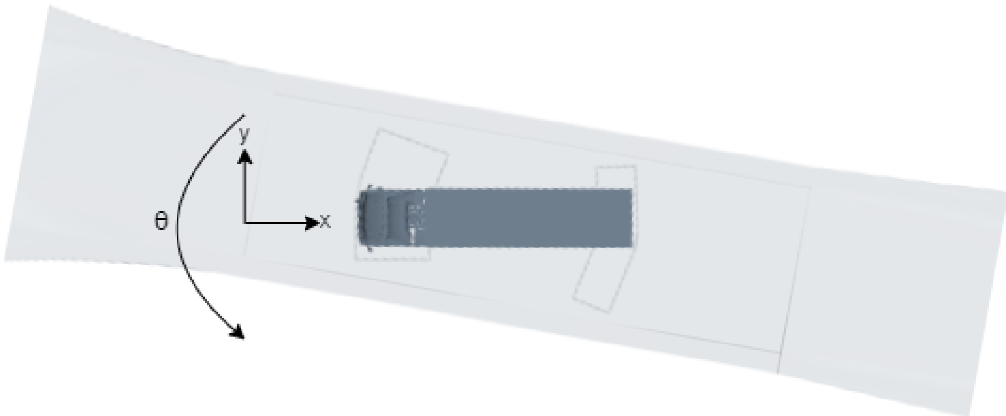

Figure 3.1: Truck geometry at -10 degree setting in the wind tunnel environment with corresponding coordinate system and angle convention.

The truck geometry used is an FH model with a short trailer. The geometry model was prepared at Volvo GTT to ensure good agreement with the truck tested in the wind tunnel. The model includes all details from the CAD available, including chassis and drive-line. The cooling packages are represented by porous media. The same truck model will be used for the majority of the simulations.

Reference Probes

When studying the normalized coefficients, C_d , C_s , and C_p , reference velocity, V_∞, and reference pressure, p_∞, are needed to scale the coefficients according to Eq. (2.13), Eq. (2.14) and Eq. (2.15). In a wind tunnel environment, it is not obvious where to obtain V_∞ and p_∞. In theory, it should be in the free stream flow far away enough not to be affected by the object that is simulated. This is not possible to achieve in a wind tunnel environment simulating trucks in full scale since no such large tunnels exist. Hence V_∞ and p_∞ will get affected by the obstruction of the truck, but the practice is to select a probe placement in the tunnel such that this effect is minimized. In the NRC tunnel, a point upstream the truck in the converging nozzle is used.

Different approaches can be used to acquire V_∞ and p_∞. One way is to use open road simulations, as Cyr, Ih, and Park [23]. This is based upon the fact that the non-dimensional parameters should be the same on the vehicle no matter if it is inside a wind tunnel domain or in the open road environment. The method uses the C_p values together with the known references from the free stream obtained from the open road simulations and combines those with the C_p values obtained in the wind tunnel. The C_p and C_d values in the wind tunnel are then corrected according to the difference obtained from the open road simulations. This correction needs two points since there are two unknown parameters, V_∞ and p_∞. This method assumes that the relation between the two points is the same in the wind tunnel environment and in open road condition to work, this is not necessarily the case for the study to be conducted here. This method comes from a study on a car geometry and hence the blockage ratio is significantly less and using this method does not seem appropriate in this work. Therefore it was decided to try to mimic the method used in the wind tunnel test setup. Doing this would probably generate similar results as for Ljungskog, Sebben, and Broniewicz [24] were it is stated that a key component in simulating a wind tunnel environment is to obtain the reference pressures in the same way as it is done in the wind tunnel. The methodology used to find the references is not the same in the tunnel used in their work as the one used in this thesis, but the idea remains the same.

No measurements for the geometry upstream of the test section is available and the reference probe positions are hard to estimate. The method used to find the position for the reference probes was to do the same calibration as the one done in the wind tunnel but backwards with the scaling parameter for V_{ref} fixed. This scaling parameter was not given as an exact number but only acquired by a discussion with the NRC engineers by Forsgren and Tenstam [22]. To do the calibration backwards to obtain the probe positions was to remove the error from an uncertain position of the probes and also the exact value of the scaling factor. The idea is to use the same methodology but without assuming any uncertain or estimated values.

Ekman, Larsson, Virdung, and Karlsson [25] mentions that the accuracy of the position of the reference probe in the wind tunnel affects the final force coefficients, this can also be analysed in the simulated environment. The original mesh size in the region where the reference probes are placed in the simulated wind tunnel environment is quite large. This makes it convenient to analyse how the reference value changes between the cells in this region instead of how it changes with physical distance. This was done by comparing the values of the cell containing the assumed position of the reference probe and its neighbours. This is visualised in Fig. 3.2, where the reference probe for V_∞ is shown from above as a red sphere in the grid with the 8 cells surrounding it. The grey area in the figure is the wind tunnel wall with the opacity reduced. The difference for the reference between the cells was then transformed into a final difference for C_d . This estimates the sensitivity of which cells the reference probe ends up in when it is close to an edge between two cells. This study was conducted for steady-state RANS in an empty tunnel, for simplicity.

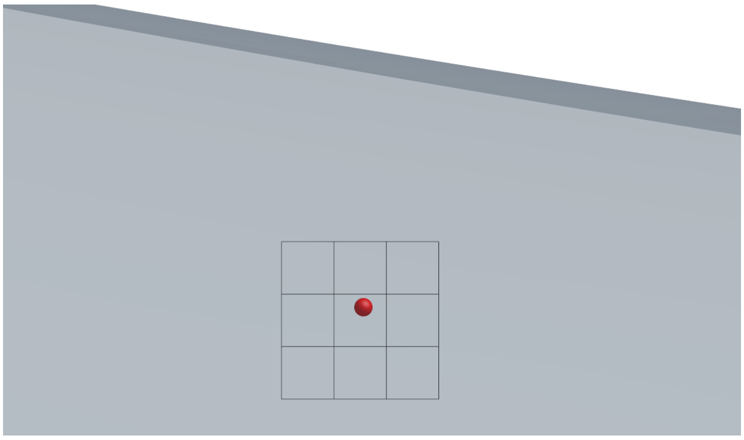

Figure 3.2: Cells around reference probe close to the wind tunnel wall.

Pressure Probe Position Uncertainty

Upon positioning pressure taps on the physical test object, the exact location may often be subject to uncertainty. To evaluate the error from the positioning of the pressure probes on the truck, small cylinders will be used around each probe. The cylinders have a radius of 25 mm and a height of 10 mm. To find a suitable statistical error of the positioning, all the values in the cylinders are used to find a standard deviation of the pressure and this is then used to estimate the error from positioning. This error will describe what error level could be assumed from the placement of the probes in the wind tunnel tests and also include the error from lack of modelling of the actual probes in the simulations. The probes have not been physically modelled in the simulations but have only been added as point measurements which will neglect the effects of the taped probes on the surface. The probes are placed on the truck in the simulations with a wall distance between 1 and 1.2 mm in the simulations, this placement is to make up for the small thickness of the physical pressure probe. The error from the pressure probes placed on the truck will be calculated separately for each probe in the upcoming sections.

Blockage Ratio Effect

There were some challenges defining how to measure the C_p values correctly in the simulations, so an analysis was made on the blockage ratio influence on this property. This analysis was made in the virtual wind tunnel environment. This was done by simulating a box with rounded corners as a bluff body of different cross-section areas to see how blockage affects the stagnation pressure prediction. To simulate this, steady-state simulation using k-ε turbulence model was used as described by Josefsson [4]. The geometry model was based on a rectangular block with rounded corners to mimic a simple truck. The height, length and width of the block was based on measurements from the truck simulated. The different sizes tested were half scale, full scale and 1.5 times full scale, those will be referred to as 0.5, 1.0 and 1.5 respectively. The method to estimate the C_p values are based on the approaches decided earlier, using probes upstream the wind tunnel test section in the converging nozzle and using these to predict the stagnation pressure.

Validation Parameters

To validate the simulation methodology different quantities in the wind tunnel are measured. The quantities used in the work will be the two force coefficients, C_d and C_s and the pressure coefficient, C_p . C_d is the drag coefficient and is the most important quantity. For this purpose C_d is calculated according to Eq. (2.13) in the theory section. C_s is the side force coefficient and is calculated similarly as C_d according to Eq. (2.14). C_d and C_s depend on the force in x and y direction, respectively. The forces arise from pressure difference and shear stresses. For the truck evaluated in this work the dominant part of the force is generated from pressure difference, which highlights the importance of pressure prediction. C_d and C_s also depend on the density, frontal area and free stream velocity. The density is assumed to be constant since incompressibility is assumed and the frontal area is set by the current truck geometry and is equivalent to the frontal area used in the wind tunnel test. The free stream velocity is calculated as mentioned earlier. This leaves C_d and C_s values with two error factors, both the overall simulation accuracy and the free stream velocity depending on the reference probe position as discussed earlier.

The other quantity that is being used to validate the methodology is C_p . C_p is calculated according to Eq. (2.15) from the theory section, were the index i correspond to each pressure probe in the tunnel. C_p is, as the force coefficients, depending on the free stream velocity, but also on the free stream pressure, which also includes an uncertainty. To evaluate C_p the difference, ΔC_p , between the simulations and wind tunnel results will be used. ΔC_p (Sim - WT) is defined as Eq. (3.2), where the notation (Sim - WT) refers to the simulation value minus the wind tunnel value.

$$\Delta C_{p_i}(Sim - WT) = \frac{p_{i,sim} - p_{\infty,sim}}{\frac{1}{2}\rho_{sim} V_{\infty,sim}^2} - C_{p_i,wt} \tag{3.2}$$

Analyzing Eq. (3.2) shows that the final error will depend on the choice of $V_{\infty,sim}$, $p_{\infty,sim}$ and the pressure, $p_{i,sim}$. $p_{\infty,sim}$ will offset the error and $V_{\infty,sim}$ will scale it.

This thesis will consider Yaw Weighted Average (YWA) quantities of the truck. YWA is derived to give a good representation of how the truck performs aerodynamically overall in a statistically averaged wind angle spectrum. Simulating the truck with a yaw angle essentially means that a side-wind component is added. This is to get a better comparison with reality, as the wind does rarely come from straight ahead but mostly has a side component hitting the truck. To get a C_d value representative for the truck the YWA is used. A weighted function of the C_d values for different yaw angles is derived to be representative for driving a truck in Europe according to the work by Berglund. [26]

3.2 Convergence Criteria

For fuel economy, the most important quantity from the simulations of heavy vehicles is the drag coefficient, C_d . To make this quantity comparable between different setups and geometries it is convenient to reduce it down to only one value, an average. The average of the drag signal is computed by averaging over a certain time span. This average can then be described as in Eq. (3.3) where the true mean, $\overline{C_{d,T=\infty}}$, is the calculated mean, $\overline{C_{d,T=\text{finite}}}$, plus a statistical error in the measurement, ϵ. The true mean can be reproduced when the averaging time, T, is stretched to infinity. The ϵ depends on the evaluation time interval and the variation of C_d . It is a quantity describing how uncertain the solution is, statistically. This limit can also help define if a solution is significantly different from another or if it is an element of uncertainty.

$$\overline{C_{d,T=\infty}} = \overline{C_{d,T=\text{finite}}} + \epsilon \tag{3.3}$$

ϵ is the error of interest but how to determine it is not straightforward. The first thought that comes to mind is to use the equation for the standard deviation, Eq. (2.21). This is not a valid formula to use in this application since all samples are not independent of each other. The time history strongly correlates between each time step because of the small time-steps used according to Norman and Howard [27]. To transform Eq. (2.21) into a form more applicable to CFD simulations Norman and Howard [27] suggest Eq. (3.4), where the actual number of samples is changed to an effective number of samples, $N_{\text{effective}}$.

$$s_{\bar{x}} = \frac{s}{\sqrt{N_{\text{effective}}}} \tag{3.4}$$

Eq. (3.4) infers that the standard deviation of the mean is proportional to the standard deviation of the signal divided by the square root of the effective number of samples. The effective number of samples is essentially some factor multiplied with the sampling time. This is because from logical reasoning, the standard deviation of the mean should decrease as the sample is taken for a longer time, as long as the sample is fluctuating around the same value.

The convergence of the DES simulations is challenging to define and very case dependent. Different methods were analyzed to find one criterion suitable for this thesis work. The work from Elofsson, Mercier, Duncan, and Boissinot [28], Sterken, Sebben, and Löfdahl [29] and Mocket, Knacke, and Thiele [30] were considered as good starting points to find a convenient method. Also, the paper from Norman and Howard [27] was addressed to see how different methods could be compared. All of those methods use one or a few parameters, for example, C_d , C_s and C_l, from the simulation to analyze the fluctuations, and from those fluctuations decide to what degree the solution is converged. To keep in mind during this analysis is that for trucks used in this work the C_d value oscillates with large amplitude and long time scales. These oscillations origin from the wake behind the truck and add a large uncertainty in the averaging since not too many of those long periods can be sampled due to the cost of the simulations. It should also be kept in mind that engineering judgment and expertise in the behaviour of the simulated case can also be of interest when deciding upon how long averaging intervals are needed.

The convergence will be analysed in the simulated wind tunnel environment since this is what is of most interest in this work. This is however a more complex environment to achieve a good convergence in compared to an open road set-up as mentioned by Josefsson [4]. This will be addressed by increasing the computational time if needed or let the convergence limits be wider as long as they are defined sufficiently. The upside of analyzing the wind tunnel environment is that most certainly the results will be applicable in the open road simulations with less computational expense. The data will further be assumed not to have any initial transient. The effect of the initial transient will be discussed in an upcoming section.

3.2.1 Visual Inspection

The simplest way of judging if enough data is sampled is to visually look at the signal and from there decide if the interval is long enough. This can be done by analysing if a signal oscillates with approximately the same amplitude around the same mean and cover a sufficient amount of periods and flow passages. This visual method requires a good understanding of the behaviour of the case that is simulated. This is a method that in a lot of cases are sufficient but it leaves an uncertainty of what confidence one has in the solution. Using this method also makes it necessary to always manually check in each simulation if it is converged and hence introduce a significant human dependence into the analysis. This might create some inconvenience in an industrial context where a standardized methodology is needed to guarantee a consistent quality of each case.

3.2.2 Moving Average

The approach that is used by Elofsson et al. [28] is of interest because of its simplicity. This approach only treats the moving average of the force coefficients and how those moving averages fluctuate. A moving average, $MA(t_i, I)$, is defined as Eq. (3.5) for a time t_i and a interval, I. The moving average is calculated for all time steps starting from the interval length, I, and up to the end of the time series. The interval length correspond to a number of time steps, for example $I = 1000$ time steps for a simulation with 0.001 s time steps generate 1 s moving average for the signal.

$$MA(t_i, I) = \frac{\sum\limits_{i-I}^{i} C_d(t_i)}{I} \tag{3.5}$$

Different averaging intervals are used, and for those different amplitudes are observed in the moving average. Elofsson et al. tested average interval lengths from 1 up to 10 seconds on a simulation of 60 seconds in total. The method constructs confidence intervals for the different average interval lengths by taking the difference between the maximum and the minimum value of the moving average for the entire run of 60 seconds. The significance of those intervals has a very strong dependence on how long the average intervals are compared to the total time of the data set, and may introduce an element of inconsistency in the analysis.

The confidence intervals generated by this method can be used to see what confidence the results have. However, some care needs to be taken before usage. The average interval length must be long enough to cover all the physical characteristic movements that are appearing, for example, a fluctuation in the base wake. This factor sets a minimum time to run dependent on how long the wavelengths are for the fluctuations. When this factor is set, the simulations need to run long enough to have the signal covering enough time for the moving average to be represented properly. This could be set in relation to the moving average length, for example, the total time is set to 6 times the longest moving average interval as Elofssons et al. does. This would ensure that the average reaches its maximum and minimum during the simulated time. For this work, it was considered to have the average intervals of 1/3 of the full time and shorter.

The downside of this method is that it cannot provide a confidence limit for the full length of the time series, but only for shorter averages. This gives a limit only for the shorter average and then it follows that the confidence interval for the full-time series should be less than those. Thus if 1/3 of the full-time series is used to set the confidence interval for the moving average, the confidence is for a signal 3 times shorter than what the actually average will correspond to. This method would perform very good in a situation where the same fluctuations appear for more than one simulated case. If this applies then only one simulation could be used as a reference and run that for long to set the confidence interval for a certain average interval. These limits could then be used for the other simulations. This would make it possible to save time in the other cases but would also assume that those would converge in the same manner as the reference. For an industrial purpose where the behaviour of the next case to be run is unknown, this assumption does not hold.

3.2.3 Running Average

Another way of defining a converged solution is presented by Sterken et al. [29] where the running standard deviation of the running force coefficients signals, Running $\sigma[C_d]$, and the running standard deviation of the running average force coefficient signals, Running $\sigma[\overline{C_d}]$, together with the running average of the force coefficients signals, Running $[\overline{C_d}]$, were analyzed. This paper presents how the running standard deviation of the raw force signal converges to a constant value and how the running standard deviation of the running average of the force coefficients approaches zero as the sample time is increased.

A check of the convergence using the running average of the force coefficients can be used together with its running standard deviation in the following way. First the running average is calculated and simultaneously the standard deviation of the sampled data is calculated. This method would show how the running average would converge towards its true value after a sufficient amount of time and the standard deviation of the running average would converge to zero as the mean approaches a constant. The suggestion from Sterken et al. is to use limits for $\sigma[\overline{C_d}]$ to tell if the solution is converged or not. The limits suggested is around 0.002-0.004, these have to be decided for the specific case. Worth to mention is that the limits set by Sterken et al. were based upon simulations from a car geometry which is significantly different from a truck geometry.

The idea of the standard deviation of the running average of the force coefficients, Running $\sigma[\overline{C_d}]$, is that it should decrease after a certain stage has been reached. This stage is when enough data has been sampled to cover the biggest fluctuations and longest time scales and further just make the standard deviation smaller. When it is starting to decrease it means that Running $[\overline{C_d}]$ starts to stabilize around the mean value. In order to determine if the solution has converged therefore require a standard deviation that is decreasing but also that it has been run for a sufficient amount of time for the specific case. Since the raw signal might start larger fluctuations after a while and those are not seen in the standard deviation before they occur. This again raises the question of how long the minimum average interval should be to capture the longest time scales of the simulation.

This method does not give a useful confidence interval of the final mean value since the samples used are not independent of each other. The limit set for $\sigma[\overline{C_d}]$ cannot be used in itself since the samples are strongly correlated with each other.

3.2.4 Repeat Reference

Norman and Howard [27] analyze a few different methods for determining the confidence in a converged solution. The first method described is the Repeat Reference (RR) method. This method is based upon taking the signal and splitting it into parts and generate an estimate of the confidence of the signal for a certain length based upon the average over all the split parts of that certain length. The equation for the error, ϵ, dependent on a specific interval length, T_ω, is shown in Eq. (3.6). Here $\hat{\phi}_{T_\omega}$ correspond to either the standard deviation or the mean of the certain interval T_ω and $\hat{\phi}_T$ correspond to the same parameter for the entire signal.

$$\epsilon(T_\omega) \approx \frac{\sqrt{\left\langle \left(\hat{\phi}_{T_\omega} - \hat{\phi}_T \right)^2 \right\rangle}}{\hat{\phi}_T} \tag{3.6}$$

This method works well to set confidence for the short lengths since then there is a lot of intervals generating data and hence making the method more stable. As the intervals get longer the number of intervals also reduce, Norman and Howard estimate that using intervals of 1/3 is the limit of how much one can stretch this method and this limit would mean that the average is taken from only three intervals.

This method is very simple to use to create confidence intervals, but just as for the moving average method, this one does not give any estimate for the full length of the signal. It only gives a good estimate for a subset of data. Norman and Howard used this method as a reference one but that was for intervals ten times shorter than the full signal length. They conclude that for their signal the RR method does get noisier when the estimate is used for more than 10% of the full signal.

3.2.5 Estimated Bandwidth Limited Gaussian White Noise

Another method discussed by Norman and Howard [27] is the work done by Mocket et al. [30]. This work presents a more sophisticated method for determining if the solution is converged to a certain limit or not. To determine if the solution is converged Mocket et al. uses a method where the error, ϵ, is estimated by assuming it to be a bandwidth-limited Gaussian white noise as in Eq. (3.7). This gives a formulation for the error dependent of the mean, $\hat{\mu}_x$, standard deviation, $\hat{\sigma}_x$, length of the interval, T, and the bandwidth, B. The bandwidth is estimated by fitting the error from Eq. (3.7) to the error from the RR method , Eq. (3.6), and find B as a curve-fitting parameter for each signal. This fit is done in such a way so that B is chosen conservative and the maximum error of the RR method is fit to the minimum error of bandwidth-limited error. The variance and error is related according to Eq. (3.8).

$$
\begin{aligned}
\epsilon[\hat{\sigma}_x] &\approx \frac{1}{\sqrt{4BT}} \\
\epsilon[\hat{\mu}_x] &\approx \frac{1}{\sqrt{2BT}}\left(\frac{\hat{\sigma}_x}{\hat{\mu}_x}\right)
\end{aligned}
\tag{3.7}
$$

$$
\epsilon \approx \frac{\sigma[\hat{\phi}]}{\hat{\phi}} \tag{3.8}
$$

The parameter B can then be used to predict the confidence interval at the end of the signal and give a conservative confidence interval of the mean.

3.2.6 Spectral Method

The method comparison by Norman and Howard [27] includes the method they mentioned as "Spectral Method Heidelberger and Welch". This method by Heidelberger and Welch [31] proposes how to set confidence limits for an averaged value. This method has the assumption that the time series converge to a steady-state solution and that this can be modelled as a stationary covariance process. This means that the mean is constant in time and that the variance of two points in the time series don't depend on time but only on the distance from each other according to Taboga [32]. Using this one can find how the variance of the mean is depending on the power spectral density of the time series. This can then be used by splitting up the available data in different batches and find a mean of the variance over those batches to determine a fair variance of the mean.

When this method was applied the results did not match the expectations very well. Due to time limitation, this method did not get analyzed further on available data. This method does give very good results for determining the confidence level in agreement with the RR method for a long time series [27] so it could be of interest to examine this method further in the future.

3.3 Initial Transient

Running unsteady simulations always introduce a start-up transient at the beginning of the simulation since it is initialized from a certain state, a RANS solution for example. This transient introduces an uncertainty as when to start the averaging time interval. The transient adds a bias and it is of interest to start the averaging interval after this transient has decayed. When the initial transient has decayed it can further be assumed that the process is statistically stationary as Mockett et. al refers to it [30].

Norman and Howard [27] evaluate four different methods for estimating the initial transient and how much time must be removed in the beginning. To discuss those methods a stationary process needs to be defined. Strict and weak stationarity is mentioned by Norman and Howard but the methods they test only assume weak stationarity or less. Strict stationarity means that the process has a joint statistical distribution that is the same over the entire time domain. The weak stationarity means that the mean, variance and autocovariance is the same for the time domain. The method from Heidelberger and Welch [33] tests for the weak stationarity and the method by Mockett et. al [30] only tests for mean and variance stationarity. The other two methods tested by Norman and Howard test for stationary mean and variance from Chodera [34] and only for stationarity of the mean from Geweke [35].

Norman and Howard conclude that the method from Geweke [35] is the best for predicting the stabilization time. They also mention that the method from Mockett et al. performs almost as good but it overpredicts the length of the initial transient. Because of project time limitations, only one method was evaluated in this work. This was the method used by Mocket et al, since this method uses the same parameters as the convergence method, estimated bandwidth-limited Gaussian white noise, from Mocket et. al [30]. The method from Geweke could however be of interest since this predicted the initial transient more accurately and thus might reduce the computational cost slightly compared to the method of Mocket et. al that overestimated the initial transient.

The method to find the initial transient proposed by Mockett et. al [30] is based upon finding a minimum value in error. This minimum is the product of the estimated variance of the variance, $\sigma[\hat{\sigma}_x]$, and the estimated variance of the mean, $\sigma[\hat{\mu}_x]$. This variance is estimated for intervals from $[t, T]$ were t is the starting time and T is the final time. The starting time, t, is ranging from $(0, \frac{T}{2})$ since otherwise there could be minima introduced since the total time is shortened too much and hence the statistical reliability is lowered too much. The t that generates the lowest product from the two estimated variances are then used for $t = t_0$, where t_0 is where the initial transient should be gone and can be used for starting the averaging for the mean values.

The variances $\sigma[\hat{\sigma}_x]$ and $\sigma[\hat{\mu}_x]$ is computed by assuming the error to be distributed as white Gaussian noise, as for the method used for the convergence earlier. This assumption leads to setting $\epsilon[\hat{\sigma}_x]$ and $\epsilon[\hat{\mu}_x]$ according to Eq. (3.7), where the error depends on the variance according to Eq. (3.8). This is then calculated as before, see section 3.2.5, to generate a separate B for each of the variances. Then the product, $\sigma[\hat{\sigma}_x] \cdot \sigma[\hat{\mu}_x]$, is calculated for different starting times and where this product is minimal, the starting time, t_0, is set. The underlying thought is that the error will decrease when t is increased up until the initial transient is gone because of the bias from the initial transient increase the variance. However, when t is increased further the variances will again increase because the total signal gets shorter. This combination should then give an appropriate starting point were enough of the initial transient is removed compared with the error received from shortening the sample.

3.4 Mesh Analysis

The spatial discretization of the domain is one of the errors in CFD simulations and it gives a numerical error due to the approximations done between cells. The error is based on the terms truncation in Taylor expansion and gives a direct numerical error according to Versteeg and Malalasekera [6]. These errors all appear in each flow quantity solved for. In theory, it is possible to eliminate this error by increasing the mesh resolution. This is not of interest as it increases the computational cost of the simulations. Therefore the mesh should be refined in an efficient way to make an acceptable trade-off between accuracy and computational cost.

It is not straightforward how to generate a mesh for complex geometry. It is of great importance when the computational domain is big and complex that the mesh is constructed efficiently. Therefore the use of refinement regions can be of interest. Doing refinements in certain regions is called Block-Structured Grids [6]. Josefsson has previously done some studies on different refinement regions [4]. One aspect of the mesh study here is how the results get affected in a wind tunnel environment. Josefsson's work included a mesh study that was performed in an open road environment and was therefore not fully applicable in this work.

3.4.1 Refinement Regions

The mesh refinements are going to be limited to certain regions and be scaled according to a base size of the domain. This scaling will be done by reducing the cell size by half according to the previous size and hence increase the number of cells in those refined regions by 8. This scaling is done because in the CFD software used, all refinements are scaled according to a base size. This base size is used to create relative refinements in the entire computational domain. The difference between the mesh setups will be compared and then the setup that yields results that are best compared to the computational cost will be used for further analysis.

Initial Refinement

The initial mesh setting in the simulations includes use of a base line setting in the domain and then different boxes to refine certain volumes. The mesh for the prism layers are also refined for all the surfaces in the test section of the wind tunnel. There are 5 different box refinements in the domain. The first are two boxes that scales down the refinement around the truck. Those refines the cells from the mesh far upstream and downstream the domain. The next refinement is a ground refinement, which refines the floor in the test section under the truck. There is also a refinement around the cab of the truck, this refinement is created to capture the details in the flow appearing because of the complexity of the cab. The last refinement is at every wheel. Those are created to capture the interaction between the wheels and the ground. The mesh is shown for two planes for the test section in Fig. 3.3. The two planes used are the y=0 plane and the z=2 plane. In the figure the refinement around the cab is clear. Then the inner box is covering the cab refinement and the entire truck and outside of this the outer box is visible.

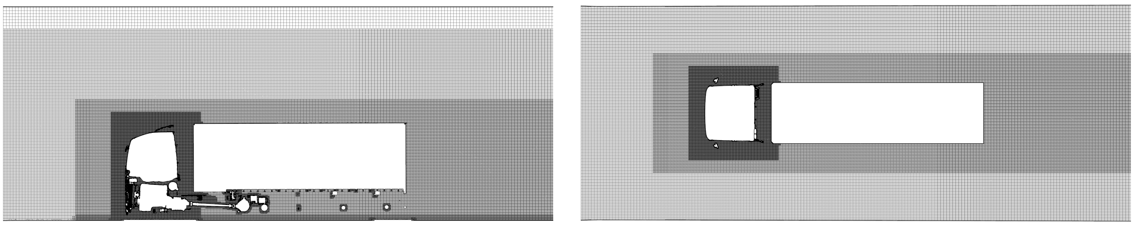

(a) y = 0 plane

(b) z = 2 plane

Figure 3.3: Initial mesh settings visualized in the y=0 and z=2 planes.

The mesh refinements around the cab in the initial setting and the refinements that will be analysed is presented in Fig. 3.4 for the side view. The refinement regions are presented as green boxes and are mentioned as initial cab, trailer, underbody, and front cab for the different regions.

(a) Initial cab (100% of cab)

(b) Trailer (100% of cab)

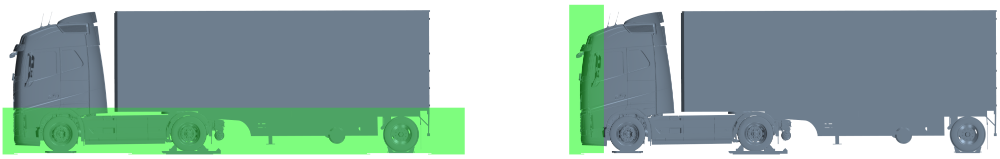

(c) Underbody (50% of cab)

(d) Front cab (50% of cab)

Figure 3.4: Mesh refinement regions for initial cab, trailer, underbody, and front cab in side view. The relative size of the cells compared to the cab refinement is shown in parenthesises.

Trailer Refinement

The first refinement that was tested to improve the accuracy around the truck was around the trailer. This is an extension of the refinement around the cab in the initial setting to cover the entire truck, see Fig. 3.4(a) and (b). The cells in this refinement is 100% of the size of the cells in the cab refinement. This was chosen to test since a lot of the pressure probes tested in the wind tunnel is placed on the trailer and hence the result from those probes should be reliable. The trailer refinement that extended the cab region over the entire truck is not affecting the limitations that arise from the CFL condition. This is since the local velocities in those cells is not as high compared to the cells already present in the cab region. This refinement would also capture more of the smaller movements in the wake region close to the truck which is of great interest. This refinement was deemed necessary so it is included in the two refinements of the underbody and the front.

Underbody Refinement

The second attempt to improve the mesh setup was to add refinement of the underbody to the trailer refinement. This refinement region is visualized in Fig. 3.4(c). The cells in this refinement is 50% of the size of the cells in the cab refinement. This was made in addition to the trailer refinement as a new region. This refinement generates a lot more cells in the computational domain because of the details of the chassis but is considered worth to test because this region is of great interest for the zero degrees yaw case. The airflow has to travel underneath the truck to exit in the back and affect the base wake. This raises the question of how well the flow underneath has to be resolved to make sure the base wake is predicted accurately. This region affects the CFL condition in the front region where the flow accelerates underneath the truck. This would mean that there is a risk of losing information in the temporal resolution and hence generate another error.

Front of CAB Refinement

The third attempt to increase the mesh settings was to add refinement in front of the cab. This refinement region is visualized in Fig. 3.4(d). The cells in this refinement is 50% of the size of the cells in the cab refinement. This refinement, as for the underbody refinement, was added to the trailer refinement. This made the cells in this refinement to be half the size of the trailer refinement. This refinement was motivated by the fact that a lot of separations occur around the front corners of the cab, a-pillars, and hence will affect the flow all the way downstream. This refinement is not as expensive as the underbody refinement and therefore would be more feasible to implement. This region affects the CFL condition strongly. Most of the cells with the highest CFL number are placed in this region of the domain which makes this refinement require a higher temporal resolution.

3.4.2 LES resolution

To find if the mesh size is satisfactory in the LES part of the domain, there are some different methods to use. One way is to compare the ratio between modeled and total shear stress, another is to compare the ratio between modeled and total turbulent kinetic energy. In this thesis the two-point correlation will be used in different region of interest in the domain. This method was presented by Davidson [36]. The method uses two-point correlation for the fluctuating part of the velocity, v', as Eq. (3.9) to create the normalized correlation coefficient, $C^{norm}_{v'_j v'_j}(i_A, i_B)$. The coefficient depends on which fluctuating velocity component is used and which coordinate direction is used. The indices i and j represent the coordinate and velocity component respectively, such that $i, j \in \{x, y, z\}$. The index k denotes what cell is being evaluated. This is used to see if the largest eddies are described by enough resolution in the LES region. This is done by looking at how many cells are needed to remove the correlation between two points. According to Davidson the largest scales should be resolved by a minimum of 4 cells for a coarse LES but preferably 8 cells or more. Although, 8 cells is usually not enough to be a well resolved LES according to Davidson. Davidson suggest that the poorest resolved direction should be the one determining the resolution according to this method.

$$\begin{aligned} C^{norm}_{v'_j v'_j}(i_A, i_B) &= \frac{\overline{v'_j(i_A) v'_j(i_B)}}{v'_{j,RMS}(i_A) v'_{j,RMS}(i_B)} \\ v'_{j,RMS}(i_k) &= \sqrt{\overline{v'^2_j(i_k)}} \end{aligned} \tag{3.9}$$

This method is motivated by making sure that the largest turbulent length scales, largest eddies, are resolved well for the flow. This is to ensure that the cascade process is initialized correctly. According to Davidson [8] the cascade process is the phenomenon where the energy is transferred from the mean flow to the large turbulent structures and from those successively transferred from larger to smaller eddies until dissipation occur in form of thermal heat at the smallest turbulent length scales. The largest turbulent length scales can be described by the integral length scale, $L_{int}(v'_j, i)$, in Eq. (3.10). The normalized correlation factor is then integrated up to infinity, which in this work is considered when the correlation factor crosses 0 or starts to increase noticeably.

$$L_{int}(v'_j, i) = \int_0^\infty C^{norm}_{v'_j v'_j}(i, \tilde{i}) d\tilde{i} \tag{3.10}$$

The two-point correlation was used by Ljungskog [37] in the wake of a SUV car model. Ljungskog uses 8 cells as a limit to describe the largest eddies, but finds in his result that the correlation spans over 10 cells. Ljungskog test the correlation for the stream-wise velocity, V_x, for two lines in the x and z-direction in the wake of a SUV car.

The investigation was applied to three regions, wake, side and underbody, according to Fig. 3.5. To describe the regions three lines are taken for each region, one line for each direction; x, y, and z. The coordinate system used is the same as earlier in the report. The values along those lines were then correlated upwards along the positive direction for each line. The correlation is limited in the last cells of each lines. The correlation for those cells are forced to diminish when the number of cells are limited in the end of the lines which makes the result look like the resolution is reducing. This is just a numerical limitation for a finite line of cells and makes the last cells for each line unusable for analysis.

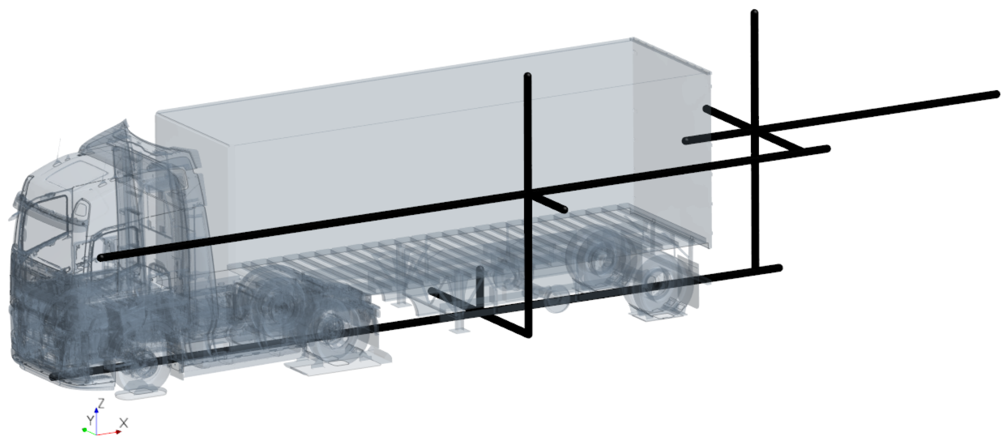

Figure 3.5: Coordinate systems used for two-point correlation. Wake, side and under system.

The lines used in the different systems are placed according to Table 3.1 for clarification. To understand where those are localized in space the outer measurements of the truck is also listed in the table.

Table 3.1: Limits of the truck and list of lines used in the systems of lines for two-point correlation.

System	Line	x (m)	y (m)	z (m)
Truck	N/A	1.9 to 14.0	-1.3 to 1.3	-0.6 to 3.5
Wake	x-line	14.2 to 20.1	0.0	2.0
Wake	y-line	15.5	-1.6 to 1.6	2.0
Wake	z-line	15.5	0.0	-0.4 to 4.0
Side	x-line	2.2 to 16.0	-1.6	2.0
Side	y-line	10.3	-2.8 to -1.6	2.0
Side	z-line	10.3	-1.6	-0.4 to 4.0
Under	x-line	2.2 to 16.0	0.0	-0.4
Under	y-line	10.3	-1.6 to 1.6	-0.4
Under	z-line	10.3	0.0	-0.4 to 0.3

3.5 Frequency Content

Simulating trucks and primarily focusing on the C_d of them puts the focus on the base wake since this is a part contributing significantly to the drag according to Hucho [3]. This brings up the interest of how this wake and drag signal behaves when it is resolved in time. Elofsson et al. [28] studied the relevant time scales by using spectral analysis of the drag signal. Elofsson et al. found that for the 5 degree yaw case the drag signal depends mostly on the low-frequency signals of 0.25 Hz meaning a time scale of 4 seconds and the side force is dominated by 1-2 Hz fluctuations. Elofsson et al. also analyses the C_p fluctuations on different points on the truck and find out that the strongest fluctuations appear on the rear end of the truck.

The drag signal is sampled with a certain time step and for a certain length. These parameters give two important limitations in the frequency domain. The time step length limits the highest frequency that is resolved according to the folding frequency, the second limitation in the frequency domain is limited by the sampling length, from the theory section 2.5. This limitation is based upon how long sample is taken and will limit the lowest frequencies resolved. The lowest frequency resolved is the inverse of the sampling length. These two limitations are crucial when analysing the frequency domain. This is since if data is sampled with too long time steps or for too short time relevant information in the frequency domain might be omitted.

3.6 Inner Iterations

Simulating time-resolved flow using an iterative implicit method includes the choice of inner iterations in the solver. The inner iterations are used similar to a steady-state solver in each time step that makes sure the equations converge in each step. This is one major source of the total computational cost since it scales linearly in time with how many inner steps are taken. Common guidelines are to take between 5-10 steps according to Ross and Herrmann [38], but these inner iterations are dependent on the length of the time steps used in the simulation. This introduces a coupled problem where one can increase the time step size but this might directly translate into an unconverged solution in each time step. To evaluate if a solution is converged or not the residuals can be monitored for each time step. The residuals are the errors that occur in the discretized flow equations due to the iterative method. This error is purely a numerical error and is possible to decrease by taking more iterative steps. The residuals are obtained for every cell element in the domain and to make it more convenient to use, the absolute value of all the local residuals in each cell are added together to create a global residual. The residuals have a different value depending on what flow quantity being analysed and therefore a normalization method is used to make all the residuals comparable to each other as stated by Versteeg and Malalasekera [6]. The normalization used in this project is the standard procedure in Star-CCM+ that is based on dividing the residual by the largest one occurring in the first five iterations [11]. The residuals can be reduced down to machine precision, but this is not of interest since other sources of errors are much larger then that. Therefore it is of more interest to drop the residuals to be the same order of magnitude as the other errors in the simulation, from the modelling and discretization. Iterating for longer is just a waste of computational time since it will not significantly reduce the total remaining error in the simulation according to Windisch [39].

Ekman et al. [25] used a preset limit of 10^{-5} for all the normalized residuals to ensure convergence. This limit results in 3 inner iterations for the finest time step up to 10 for the largest. The factor between the time steps was 100 from smallest to largest, and this work showed that increasing the time step significantly changed the number of inner iterations needed to reach the same order of convergence. For this thesis, the six residuals monitored were not behaving similar to each other, and having one single limit for all residuals did not make sense. The residuals were not used as limits for this work but instead, the difference in the residuals for different time steps were analysed to see how they differed.

This inner convergence is also coupled to the Under Relaxation Factors (URF) used in the simulations. The URF is added for the segregated velocity, V_{URF}, segregated pressure, P_{URF}, and $k-\omega$ turbulence, KO_{URF}. Those factors are used to reduce the risk of a solution to diverge, but doing so also slows down the convergence in each inner iteration. There are different recommendations on how to set those URF values. According to Ross and Herrmann [38], they can be set in either a recommended setting or an enhanced stability setting. The recommended setting values are $V_{URF} = 0.8$, $P_{URF} = 0.3$, and $KO_{URF} = 0.7$. The values for the enhanced stability are $V_{URF} = 0.7$, $P_{URF} = 0.1$, and $KO_{URF} = 0.6$.

Since this thesis includes a study of how the results get affected by different temporal discretizations, a study will also be conducted on how those time steps affect the residuals. This will be done together with a study of how the under relaxation factors affects the residuals.

3.7 Simulations

All the CFD simulations carried out in this thesis will be done in Star-CCM+. The simulations are listed in Table 3.2. The table lists the key differences between the simulations in such a way that they are comparable to each other. The first column gives the descriptive name of the simulations. The first setting, in the second column, is the geometry setting, this is split into truck and block. The "truck" refers to the truck geometry mentioned earlier and the "block" geometry is the geometry used for the study of the stagnation pressure. The second setting is the mesh setting. The "initial" mesh refers to the settings used at Volvo GTT when the thesis was started and "trailer", "underbody" and "front cab" refers to different refinement regions. The third setting is the time step of the unsteady simulations, this refers to the length of the time step or to "RANS" if steady-state Reynolds Averaged Navier-Stokes (RANS) solver was used. All the unsteady simulations are initialized from a RANS solution of 1000 iterations to make sure they start from flow conditions more similar to the end results. The fourth setting is for the Under Relaxations Factors (URF) which is referred to as "R" for Recommended settings and "ES" for Enhanced Stability settings. The name "NURF" refers to New Under Relaxations Factors. The fifth setting is for the number of Inner Iterations (II) used in the simulation. This will be set to 8 or 10 for unsteady simulations and maximum 10000 (10K) for the RANS solver. The sixth setting is which yaw angles the simulations have been run for. This setting refers to either separate angles of 0, -2.5, -5.0, -7.5, or -10. degree or as "Full" for all of them as a full yaw sweep. The last setting, T, is the length of the simulations in terms of T^*. For "1ms" the 31(62) T^* means that the 0 degree yaw was run for 62 T^* and the remaining angles 31 T^*.

Table 3.2: List of simulations and their settings included in the thesis.

Simulation	Geometry	Mesh Setting	Time Step	URF	II	Yaw	T
0.1ms	Truck	Trailer	0.1 ms	R	8	0, -5	20 T^*
NURF	Truck	Trailer	1 ms	R	10	0	15 T^*
1ms	Truck	Trailer	1 ms	ES	10	Full	31(62) T^*
2ms	Truck	Trailer	2 ms	ES	10	Full	31 T^*
4ms	Truck	Trailer	4 ms	ES	10	Full	31 T^*
8ms	Truck	Trailer	8 ms	ES	10	Full	31 T^*
Mesh Initial	Truck	Initial	1 ms	ES	10	0	31 T^*
Mesh Trailer	Truck	Trailer	1 ms	ES	10	0	62 T^*
Mesh Underbody	Truck	Trailer & Underbody	1 ms	ES	10	0	31 T^*
Mesh Front CAB	Truck	Trailer & Front CAB	1 ms	ES	10	0	31 T^*
Half scale Block	Block	Initial	RANS	ES	10 k	0	N/A
Full scale Block	Block	Initial	RANS	ES	10 k	0	N/A
1.5 scale Block	Block	Initial	RANS	ES	10 k	0	N/A

Table 3.2 will serve as a summary of all simulations referred to in this thesis. Each part of the report will treat different simulations in groups where parameters are changed individually. Each setting will be further described in each part of the thesis.

4

Results

The results will be divided into seven parts. The first four is; wind tunnel, convergence criteria, initial transient, and mesh analysis. Those are followed by the results for absolute accuracy and temporal resolution. Lastly the results for the inner iterations is presented.

4.1 Wind Tunnel

There are two main results from the wind tunnel setup. The uncertainty of the reference probes and the blockage ratio effect on the stagnation pressure. They will each be presented individually.

4.1.1 Reference Probes

Since the reference velocity, V_∞, and reference pressure, p_∞, is taken from one single point it was of interest to see how the position affects the value. It was found that the difference in one cell step for the initial setting had an impact on the C_d of 1.75%, this was deemed too much since the goal of the error estimation was to predict better. So one mesh refinement was done covering the reference probes. This refinement was done by enlarging one of the already existing refinements for the outer region around the truck to also cover these probes. By doing so the error was reduced to 1.18%. This was deemed sufficient and therefore this setting was used for the continued work.

The pressure coefficient at a point depends on the pressure relative to the free stream velocity and the free stream pressure. To obtain the pressure coefficient C_p for the different positions in the simulations the dynamic and static pressure from the reference probes were used. Using these references introduced an offset error in C_p for the stagnation point in front of the truck. According to Bernoulli's equation, Eq. (2.16), the C_p in the stagnation point should be equal to one. This was not achieved in the simulations and therefore it was decided to correct this offset according to the stagnation point to make the difference between simulated and tested C_p in the stagnation point equal to zero. This is motivated by the fact that the pressure in this area is quite well known and the error from this source was hard to identify and the work could not continue unless this problem was solved. It was judged that some lack of geometrical detail of the tunnel could be responsible for the offset. This issue is most likely depending on how the reference pressure and velocity are obtained and it shows that the method used to find it is not predicting it good enough. This could be partly because of how the reference static pressure is taken close to the wall and that the modelling this far upstream is not sufficient enough.

4.1.2 Blockage Ratio Effect

The study concerning how the blockage ratio affects the stagnation pressure were conducted on the three simulations Half scale Block, Full scale Block, and 1.5 scale Block from Table 3.2. This study showed that the blockage ratio is not strongly correlated to the stagnation pressure prediction. The results for the three different scales, 0.5, 1.0, and 1.5 are shown in Table 4.1.

Table 4.1: Stagnation C_p for different scales and corresponding Blockage Ratio (BR).

Scale	0.5	1.0	1.5
C_p	0.9914	0.9905	0.9887
BR (%)	2.66	10.62	23.90

From Table 4.1 one can read that increasing the blockage ratio from 2.66 to 23.9 per cent only increase the error by 2.7 pressure counts from 0.9914 down to 0.9887 for C_p . This makes the C_p change in the stagnation point to be 0.13 pressure counts per 1% of blockage ratio change. Therefore this effect is negligible in this study and the error in C_p can not be described by the blockage ratio.

The velocity fields for the bluff bodies for the y=0 plane is shown in Fig. 4.1. The body is visualised as the grey area in the figure and the velocity is set to be 25 m/s in the domain which is the dark blue colour and it is visualized up 35 m/s to which is the yellow colour. Here it is visible that the increased blockage effect increases the effective velocity around the truck and thus decrease the effective pressure around the body according to Bernoulli's equation, Eq. (2.16). This is in line with the result from Steen et al. [21] where they conclude that this is the difference when going from the open road to wind tunnel simulations. One can see in Fig. 4.1(a) that the blockage ratio of as little as 2.7% already accelerates the flow in the upper region of the tunnel, far from the body.

(a) Velocity field for y=0 plane for half scale bluff body

(b) Velocity field for y=0 plane for full scale bluff body

(c) Velocity field for y=0 plane for 1.5 scale bluff body

Figure 4.1: Velocity plane y=0 for bluff bodies in the wind tunnel environment. The velocity is set to be 25 m/s for an empty tunnel.

4.2 Convergence Criteria

This section will cover the convergence results from this work. It will state the different results from different methods and also compare the methods on the same signal to determine differences. Then the final method used further in the thesis will be stated. The simulations used to evaluate the different methods are 4 yaw sweeps for different time steps, referred to as 1 ms, 2 ms, 4 ms, and 8 ms in Table 3.2. Those simulations all include 5 angles from 0 to -10 degree yaw and the only difference between each yaw sweep is the time step. Therefore in this chapter figures and results will be referred to with a time step and a yaw angle. The time-dependent signal will be presented with T^*, according to the theory section 2.4, instead of time. To be noted is that all simulations have been run for 31 flow passages, T^*, except for 1 ms time step and 0 degree yaw, this simulation was run for 62 T^*. All results start to take the average from after 8 T^*, to remove any initial transient.

4.2.1 Visual Inspection

Starting with the visual inspection of a signal, Fig. 4.2 for example shows the variation of the drag coefficient around the mean against the non-dimensional time, T^*. The signal describes 1 ms and -7.5 degree yaw and is $31 - 8\ T^*$ long meaning that it contains 23 flow passages over the truck. Using the three targets of steady amplitude, oscillating around the same mean and covering a sufficient amount of periods, this signal can be estimated to be sufficient by sound reasoning. The amplitude is limited to about ± 40 drag counts (dc). The lowest frequency of the signal could be estimated to come from the period from $\approx 15\ T^*$ to $\approx 19\ T^*$. This period would then be about 4 flow passages long and the full signal would then cover at least about 5 to 6 of those periods if averaged after $8\ T^*$.

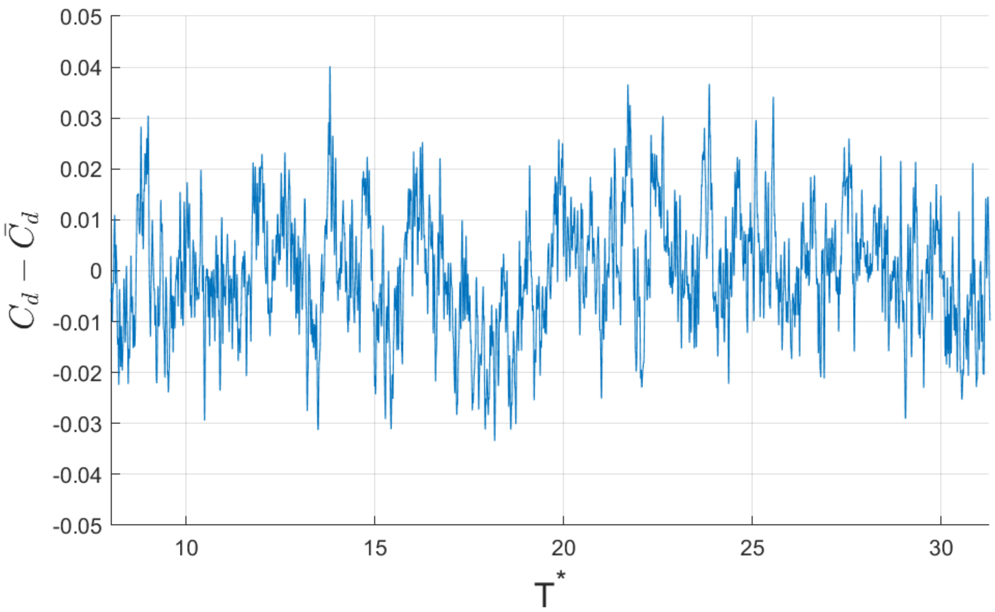

Figure 4.2: C_d signal offset by its mean value for a converged signal for 1 ms and -7.5 degree yaw.

The signal in Fig. 4.2 is one of the "nicer" looking signals that did not include any of the very long time scales. In contrast the signal obtained from the first 31 T^* from 1 ms and 0 degree yaw is shown in Fig. 4.3. This signal exemplifies a case where it is more difficult to decide whether more computational time should be invested to ensure convergence or it will be sufficient to average over the available time series. This case is a clear example where it would be appreciated to have a method that calculates the confidence for the average.

Judging by visual inspection does not give a clear relation between computational cost and statistically significance of the results. Therefore individual decisions might cause some simulations to run for a very long time, generating a small, but still unknown, confidence interval of the mean value while others decide upon a very short time having a large corresponding confidence interval. This would simply occur

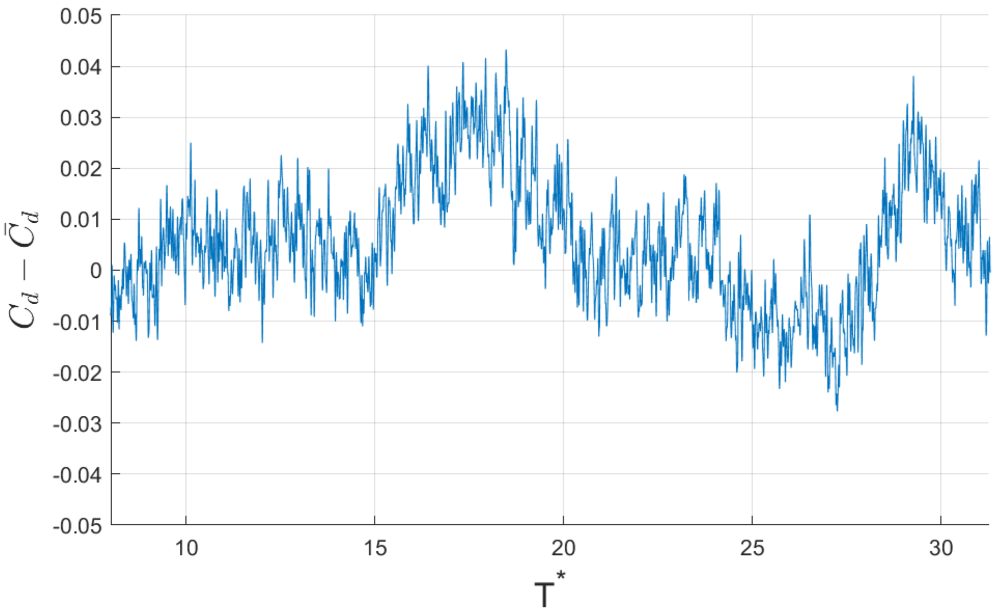

Figure 4.3: C_d signal offset by its mean value for a less obvious converged signal for 1 ms and 0 degree yaw up to 31 T^*.

since different individuals value the computational cost versus estimated statistical significance different. Therefore it is of interest to find a method that calculates the confidence interval for the mean value of interest and shows how this is related to the computational time. Having a confidence interval would also give a clear answer to the question in design whether a geometry modification gives a true change in drag or if it stemming from an error based on the uncertainty of the drag.

4.2.2 Moving Average

The moving average method will be considered for the 1 ms and 0 degree yaw case. This is because this method needs a very long signal to generate any useful results and this simulation is the longest signal of 62 T^*. The method is started after 8 flow passages because of the initial transient in the signal. The method is shown in Fig. 4.4 for three different average intervals, 2, 10, and 20 T^*. This figure shows how the moving averages change along time and it also shows that the averaging start later as the length of the average interval increases. The legend shows the length of the average intervals and also shows the confidence interval of the mean. The confidence interval for each signal is based upon the difference between maximum and minimum of the signal. It can be seen as expected that the largest confidence interval of ± 24 dc is obtained for the shortest average interval of 2 T^*. The confidence intervals then decrease gradually until the average interval length of 20 T^* where it is ± 7 dc. However, for the long average of 20 T^*, the overall accuracy is lower since it covers only about 1/3 of the signal. This gives a risk of not covering a sufficient amount of oscillations of the lowest frequencies to adequately describe the full width of the fluctuations of the mean.

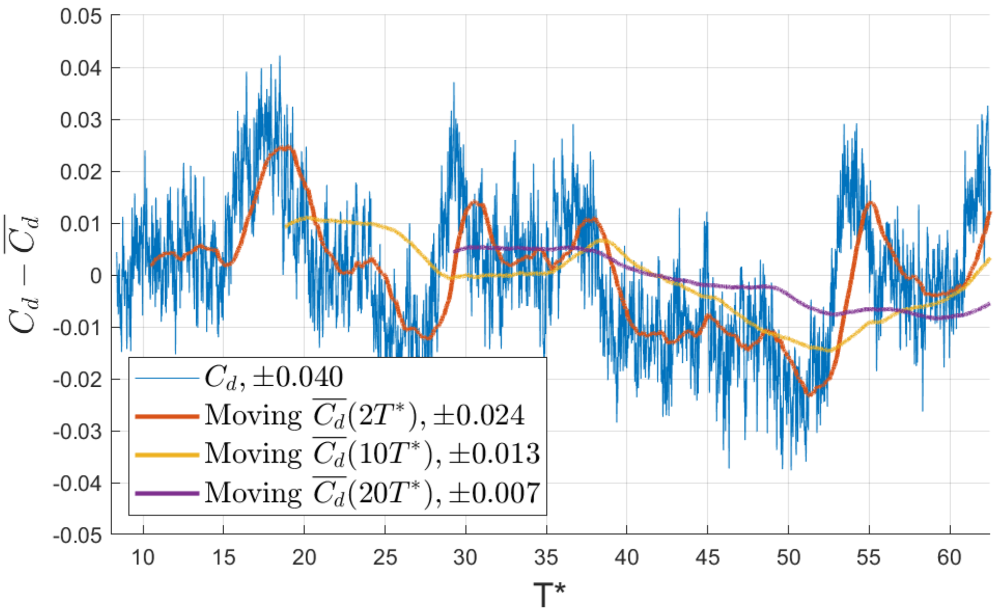

Figure 4.4: Moving averages for length of 2, 10 and 20 flow passages for C_d including their corresponding confidence intervals for 1 ms and 0 degree yaw.

The limits generated from this method is questionable if they can be used from one simulation to another. The objective is to determine the error for a new simulation, and then the question is for how long it has to run. That means that if this method is used, the simulations have to be run for a certain amount of time to start with and then use a, not too long, average window over the signal to determine the uncertainty. This could be done for example 1/3 of the signal as for 20 T^* or as 1/6 of the signal which would be 10 T^*. The difference between the two from this signal would then be as large as ±7 dc to ±13 dc or as a relative increase almost 100%. The limit used for further comparison will be the 20 T^* moving average. This is because it covers about 1/3 of the signal and is then comparable with the limits from the RR method, which also use up to 1/3 of the signal.

4.2.3 Running Average

To visualise the running average method the results from 1 ms and -7.5 degree yaw will be used. Fig. 4.5 shows how the running average levels out to a constant value. The blue line is the instantaneous C_d value and the red line is the running mean.

Fig. 4.6 shows the running standard deviation of C_d in (a) and the running standard deviation of the running average of C_d in (b). In Fig. 4.6(a) the signal behaves in a nice way for the method. This is because it grows in the beginning up to a peak and then decays to a constant value. This means that it first grows as the signal is very short and uncertain, then when enough of the fluctuations of the signal has been caught it flattens out to a constant value of about 0.012 as the signal gets longer and more stable. In Fig. 4.6(b) the signal shows a nice trend as it decays over time and ends at about 0.0015.

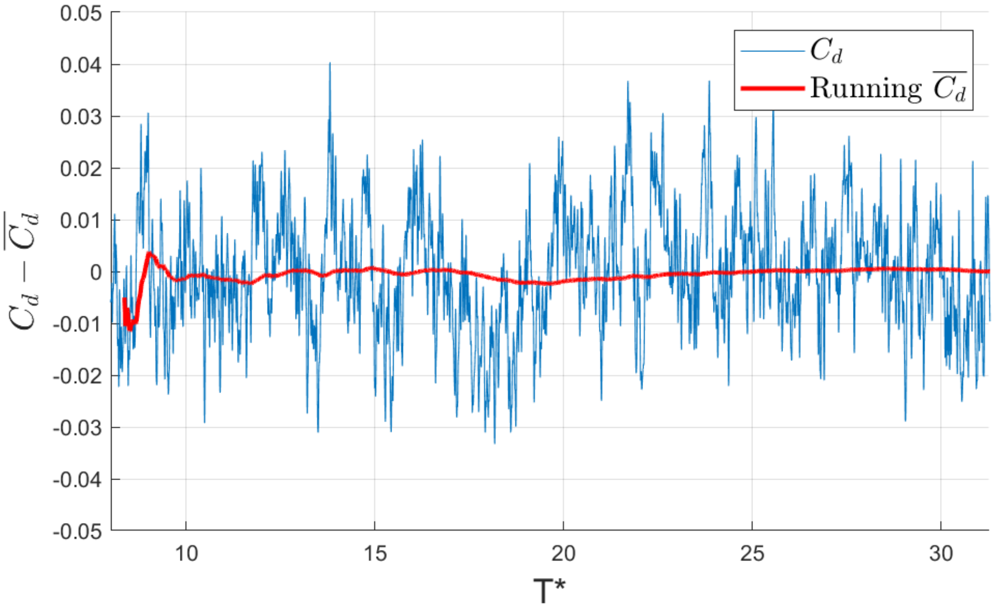

Figure 4.5: C_d and running average of C_d for 1 ms and -7.5 degree yaw.

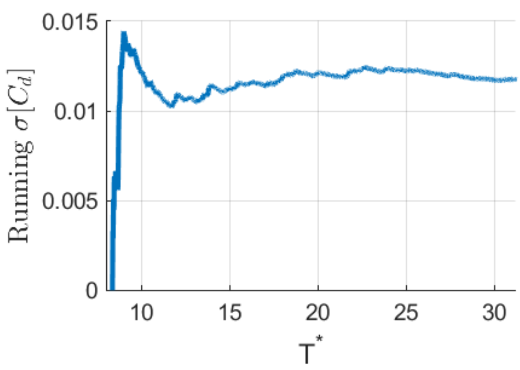

(a) Running standard deviation of C_d

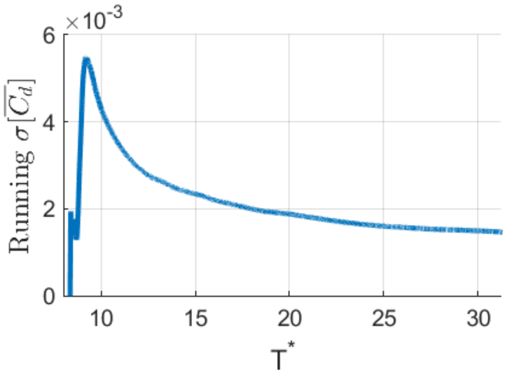

(b) Running standard deviation of running average of C_d

Figure 4.6: Running standard deviation of C_d and Running standard deviation of running average of C_d for 1 ms and -7.5 degree yaw.

This method has its limitations in how much data is collected and that one needs to run for at least enough time to capture one larger fluctuation if those exist. One can be mislead at the beginning of the simulation that it has converged since the standard deviation would decrease but that could change drastically if a larger fluctuation appears. To handle this problem the longest time scales needs to be known for the simulations and a minimum run time longer than that need to be set.

4.2.4 Repeat Reference

Results from the Repeat Reference (RR) method are shown for a representative data set in Fig. 4.7. The lines in the figure are as follows, blue is the instantaneous C_d value, red is the running mean of C_d and green is the confidence interval from the RR method. This figure shows the RR method applied to 1 ms and -2.5 degree yaw, and the signal is 31 flow passages long. This figure illustrates the method when the data is divided from 100 down to 3 subsets as the solid part of the green curve. From 3 splits, it is illustrated as the green dashed line. The splits could also be made in constant time steps but this would omit some data from each interval and hide some of the behaviour of the method.

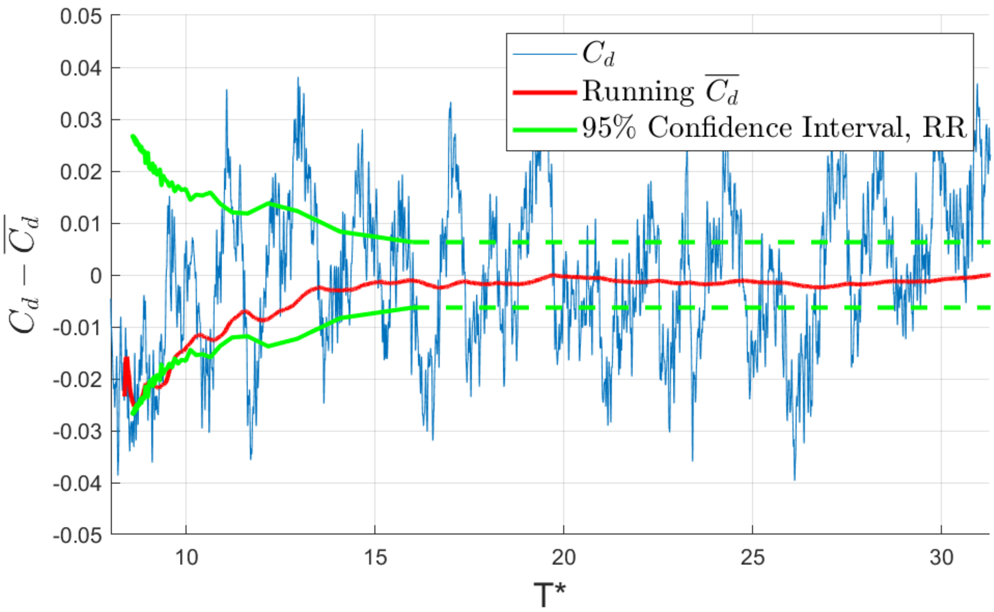

Figure 4.7: C_d and moving average of C_d together with the confidence interval generated with the Repeat Reference (RR) method from 100 to 3 splits for the 1 ms and -2.5 degree yaw simulation.

The confidence interval generated from the RR method in Fig. 4.7 can be interpreted in different ways. One way is to use the last point as the final interval, which is the dashed green line in the figure. This covers the running mean of C_d throughout the rest of the simulation. This is only based on one point estimated from three subsets of the signal and is therefore quite sensitive to the data. Another way of using this method could be to say that the confidence interval is only meaningful at the beginning of the signal up to 1/10 of the final time based on the results from Norman and Howard [27]. Unfortunately, this does not give that much useful information as the confidence of the first 10% of the signal is very wide if it is to be used at the end of the signal. This shows the need for a method that uses the well-known information from these first 10% and predicts the final confidence interval.

4.2.5 Estimated Bandwidth Limited Gaussian White Noise

The last method evaluated for finding the confidence intervals of C_d is the estimated bandwidth-limited Gaussian white noise method. This method will be visualised on the 1 ms and -2.5 degree yaw case, of length 31 T^*. This method uses the RR method discussed earlier to predict the confidence interval at the end of the signal. In this work, the first 1/4 of the time series in the RR method has been used to tune the B parameter and the tuning result is shown in Fig. 4.8. The figure shows the confidence interval $\epsilon[\mu]_{RR}$ for the RR method as the blue line and the fitted confidence interval $\epsilon[\mu]_B$ with B as the orange line. The point used for fitting is marked with a red circle. This point made the confidence interval conservative by finding a B such that the error, $\epsilon[\overline{C_d}]$, from Eq. (3.7) are larger at all times compared to the error from the RR method, Eq. (3.6).

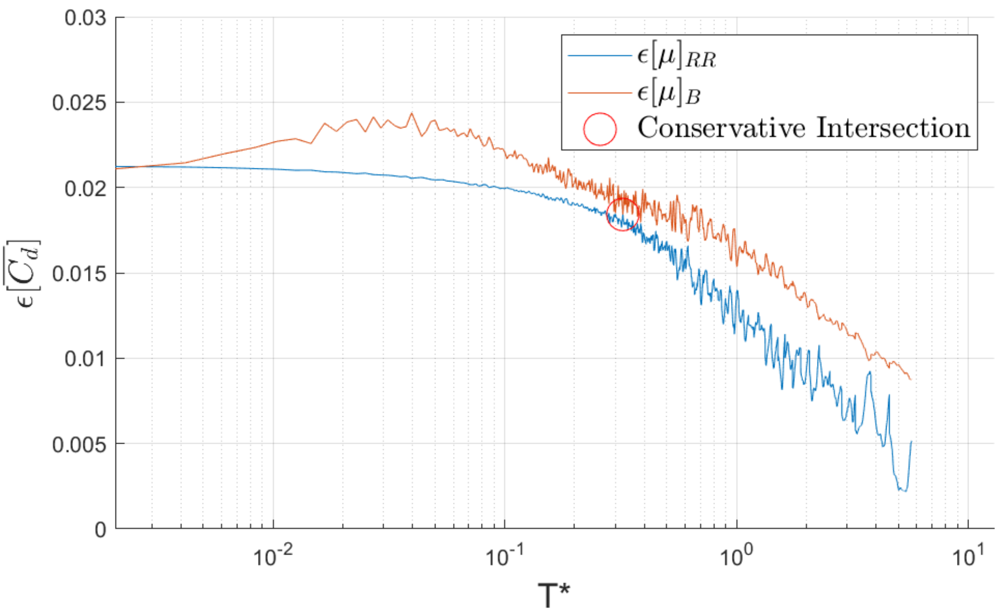

Figure 4.8: Fitting the error estimated from Repeat Reference (RR) method and the Bandwidth (B) limited method for the 1 ms and -2.5 degree yaw simulation.

The final confidence intervals together with the raw C_d signal and the running mean of C_d are shown in Fig. 4.9. The blue line is the instantaneous C_d and the red line is the running mean of C_d . The figure shows how the confidence intervals are approximated for the entire signal. The confidence levels shown are the green lines and correspond to 95% confidence levels.

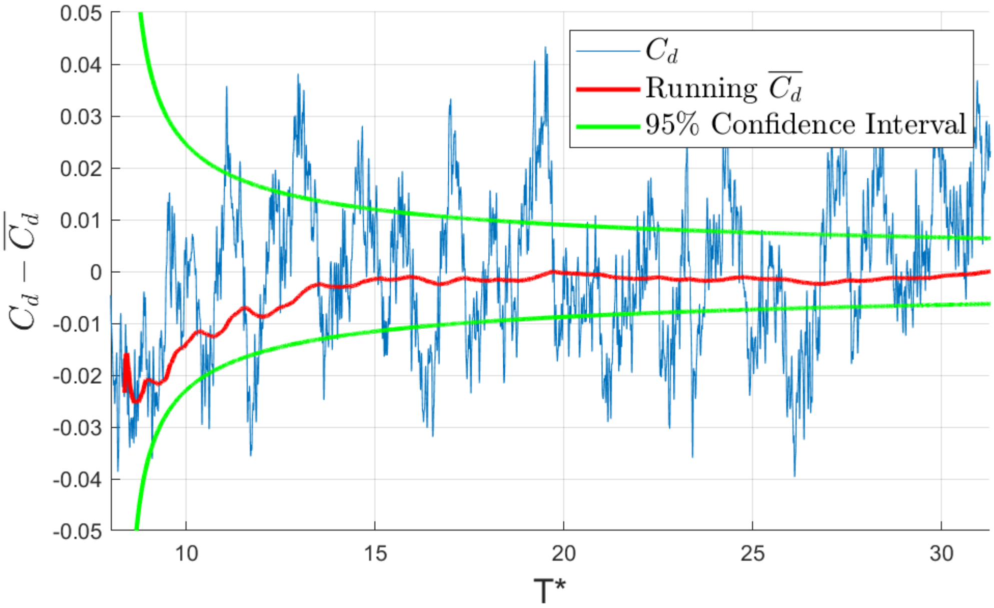

Figure 4.9: C_d and moving average of C_d together with the confidence interval generated with the Bandwidth (B) limited method for the 1 ms and -2.5 degree yaw simulation.

4.2.6 Comparison

To evaluate the performance from the different methods described, all were applied to the 1 ms and 0 degree yaw simulation. This was the simulation that was the slowest to converge in the wind tunnel environment. Because of this, it was considered a challenging case to apply the method onto because then the methods would most probably perform better on the other cases. The time series and the running mean are shown in Fig. 4.10. The data is starting to be averaged after 8 flow passes to remove any initial transient. This reduces the useful signal to a length of about 54 T^*.

As one can see in this figure the time series contains large fluctuations in the data and it is difficult to conclude visually how well the data has converged. Therefore, visual inspection is not a good option for this type of signal. The second method to analyse is the moving average method. The result from this method was given in the section evaluating this method individually, section 4.2.2. To recall the results from this section two confidence intervals were estimated, the first one using an average length of 10 T^* giving limits of ± 13 dc and the average length of 20 T^* giving limits of ± 7 dc. The average length of 20 T^* is about 1/3 of the total length used for averaging and will because of that be considered comparable with the other methods.

The next method to be used is the running average method. The running standard deviation of C_d is shown in Fig. 4.11(a). This figure shows a different behaviour than for an ideal shape as the one visualized in Fig. 4.6(a). For Fig. 4.11(a) the signals grows throughout the entire sampling time. The signal seemed to stagnate

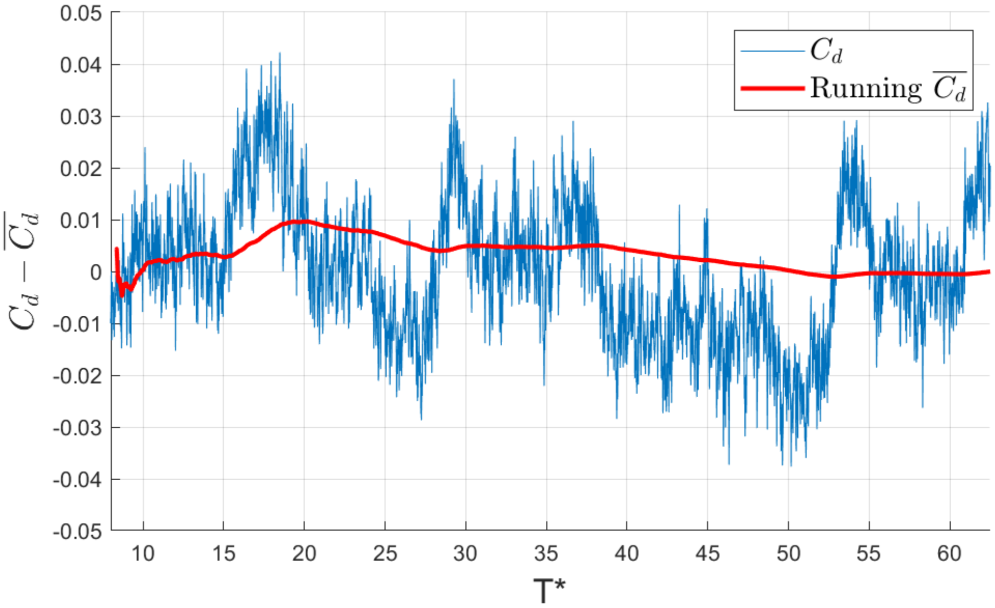

Figure 4.10: C_d and running average of C_d for 1 ms and 0 degree yaw.

after about 30 T^* at a value of about 0.012, but then it grows again after 40 T^* up to 55 T^*. This makes it hard to determine if the signal has converged to a constant and representative standard deviation. Although, the final value is about 0.013, which is in the same range as for the 1 ms and -7.5 degree yaw case mentioned earlier. Furthermore, Fig. 4.11(b) shows the running standard deviation of the running average of C_d . This signal shows an unexpected increase from 45 T^* to 60 T^* which rejects the perception of a converged signal. This value ends at about 0.003 which is almost twice as high as for the 1 ms and -7.5 degree yaw case.

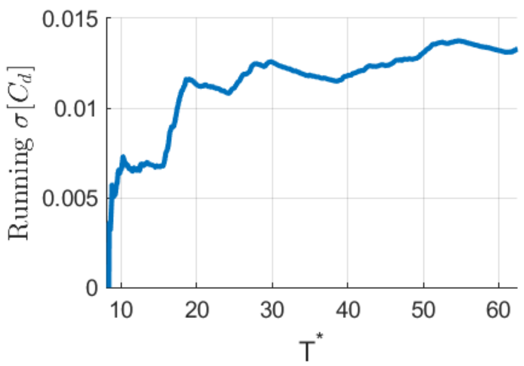

(a) Running standard deviation of C_d

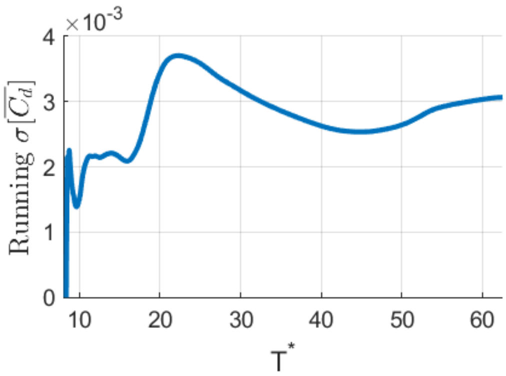

(b) Running standard deviation of running average of C_d

Figure 4.11: Running standard deviation of C_d and Running standard deviation of running average of C_d for for 1 ms and 0 degree yaw.

To further analyse the convergence the Repeat Reference (RR) method is applied to the signal. The results are shown in Fig. 4.12. Looking at the confidence limits generated, they have a smooth shape from 8 T^* until a distinguish peak at $\approx 19\ T^*$. Using the last point at 26 T^* as the final confidence level this gives a confidence of ± 10 dc.

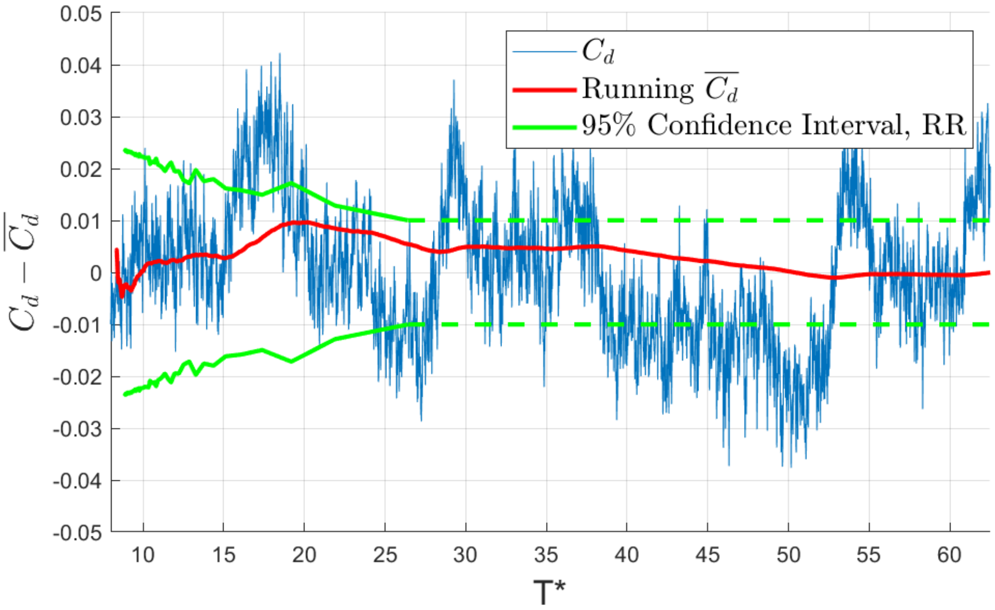

Figure 4.12: Repeat Reference (RR) confidence limits for 1 ms and 0 degree yaw.

The final method analysed is the estimated bandwidth-limited Gaussian white noise method. The result of this method is visualized in Fig. 4.13. The confidence limits shown in this figure have the final value of ± 10 dc. The resulting confidence limits flatten out at the end of the signal. This show how the method predicts a diminishing return for an increased simulation length. This means, since the model is based on a function that assumes a dependence of $1/\sqrt{T^*}$, the increased simulation time will only reduce the confidence interval with that factor. In numbers, this means that increasing the computational time with a factor of 100 will only reduce the confidence limits with a factor of 10.

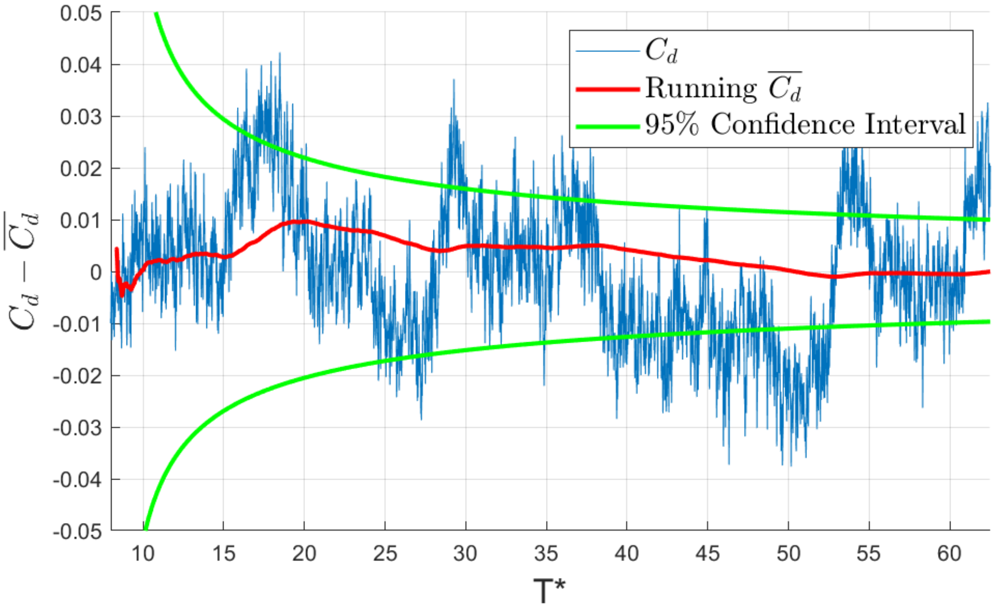

Figure 4.13: Bandwidth-limited confidence limits for 1 ms and 0 degree yaw.

4.2.7 Conclusion

Using the C_d signal from the 1 ms and 0 degree yaw case is a challenging way of testing the different methods discussed in this chapter. The signal contains large and slow fluctuations. This makes some of the methods very unreliable. Firstly the visual inspection is not enough, this gives no limits and does not tell if the signal is converged. The running average method does indicate that the signal might not be converged, but it does not indicate how large uncertainty is still present. The methods resulting in a final limit is the moving average, RR and bandwidth limited method. The moving average method is useful when the signal is well known and the length of the average and sampling is known to be sufficient to capture enough tops and bottoms. This might not be the case for all simulations and therefore this method is also not satisfactory. The RR method does give a good prediction at the beginning of the sample but it does not give one single value at the end that can be used as confidence limits. Using the last point, as done in this chapter, is not satisfactory since this point is unreliable as only three intervals are used for averaging. The final method, the estimated bandwidth-limited Gaussian white noise method, is judged to be the most appropriate method. This method uses the RR method and predicts a final value at the end. This was considered the most stable method in an industrial application. The three last methods did give very similar confidence limits, but the bandwidth-limited method is deemed to be most efficient on simulations with unknown time development. However, this method has some down sides that have to be considered. The method does predict the confidence interval conservatively which does mean that the actual confidence interval probably is smaller. This makes the method require more computational time than actually necessary to reach a certain confidence. The method is also sensitive to the averaging starting point as it affects the confidence limits. If the starting point is known this method could be used as a stopping criterion for simulations. Stopping criterion, as in stopping a simulation when a given satisfactory confidence has been achieved.

Having this result stated, the estimated bandwidth-limited Gaussian white noise method will be used further in this thesis to determine confidence limits of simulations. Even though this method could be used with some precautions as a stopping criterion, this has not been done in this thesis. The method has instead only been used to determine the limits of simulations run for an already set amount of time steps. Precautions, in this case, refers to not simulating for too short time for example, since then false impressions can result from the method. Furthermore, if a confidence limit is mentioned for an unsteady signal in the thesis, this method is the one applied.

4.3 Initial Transient

The method applied to find the initial transient was tested on the simulations of 4 yaw sweeps for different time steps, referred to as 1 ms, 2 ms, 4 ms, and 8 ms in Table 3.2. Those cases gave a variation of results as some of the cases got very small starting times, t_0, while others got very long. The shortest t_0 was estimated to be $t_0 = 0.1\ T^*$ and the longest $t_0 = 14.6\ T^*$. However, the longest is one out of 3 outliers for those 20 simulations. The mean of those 20 was $\overline{t_0} = 3.2\ T^*$ and the median was median$(t_0) = 1.8\ T^*$. All t_0 from those 20 simulations are shown in sorted order from smallest to largest in Fig. 4.14. In this figure the three outliers for large t_0 is visible for simulation point 18, 19 and 20 in the figure. Those three outliers came from 4 ms and -2.5 degree yaw, 1 ms and -10 degree yaw, and 2 ms and -2.5 degree yaw respectively. The remaining simulations keep the t_0 below 5 T^*.

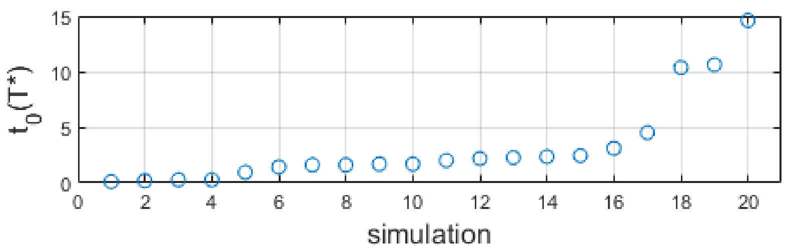

Figure 4.14: Sorted length of the initial transient, $t_0(T^*)$, for 20 simulations.

Fig. 4.15 shows an example of the offset C_d value together with the product of the statistical quantities, $\sigma[\hat{\sigma}_x]$ and $\sigma[\hat{\mu}_x]$. The signal comes from the 4 ms and 0 degree yaw simulation. Here one can see that the method finds the minimum at $t_0 = 1.6\ T^*$. How the minimum is found is seen in the lower graph of Fig. 4.15, where the product of the two variances is shown. For this case, the minimum is clear since the product grows clearly in both directions. Judging the C_d signal in the upper graph visually could be done in different ways, but one could be to start at about 1.1 T^* where the signal reaches -0.02 in this figure. This would then be very similar to what the initial transient method predicts.

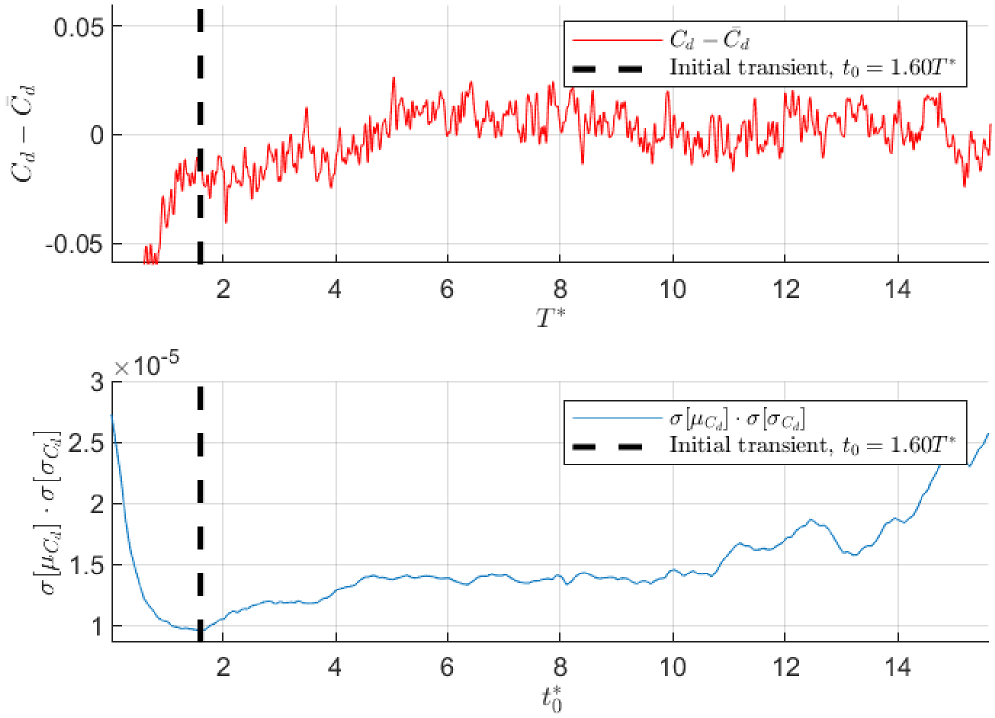

Figure 4.15: Initial transient finding method, instantaneous C_d value in the upper graph and minimized variance in the lower graph.

The method predicts a very small t_0 in a lot of the simulations, as seen in Fig. 4.14. This is most probably because of the bias included in the initial transient for the simulations conducted in this work is fairly small compared to the general fluctuations in the signal. This could be because the simulations are initialised from a RANS solution and therefore does not have a distinct initial transient. This would, for the method used here, give a very small t_0 as the total time for averaging is worth more for the statistical error, than the bias included from the initial transient. The value used for determining t_0 is the C_d signal. This signal includes all the effects on the truck from the flow and thus has a very complex dependence. The initial transient might add and remove forces that contribute to C_d in such a way that the signal seems to have reached a statistically stationary state earlier than the actual time. This would give a false interpretation of the instantaneous data and also the later averaged C_d value. The signal which includes an initial transient should not be used for averaging since this signal would not be taken from a statistically stationary process. The error would not be seen in the average of C_d itself but it would appear in the confidence limits of the average of C_d . The confidence limits would be smaller than for the true signal because the total length of the signal is increased. Therefore, it was decided not to use this method for each simulation, but instead, take the result from all simulations and add a common limit to start the averaging. This limit was chosen to be $t_0 = 8\ T^*$, as this seemed to be a good compromise between computational cost and safety margin.

4.4 Mesh Analysis

The results from the mesh analysis will be divided into two parts, mesh refinement and evaluation of LES resolution. The first part will treat the results from the different refinement regions and the latter will show the result from the LES resolution in the final mesh refinement chosen.

4.4.1 Refinement Regions

For the mesh refinement analysis the simulations "Mesh Initial", "Mesh Trailer", "Mesh Underbody", and "Mesh Front CAB" is used. Those 4 simulations have the same settings except for the mesh refinement regions.

The results from the mesh study are summarized in Table 4.2. The number of cells in the initial setting contained 185 Million (M) cells, this is increased to 214 M for the trailer refinement. The number of cells for the underbody and front refinements is 306 M and 233 M respectively. This means that the trailer refinement added 29 M cells, this was deemed necessary since the ΔC_d value changed from -49 to -58 drag counts with this refinement. The changes in ΔC_d for the two other refinements were +5 and -2 drag count compared to the trailer refinement. These two were not considered necessary since the number of cells increased drastically for the underbody refinement up to 306 M cells and the change in ΔC_d was so small for the front cab refinement.

Table 4.2: Summarising table of different mesh refinements including the total number of cells, in millions (M), in the domain, C_d difference compared to wind tunnel results, ΔC_d (Sim - WT) and also the mean of absolute errors for the probes compared to the wind tunnel, $\overline{|\Delta C_p(Sim - WT)|}$.

Refinement	#cells (M)	ΔC_d (counts)	ΔC_p (counts)
Wind tunnel	N/A	0	0
Initial	185	-49	82
Trailer	214	-58	83
Underbody	306	-53	83
Front cab	233	-60	87

The mean of the absolute difference between the pressure probes and wind tunnel test, $\overline{|\Delta C_p(Sim - WT)|}$, were also compared. This was computed by averaging all the absolute errors between the probes in the simulations compared to the wind tunnel. This comparison showed almost no difference for the trailer and underbody refinement, +1 and 0 pressure counts respectively. The front refinement, on the other hand, changed more, +4 pressure counts. This could be because this refinement captured both the probes that are placed on the front corners of the cab, which include big errors. The front cab refinement also affects the CFL condition to be worse when the spatial grid is refined. The CFL condition is a limiting factor which also motivates the choice of a coarser mesh in the front region of the truck.

The results from this study motivated the usage of the trailer refinement with no additional refinements. The trailer refinement mesh is used in the simulations in the upcoming sections. The trailer refinement did generate a higher error compared to the wind tunnel tests, as seen in Table 4.2. However, this refinement is still considered necessary since it resolves more of the flow structures. The coarser mesh from only the cab refinement does omit flow structures that affects the C_d value and therefore the trailer refinement was necessary. The other two refinements differ less compared to the trailer refinement and does therefore not omit that much of the flow properties. This was chosen early in the project to be able to continue the work. However, using mainly the ΔC_d value as an indicator if a simulation has a sufficient mesh is not optimal. This is since the force coefficient is too complex and includes many factors which might omit differences from a refined mesh. Because of this a more detailed study on the mesh was needed.

4.4.2 LES resolution

To further analyse the mesh quality in the domain the two-point correlation analysis was used. This was used to verify that the mesh in the LES region is fine enough. This analysis was made on the three sets of lines presented in Fig. 3.5. The three systems are wake, side and under-system. The lines used in each system are clarified in Table 3.1. The simulation used for this study is the "Mesh Trailer" from Table 3.2. This simulation has the mesh refinement around the trailer from Fig. 3.4(b).

Wake System

The lines in the wake system show a fine resolution in most parts of the region except for some areas. The resolution is considered fine when the integral length scale is described by 16 or more cells. The region not fulfilling this in the wake system is shown in Fig. 4.16. Each figure has a scale for the number of cells describing the integral-length scale, blue, and one for the integral-length scale, L_{int}, orange. The number of cells describing L_{int} has a logarithmic scale to visualize the limits. Fig. 4.16(a) show $L_{int}(v'_y, x)$ which is the fluctuating part of the velocity in the y-direction along the x-line in the wake. This line starts close to the rear end of the truck. In this figure, most of the positions are described by more than 16 cells except from x=14.2 up until about x=14.5. This is the region close to the truck in the x-direction. Fig. 4.16(b) show $L_{int}(v'_z, y)$. This figure shows how the correlations for v'_z on the y-line reduces faster than within 16 cells and even faster than 8 cells at y=-1.2 and y=1.2. This is for the shortest integral-length scales of about 0.05m. Fig. 4.16(c) shows $L_{int}(v'_y, z)$, this is for v'_y along the z-line. For this line, the shortest length-scales are measured at the top of the line, where they again are described with less than 8 cells. This analysis shows that the resolution is good except in the region close to the wake where the smaller turbulent length scales dominate. All figures have a drop at the end of each line where they approach zero. This is not because the resolution is bad, it is because the correlation for the cells in this region stretches further than the end of the line and makes the ends of each line meaningless.

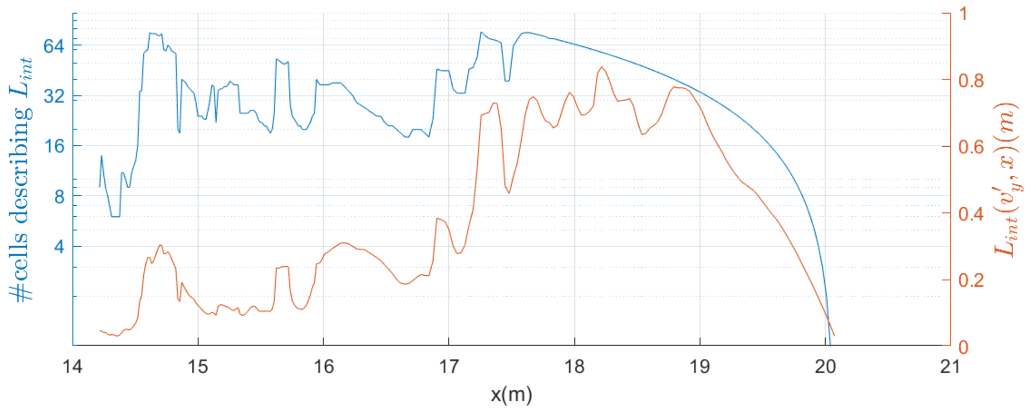

(a) Integral-length scale of the y-component of the velocity on the x-line, $L_{int}(v'_y, x)$

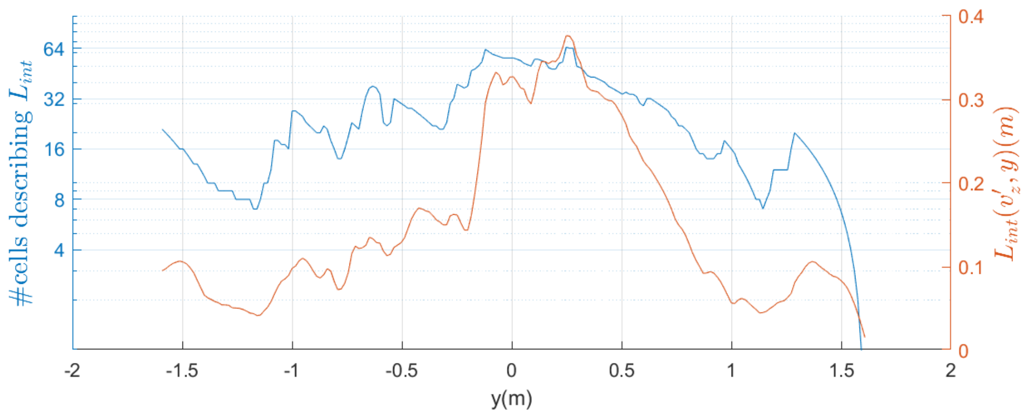

(b) Integral-length scale of the z-component of the velocity on the y-line, $L_{int}(v'_z, y)$

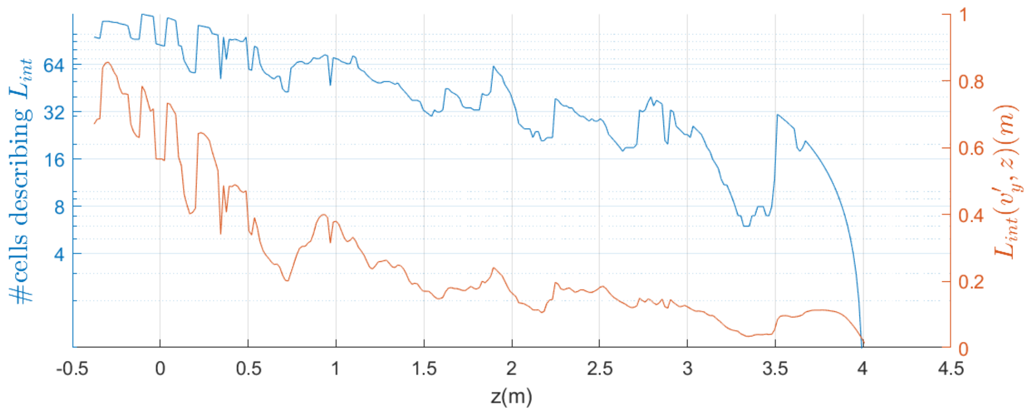

(c) Integral-length scale of the y-component of the velocity on the z-line, $L_{int}(v'_y, z)$

Figure 4.16: L_{int} and cells describing L_{int} for the system of lines in the wake.

Under System

Considering the region under the truck for lines x, y, and z, the smallest integral-length scales were obtained from v'_z, v'_z, and v'_x respectively. This region is less resolved, and the description of the integral-length scales goes down to 8 cells in many positions. Also for a few positions, some of the integral-length scales are resolved with as few as 4 and 5 cells. This is because of the smaller integral-length scales that are present underneath the truck. This does motivate a finer resolution in this underbody region if well-resolved LES is to be achieved. This is, however, very costly since this region already has a very fine resolution.

Side System

The last region evaluated was the system on the side of the truck. For the x-line in this region the lowest resolution is obtained in the beginning of the line for both $L_{int}(v'_y, x)$ and $L_{int}(v'_z, x)$. This is most likely an effect from the turbulent structures created by the rear mirrors, as the line mentioned starts in this region. The turbulent scales are very small behind the mirrors and grow larger along the x-direction. This result in a poor resolution in this region of 5 cells. The y-line for the side system shows the effect of a coarser mesh. The integral-length scales are described with 8 cells in the outer part of the line where the trailer and inner box refinement is not present. This could be resolved by extending the refinement boxes outwards in the positive and negative y-direction. Looking at the z-line the same trend as for the z-line in the wake system is seen, that the integral-length scale reduces in the positive z-direction. The resolution is above 16 cells for z $<$ 2.5 and above 8 cells for z $>$ 2.5. The integral-length scales in the least resolved direction for the under and side system is attached in Appendix A.

Conclusion of the LES Resolution

To conclude the LES resolution from the two-point correlation made for the three different systems, wake, side and under-system. The resolution is deemed sufficient with excepted regions. Most of the regions analysed prove to have a resolution of over 16 cells, meaning that the largest turbulent length scales are resolved over more than 16 cells. Some regions make this resolution drop to 8 cells, which is considered sufficient. This assumption might need to be verified further to motivate that this resolution captures the most important features of the flow. The LES resolution drops down to the 4 cell limit at some regions. This question if the resolution should be refined. The simulation setup is considered resolving fine LES and thus a resolution of 4 cells is arguably not enough. At the same time it should be kept in mind that refining the resolution does increase the computational cost for the simulations, and make them less attractive in an industrial approach. Also, increasing the spatial resolution does require a refined temporal resolution in areas of high velocity, in order to satisfy the CFL condition. Example of this is in the side and beginning of the under-system for the x-lines. The start of those lines where the resolution is poor was also placed in the front end of the truck where high velocities are present. This is also regions that are already resolved very finely. Some regions that should be considered to add a refinement are along the upper region of the trailer where the resolution should be finer, also in the wake close to the trailer.

4.5 Absolute Accuracy

This section will serve as a validation of the simulation method with the data obtained from the wind tunnel tests to obtain the absolute accuracy. This validation was based on the 1 ms simulations from Table 3.2. The 1 ms simulation will also be referred to as the base case. These simulations had a time step of 1 ms and the mesh included the trailer refinement from section 4.4. The under relaxation factors were using the enhanced stability setting and the number of inner iterations were 10 as discussed in section 4.7. A full yaw sweep is considered but only the 0 and -5 degrees yaw cases are analysed in more depth. The confidence intervals for averaged values were generated from the estimated bandwidth-limited Gaussian white noise method discussed in section 4.2, and the averaging were started after 8 T^*. The result from this section will be used as an absolute error estimation for the CFD method.

4.5.1 Force and Pressure Coefficients

To validate the simulations, the results will be compared to the wind tunnel results. The test data available from the wind tunnel test is time-averaged values for C_d , C_s and C_p , The C_p value is available from 71 probes placed on different positions of the truck. The test data contain both uncorrected values and corrected. The correction refers to if the values have been corrected to remove the effects of the wind tunnel. Since the wind tunnel environment is simulated, this work will focus on the uncorrected values.

Drag Coefficient, C_d

The first value that will be compared is the drag coefficient, C_d . This is the most important value that is being compared. The drag coefficient is calculated according to Eq. (2.13). The coefficient depends on the force created on the truck which is due to pressure differences and shear stresses. For the trucks, most of the force is generated from pressure differences so the pressure is the most important factor. The coefficient also depends on the area that is set for a specific vehicle and the density of the air. The coefficient also depends on the free stream parameter V_∞, which is also subject to error in a wind tunnel environment as discussed earlier.

It should be kept in mind that the primary objective of the methodology is to predict drag, since this is the quantity of interest for emission reduction purposes. The drag values will not be presented in absolute values because of confidentiality reasons so instead, the errors in drag counts will be presented. Table 4.3 shows the error between the base case and the wind tunnel results for each yaw angle and the yaw weighted average. The table also includes the confidence limit from the averaging in the simulations. The error is outside of the confidence limits for all yaw angles, so it is clear that they underpredicts significantly compared to the wind tunnel tests. The largest error is predicted for the 0 degree yaw case, which is also the case that has the largest confidence interval. The -2.5 degree yaw angle prediction is a bit better and the confidence range is reduced further. The angles -5.0 and -7.5

predicts a more similar error and have more similar confidence intervals and predict the lowest errors. -10 degree yaw again increase slightly both in error and confidence. The CFD method performs better for the higher angles when comparing the errors. This phenomenon could be explained partly by the long distance underneath the truck that is building up an error that contributes more to the low angles. It could also depend on the large, low frequency, fluctuations that are generated in the base wake for the small angles. For this study the yaw weighted average ends up at -45 dc error with a confidence interval of 7 dc.

Table 4.3: ΔC_d (Sim - WT) between 1 ms time steps and wind tunnel results.

Yaw	YWA	0.0	-2.5	-5.0	-7.5	-10.0
ΔC_d	-45 dc	-58 dc	-48 dc	-25 dc	-22 dc	-38 dc
Confidence interval	±7 dc	±10 dc	±6 dc	±4 dc	±4 dc	±6 dc

To visualize the results from Table 4.3 the ΔC_d (Sim - WT) difference is shown in Fig. 4.17. In this figure the trend of the error for the different yaw angles can be seen. The error is the largest for the 0.0 degree yaw and then decreases to a turning point somewhere between -5 and -7.5 degree and then again grows in magnitude. Note how the error is negative.

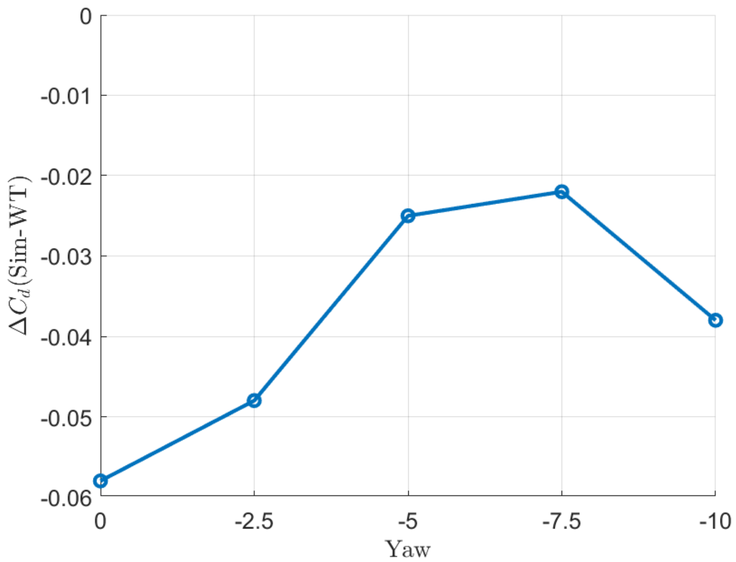

Figure 4.17: ΔC_d (Sim - WT) between 1 ms time steps and wind tunnel results.

The C_d values are based on simulations run for 62 flow passages for the 0 degree yaw and 31 flow passages for the rest of the angles. The 0 degree yaw angle was the case that took most computational power to reduce the confidence limits. This was due to large fluctuations in the drag signal from low-frequency content in the signal. Fig. 4.18 shows the running averages for all yaw angles from the starting point at 8 T^*. As seen in the figure the 0 degree yaw needs significantly longer time as the mean moves about 5 dc from 40 to 50 T^*. The other mean values converge more smoothly and do not require as long averaging intervals.

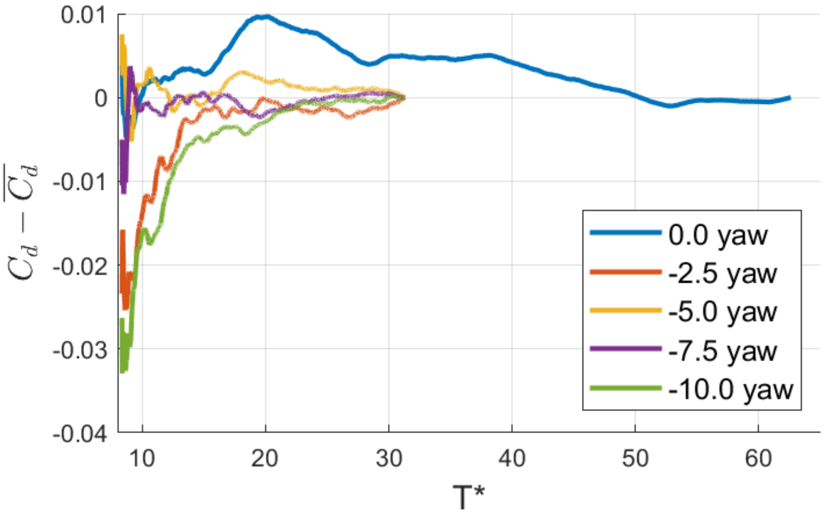

Figure 4.18: Running averages of C_d for all yaw angles, from 8 T^* to 62 T^* for 0 degree yaw and from 8 T^* to 31 T^* for the other yaw angles.

Side Force Coefficient, C_s

The drag is the most important parameter to analyze but the side force coefficient can also be of interest to see how well the CFD method works when a yaw angle is introduced. The side force coefficient is calculated according to Eq. (2.14). The side coefficient is not of much interest for low yaw values as it is very small and have little impact. But for higher yaw angles this value gets more interesting to see how it is predicted compared to the C_d value. The C_s difference is presented in Table 4.4. The simulations show the very good prediction of the C_s value for 0 and -2.5 degree yaw. The yaw weighted average value is also very small. For the higher yaw angles, the error increases drastically but so does also the absolute value. Looking at the relative error this stabilizes for the higher yaw angles but these numbers are not shown due to confidentiality.

Table 4.4: ΔC_s (Sim - WT) between 1 ms time steps and wind tunnel results.

Yaw	YWA	0.0	-2.5	-5.0	-7.5	-10.0
ΔC_s	-11 dc	-6 dc	7 dc	-27 dc	-55 dc	-88 dc
Confidence interval	±10 dc	±5 dc	±12 dc	±10 dc	±10 dc	±12 dc

To visualize the results from Table 4.4 the ΔC_s (Sim - WT) difference is shown in Fig. 4.19. In this figure the error is the smallest for the 0.0 and -2.5 degree yaw and then increases linearly for the larger yaw angles. The interpretation of this trend is not as clear as for ΔC_d since the growth of C_s is very large. The confidence interval from Table 4.4 on the other hand are quite stable for all angles other than 0 degree were it is smaller.

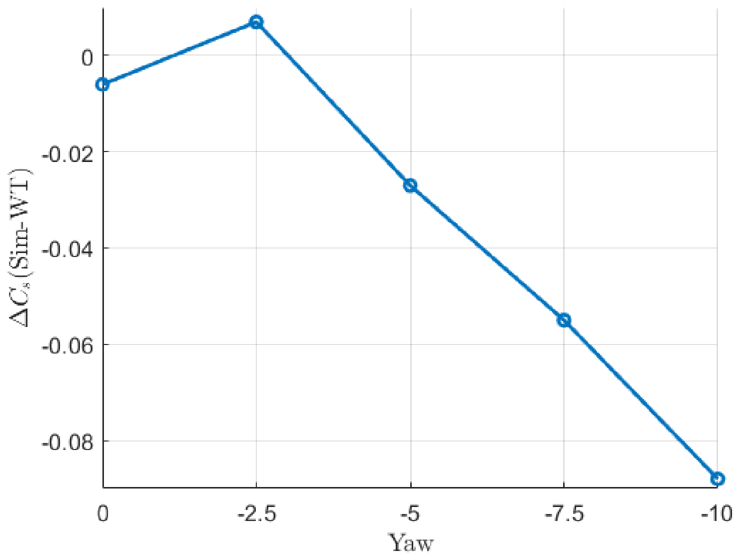

Figure 4.19: ΔC_s (Sim - WT) between 1 ms time steps and wind tunnel results.

Pressure coefficient, C_p

The pressure coefficient is calculated according to Eq. (2.15) for each probe. The probe comparison will be divided into 5 different regions to give a better view of the results. The regions are front, rear, front trailer, left, and right. The number of probes in each region is 3, 25, 5, 19, and 19 respectively. The errors for the probes will be divided into two parts, convergence and position. The convergence error is calculated as for the force coefficients according to the bandwidth-limited confidence limits. The position error is calculated by using the cylindrical discs, presented in section 3.1, around each probe to determine the standard deviation of the pressure coefficient according to the position in the cylinders.

Front Probes The first probe in the front is the one used for scaling the stagnation pressure and hence the error will be set to zero as explained in section 4.1. The third point in the front region is placed under the engine and not in the front of the truck. The second probe is placed on the front of the truck on the registration plate. The other regions probes are placed on the surface as they appear in the figures in the following sections.

Fig. 4.20 shows the probes on the geometry in Fig. 4.20(a) and the error between the simulation and the wind tunnel test according to Eq. (3.2) is shown in Fig. 4.20(b). Fig. 4.20(b) show the error between the simulation and the wind tunnel test with the error of the measurement depending on the convergence of the simulation, red, and position of the probe, yellow, and the total, blue. For the remaining analysis only the total error will be visualized.

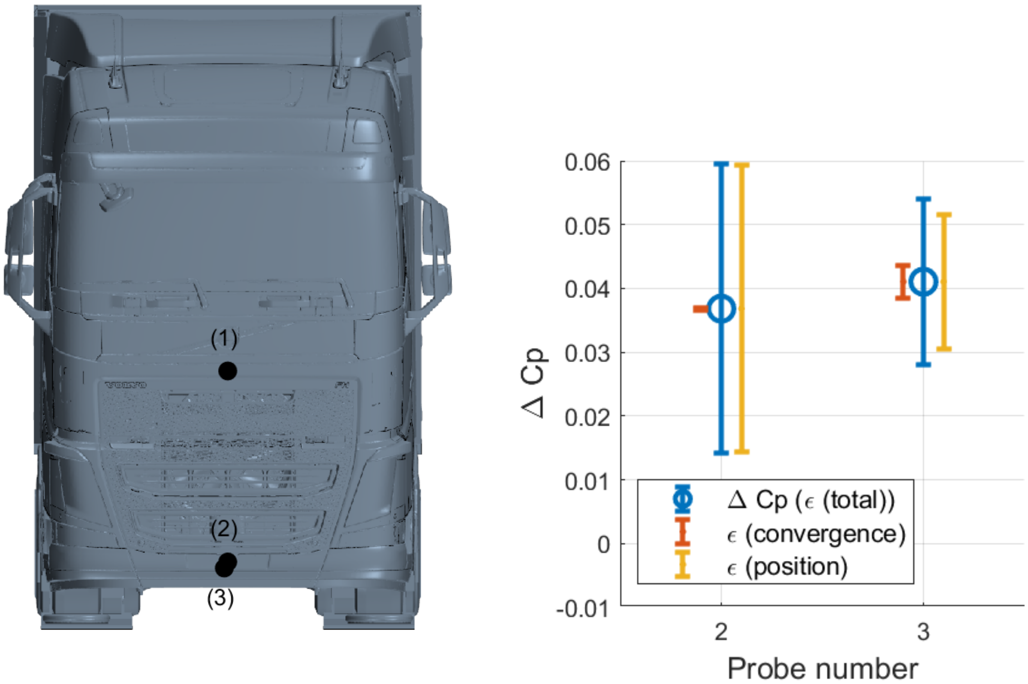

(a) Geometry (b) Error

Figure 4.20: Geometry and ΔC_p (Sim - WT) for probes on the front of the truck for 0 degree yaw.

From Fig. 4.20(b) the different error contribution from position and convergence can be seen. The majority of the error for front probe 2 and 3 is due to the position of the probes. This is not the case for higher angles were only probe 2, the registration plate probe is dominated by position. The engine bay probe for the -10 degree yaw has an error of the same size for both position and convergence. The fact that the error for probe 2 is significantly different from the tunnel experiment raises the question if there is still an issue with the scaling of C_p since both probe 1 and 2 should have similar flow conditions. Having an error of 40 pressure counts in C_p already in the front is noticeable. This discrepancy might depend on the boundary flow that builds upon the floor, alternatively on an unknown rotational structure of the flow in the wind tunnel. This rotational component is discussed by Josefsson [4].

Rear Probes The rear surface was prepared with 25 probes, those were positioned in 5 rows. Fig. 4.21 show the probes with corresponding ΔC_p for 0 and -5 degree yaw. For the 0 degrees case there is a step in pressure difference from probe line 16-20 compared to 21-25. This shows some interesting behaviour that the simulations does not capture. This overpredicted pressure might also explain how the simulation underpredicts the drag for the 0 degree yaw case. Looking at the 5 degree yaw case instead another pattern in the error is present in Fig. 4.21. The error is lower for the centre probes and higher for the probes on the edges, especially on the right side. The increased error on the upper right side of the rear shows that there might be an error in the flow separated from the side facing the flow in the simulations.

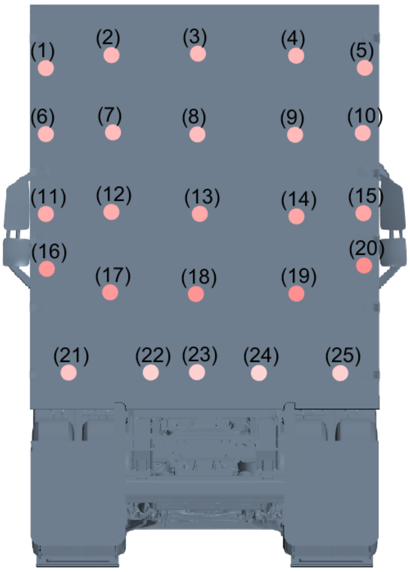

(a) 0 degree yaw

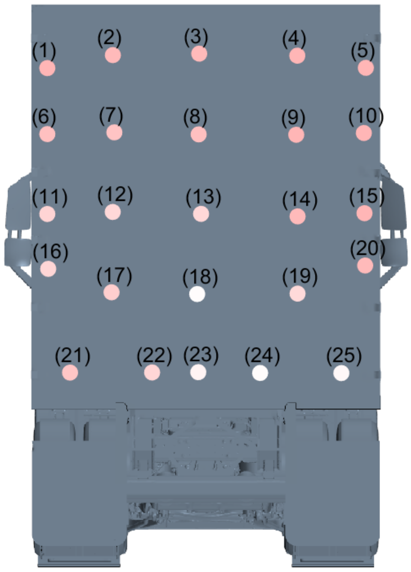

(b) -5 degree yaw

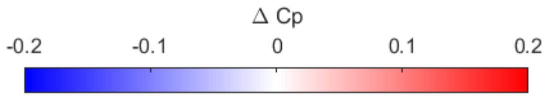

Figure 4.21: ΔC_p (Sim - WT) for probes on the rear of the truck for 0 and -5 degree yaw.

Fig. 4.22 and Fig. 4.23 shows ΔC_p with error bars for the rear probes for the two yaw angles, 0 and -5 degree. In Fig. 4.22 the error for C_p is shown as confidence intervals. This error is dominated by the convergence error and not the position. This is because there are no large pressure gradients on the rear surface and thus the uncertainty of the position is small. Looking at Fig. 4.22 for the 0 degree yaw case the trend and abrupt step in error between probe 16-20 and 21-25 is visible. The pressure is gradually overestimated more and more the lower on the rear it goes until the last row of probes where it is significantly reduced. Viewing Fig. 4.23 for -5 degree yaw a less obvious trend is present. In the upper region the error is quite similar for probe 1-10, for the next line the error reduces for the first three probes, 11-13. The next line 16-20 show a large uncertainty for the center probe, 18. This tells that there is large fluctuations in the pressure for the center of the rear surface for -5 degree yaw. Looking at the lowest line of probes, 21-25, the error gradually reduce from left to right. This is the opposite of the probes 11-15.

Trailer Front Probes The probes on the front of the trailer are placed as in Fig. 4.24. Those are placed on the trailer surface in between the trailer and the cab. There is a region with high pressure-gradients right by probe 1 and 2. These high gradient regions make the position uncertainty very large for those probes, especially for higher yaw angles.

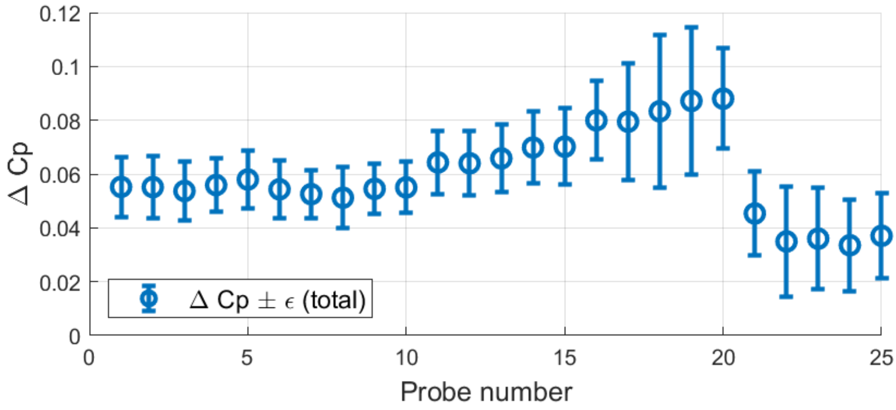

Figure 4.22: Rear probes ΔC_p (Sim - WT) error with uncertainty from convergence and position for 0 degree yaw.

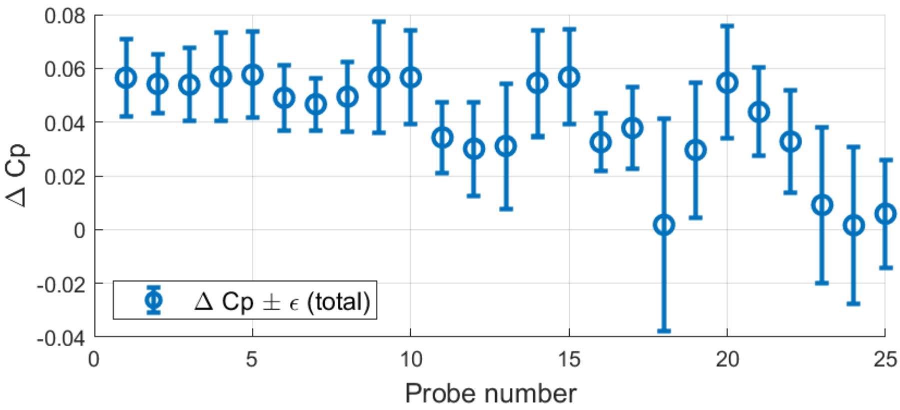

Figure 4.23: Rear probes ΔC_p (Sim - WT) error with uncertainty from convergence and position for -5 degree yaw.

The ΔC_p (Sim - WT) for the trailer probes for 0 and -5 degree yaw are shown in Fig. 4.25(a) and (b) respectively. The error for those probes are dominated by position for probe 1 and 2, probe 3-5 are dominated by convergence error. For -5 degree yaw the error for probe 2 was drastically increased because of the uncertainty around the high pressure gradient region. It became $\Delta C_{p\text{ probe, 2}} = -0.180 \pm 0.049$ while the other errors stayed in the range from 0-0.1 as for 0 degree. This made it visually convenient to exclude it from the graph and instead state it as a value.

Looking at the errors in Fig. 4.25(a) they are similar to each other except the uncertainty for probe 1 and 2. Comparing this with the error from -5 degree yaw in Fig. 4.25(b) those spread more. The error in probe 3, which is placed in the centre of the surface, increased from about 0.04 up to 0.10. This might depend on the modelling of the flow through this region and how much air is allowed to flow in between the trailer and cab. The pressure is more overpredicted in probe 3 for -5 degree yaw which indicates that the airflow through the region could be too slow according to Bernoulli's equation, Eq. (2.16). Since there is also a higher air flow through the region this increases the potential for errors. The large underprediction

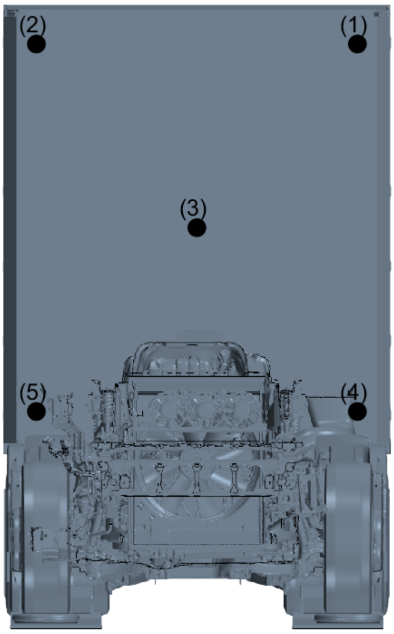

Figure 4.24: Probes on the front of the trailer.

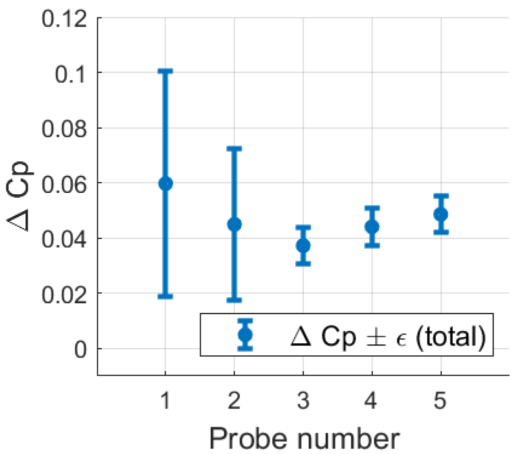

(a) 0 degree yaw

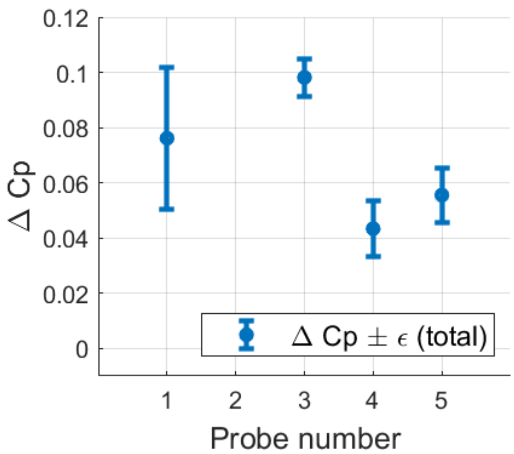

(b) -5 degree yaw

Figure 4.25: Trailer front probes ΔC_p (Sim - WT) error with uncertainty from convergence and position for 0 and -5 degree yaw. Probe 2 excluded for -5 degree yaw, $\Delta C_{p \text{ probe, } 2} = -0.180 \pm 0.049$.

for probe 2 could be because of the pressure gradients are so high so a minor change in position changes the pressure drastically. The high-pressure region created on the upper part of the trailer could be due to separations between the cab and the air deflector on the roof that generate a vortex hitting the trailer. Looking at probe 4 and 5 for both the yaw cases those appear more constant, slightly higher for -5 degree yaw. This region has low pressure-gradients and low flow velocity which raises the question if there could be a constant offset error in C_p .

Left Probes Fig. 4.26 shows how the ΔC_p value differs for the probes on the left side of the truck for 0 degree yaw. The largest errors are made for the two probes in the front of the cab, probe 1 and 2. Probe 1 overpredicts the pressure and probe 2 underpredicts it. This could depend on the large pressure gradients in this region and uncertainty in the prediction of the separation point.. Looking at the other probes on the cab a more consistent error appears especially on the lower part between the truck wheels where the error seems very consistent from the colour scale. Looking at the trailer instead a more varying error appears as it is very low for the first probe on the trailer and then gradually increase until the second last and then decrease for the last one. Looking at that behaviour the pressure seems to increase too much along with the truck which could depend on effects from the blockage.

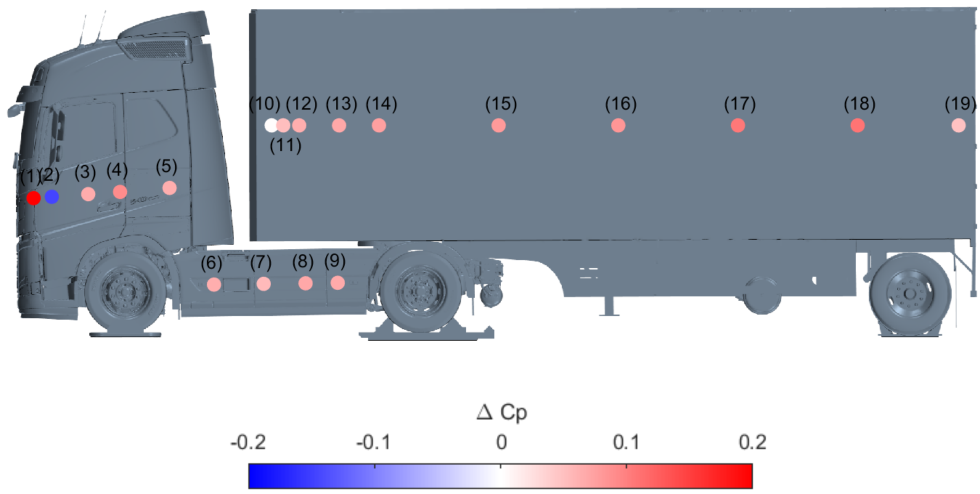

Figure 4.26: ΔC_p (Sim - WT) for probes on the left side of the truck for 0 degree yaw.

Fig. 4.27 visualize the error with uncertainty for the left side probes for 0 degree yaw. The error in the first probe are much larger than for the others, at $\Delta C_{p\ \text{probe, 1}} = 0.865 \pm 0.233$. This is very large compared to probe 3-19 which range from about 0-0.1. Therefore this probe is excluded from the graph and instead given as a value, to make the remaining probes easier to analyze. The errors for the probes on the chassis, 6-9 show a quite constant behavior whereas the error on the trailer increases from the first probe, 10, up until the second last, 18. The uncertainty for probe 11-18 is very small and tells that there is an error that builds up along the trailer that significantly increases.

Fig. 4.28 show the probes from the left side of the truck for -5 degree yaw. In this figure, a different pressure distribution is seen compared to 0 degree yaw and ΔC_p is generally lower on the cab and chassis, probe 3-9. ΔC_p on the trailer behaves similarly except for probe 10 which overpredicts the pressure more for -5 degree yaw compared to 0 degree yaw. This could depend on how the flow behaves when it leaves the gap between the cab and trailer. Looking at the error for probe 3, it

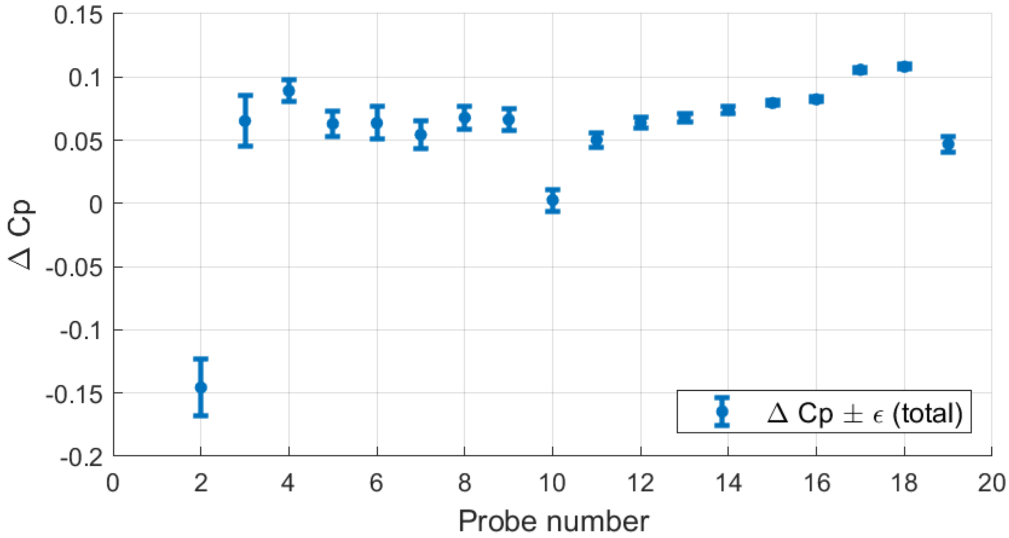

Figure 4.27: Left side of the truck probes ΔC_p (Sim - WT) error with uncertainty from convergence and position for 0 degree yaw. Probe 1 excluded, $\Delta C_{p\text{ probe, 1}} = 0.865 \pm 0.233$

reduced drastically and is now underpredicting the error. The confidence intervals increased in general for most points for -5 degree yaw. This show how the uncertainty increases for the pressure behind the object in the separated region.

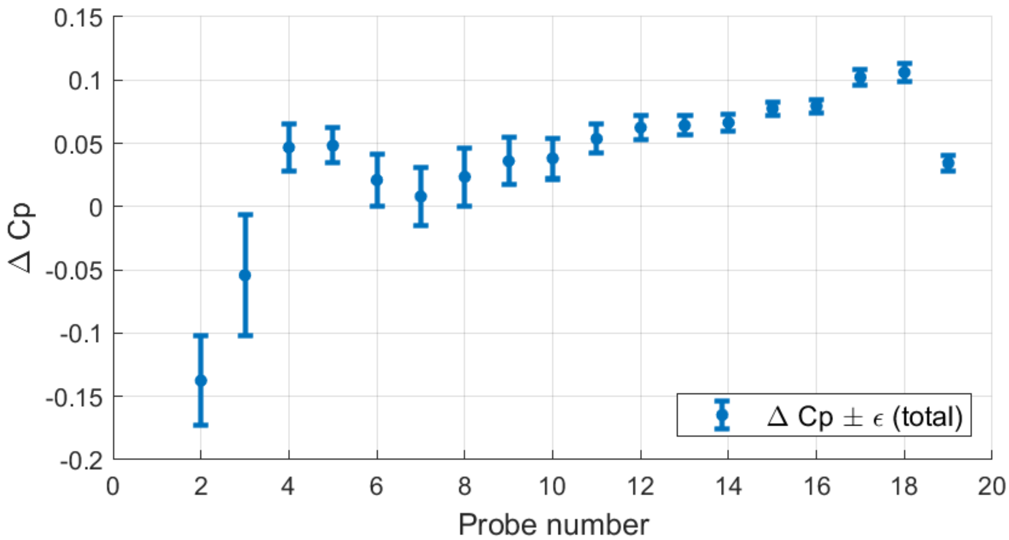

Figure 4.28: Left side of the truck probes ΔC_p (Sim - WT) error with uncertainty from convergence and position for -5 degree yaw. Probe 1 excluded, $\Delta C_{p\text{ probe, 1}} = 0.709 \pm 0.156$

Right Probes The probes on the right side will only be analysed for the -5 degree yaw case and not 0 degree yaw case due to the symmetry between the left and right-hand side. The error for each probe with corresponding uncertainty is shown in Fig. 4.29. The error in probe 1 is not as high as for the left side but still much larger than for the other probes. The error is $\Delta C_{p\ \text{probe, 1}} = 0.404 \pm 0.236$ and it is again excluded from the figure for convenience. In Fig. 4.29 it is visible how the pressure is overpredicted on the entire right surface. An interesting phenomenon present is how the uncertainty is lower for almost all probes compared to the left side at -5 degree yaw. This is most likely caused by the fact that the pressure on the headwind side fluctuates less. The exception is probe 1 and 2 which has a higher uncertainty for the right side at -5 degree yaw. The error is larger for the probes on the cab and chassis, 2-9, for the right side compared to the left. This difference will generate a shift in C_s as the pressure difference is not equally overestimated.

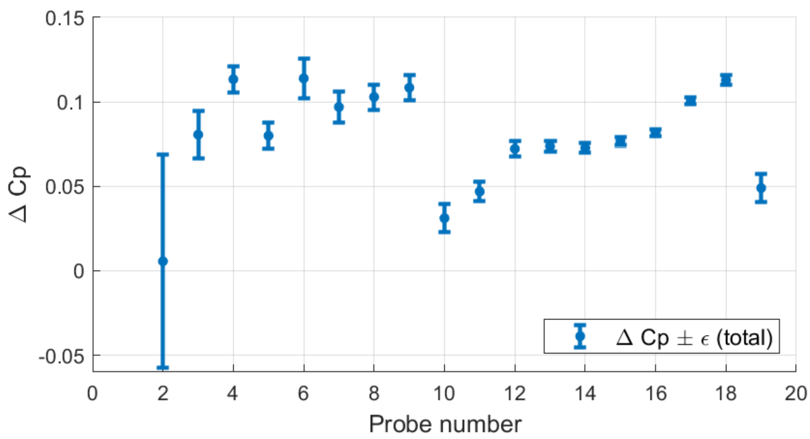

Figure 4.29: Right side of the truck probes ΔC_p (Sim - WT) error with uncertainty from convergence and position for -5 degree yaw. Probe 1 excluded, $\Delta C_{p\ \text{probe, 1}} = 0.404 \pm 0.236$

4.5.2 Pressure Difference Converted to Drag Force

The information from the probes on the rear of the trailer can be used to estimate a difference in C_d for the truck. Doing this indicates if the pressure difference agrees with the error observed in C_d . The pressure difference was interpolated over the entire rear by using a cubic method. Here four corner points were placed far away from the evaluated area to stretch the error out to the edges. The interpolation of ΔC_p is shown in Fig. 4.30. In this figure, a trend of overpredicting the pressure and hence underpredicting the C_d is present. The 0 degree yaw case shows a high overprediction area in the lower centre of the rear but this area gradually decreases as the yaw angle is increased and the overpredicted area goes out to the edges. This shows that the wake structure is not resolved properly and that it varies with yaw angle.

Integrating the ΔC_p values from Fig. 4.30 makes it possible to estimate the contribution to ΔC_d from the rear end of the truck. These values are presented in Table 4.5. In this table it is shown how ΔC_p agrees with the values for ΔC_d . It can be

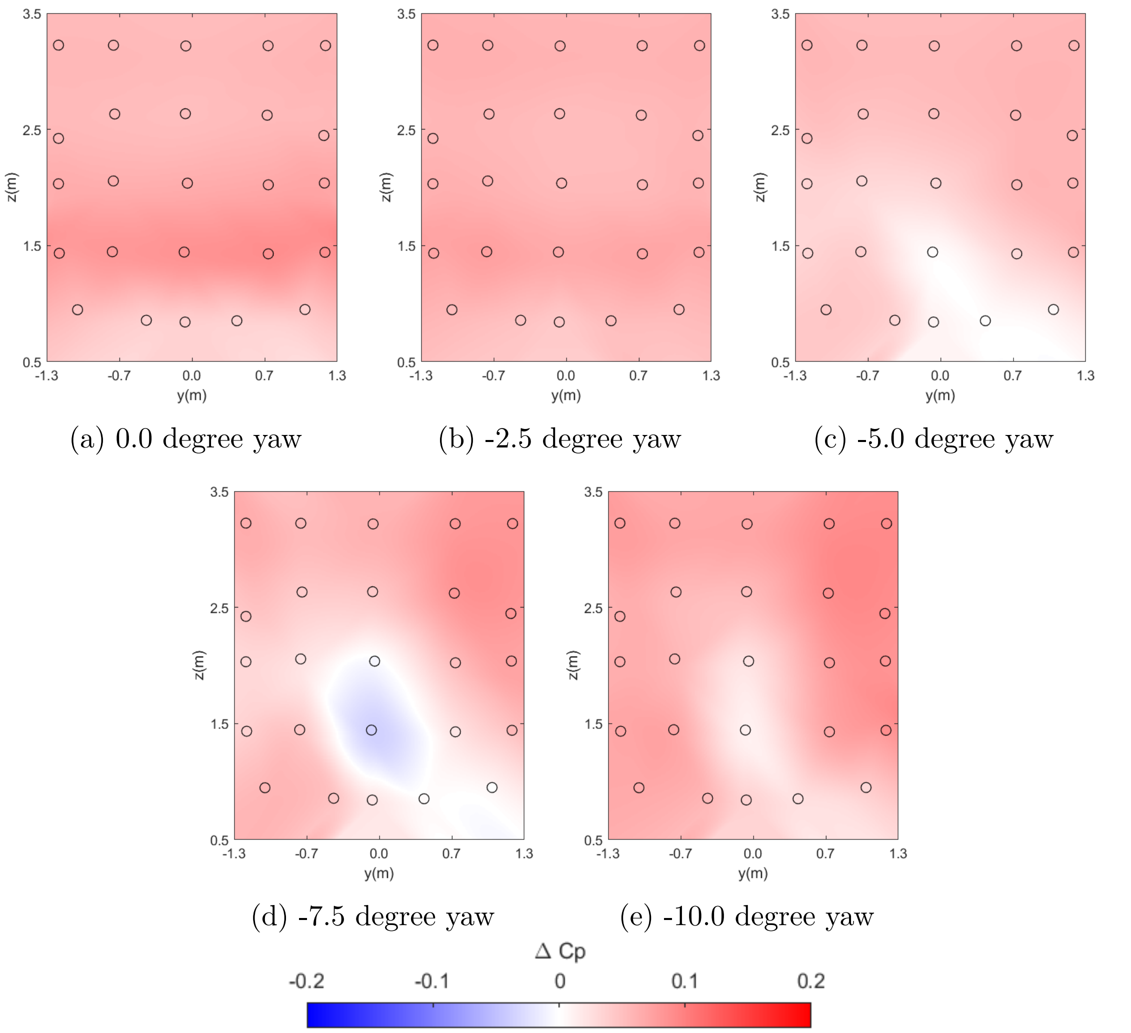

(a) 0.0 degree yaw (b) -2.5 degree yaw (c) -5.0 degree yaw

(d) -7.5 degree yaw (e) -10.0 degree yaw

Figure 4.30: ΔC_p (Sim - WT) errors interpolated from probes over rear surface

seen that the majority of the error in C_d is caused by the error in the prediction of the pressure on the rear of the truck. For the yaw weighed average the difference in C_d is reduced to -4 dc when ΔC_p is added. Furthermore, the C_d difference underestimates for the low yaw angles and overestimates for the high yaw angles. The 0 yaw case is the case that still predicts the largest error so in this case there are other factors that also contribute significantly to the error.

Table 4.5: ΔC_p (Sim - WT) contribution from the rear end of the truck to C_d

Yaw	YWA	0.0	-2.5	-5.0	-7.5	-10.0
ΔCp converted to ΔC_d	41 dc	44 dc	43 dc	29 dc	29 dc	44 dc
ΔC_d after correction	-4 dc	-14 dc	-5 dc	4 dc	7 dc	6 dc

4.5.3 Frequency Content

The frequency content to be presented is from the C_d signal. This was calculated by applying the Hann window to the time series and then using Fast Fourier Transform (FFT). The resulting Power Spectral Density (PSD) was then analysed to see if any of the frequencies showed particular importance to the fluctuations in the drag signal. It was clear that the lowest frequencies contribute the most to the fluctuations. Fig. 4.31 show the frequency content from the 1 ms and 0 degree yaw simulation. The frequency content in this signal is limited from 0.04 up to 500 Hz, due to the sampling length and time step. Fig. 4.31 shows the content from 0-1 Hz because after this the PSD decayed rapidly in comparison. This tells that most of the fluctuation magnitude in the C_d signal comes from low frequencies. There are four peaks in this region located at 0.04, 0.12, 0.35, and 0.54 Hz. The peaks are not solely at one point but spread over smaller intervals of about 0.1 Hz. The peak at 0.04 Hz is a bit unreliable since this is the lowest frequency resolved. The most important content from this figure is that the frequency content from the 0 degree yaw is dominated by signals with a lower frequency than 0.6 Hz. Transferring the peaks at 0.12, 0.35, and 0.54 Hz into the time domain those yields period times of 8.3, 2.9, and 1.9 seconds. Having periods of 8 seconds makes it very hard to statistically converge the solutions since very long time intervals are needed to capture multiple of those periods.

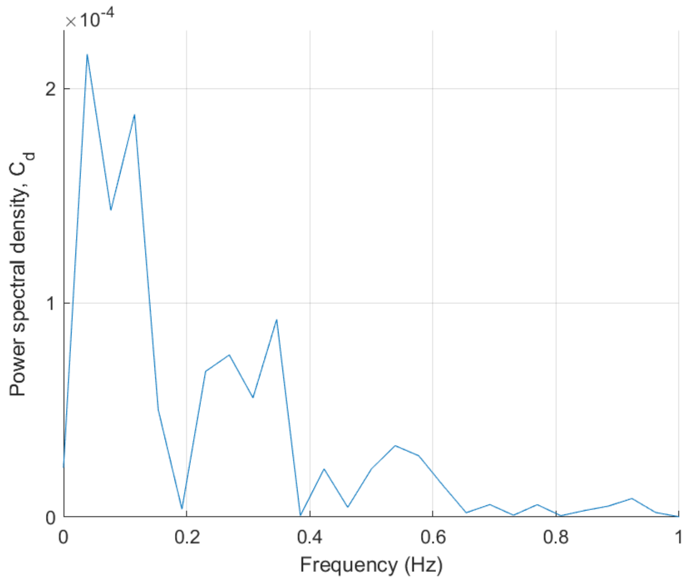

Figure 4.31: Frequency content from 1 ms simulation for 0 degree yaw. This signal has a lower limit of 0.04 Hz from the sampling length and an upper limit of 500 Hz from the time step.

Looking at Fig. 4.32 the frequency range from 0-10 Hz is shown for the 1 ms and -5 degree yaw simulation. In this figure it is shown that the signal is not totally dependent on the lowest frequencies below 0.6 Hz as for the 0 degree yaw case. For -5.0 degrees there is four peaks in the PSD, 0.18, 1.46, 3.64, and 6.19. Those correspond to the period times of 5.6, 0.7, 0.3, and 0.2 seconds. This shows that for -5 degree yaw the C_d signal includes more faster fluctuations. This might be because the base wake that generates most of the drag is not oscillating in the same way as for 0 degree yaw.

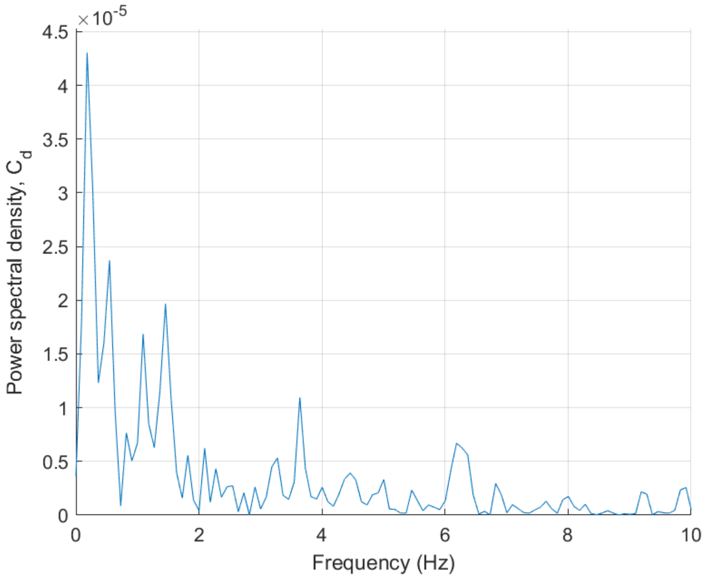

Figure 4.32: Frequency content from 1 ms simulation for -5 degree yaw. This signal has a lower limit of 0.08 Hz from the sampling length and an upper limit of 500 Hz from the time step.

To further analyze the frequency content the pressure signal from the 4 probes in the corners of the rear end was investigated, as shown in Fig. 4.33. These probes show a very clear pattern in the frequency domain where they all oscillate with a low-frequency signal of about 0.3 Hz and one a bit higher at 2 Hz.

Since the pressure in all those probes had the same frequency content, a comparison between the four was made to see how they oscillate according to each other. This comparison was done by adding a band-pass filter to the signals to show only certain frequency components. The result is shown in Fig. 4.34. The higher graph shows the pressure signal with a band filter applied for the low-frequency content, between 0.3 and 0.4 Hz, to capture the peak of about 0.3 Hz. In this graph, two interesting phenomena are seen. Firstly probe 1 and 5 are always in phase and probe 21 and 25 is almost always in phase. This means that the upper part of the rear end oscillates in the same phase and that the lower part of the rear oscillates in the same phase. The second interesting appearance is how the upper and lower part oscillates in phase in some part of the signal and out of phase in some other part. From t = 8 s to t = 11 s the entire rear end oscillate in phase as for t = 2 s to t = 5 s the upper and lower end is out of phase. This indicates that there is frequency content in the total drag signal that has a lower frequency than 0.3-0.4 Hz as the rear end include a phase shift in the upper and lower end.

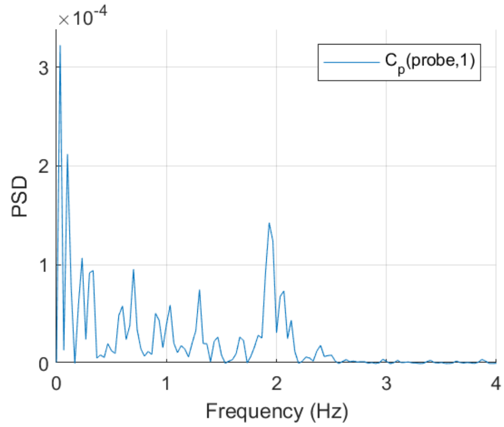

(a) Probe 1

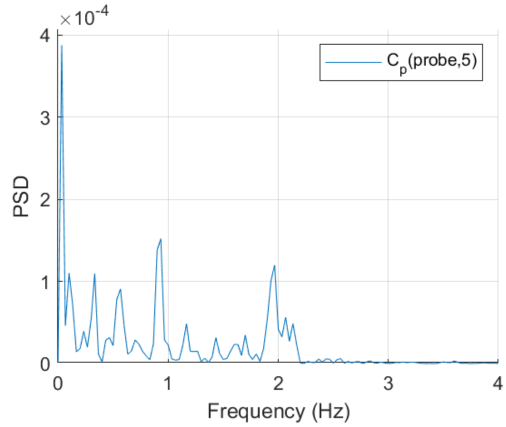

(b) Probe 5

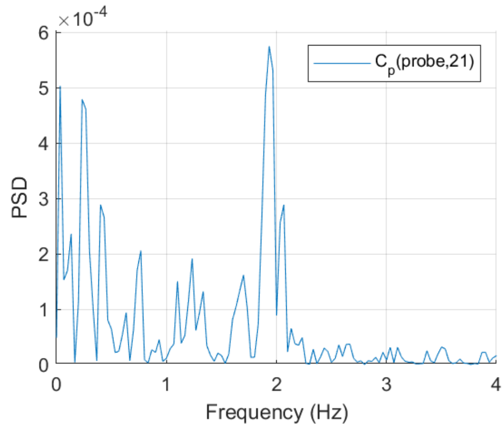

(c) Probe 21

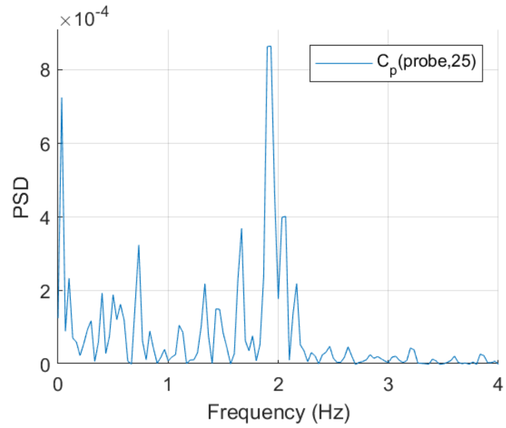

(d) Probe 25

Figure 4.33: Power Spectral Density (PSD) for the rear trailer corner probes for 1 ms and 0 degree yaw.

The lower graph of Fig. 4.34 show the same signal for the 4 probes but with a 1.75-2.25 Hz band filter instead, to capture the peak at about 2 Hz. This filter captures the peak at about 2 Hz in the signal for the probes. It shows how the upper and lower probes now always are in phase and how the left and right side instead oscillate out of phase. This shows that there is a faster vortex shedding appearing from left to right in the wake of a frequency of 2 Hz. It is also visible that this frequency content appears to oscillate in magnitude at a pattern. This could possibly be related to the behaviour seen in the upper graph of Fig. 4.34 were sometimes the upper and lower probes are in phase and sometimes not.

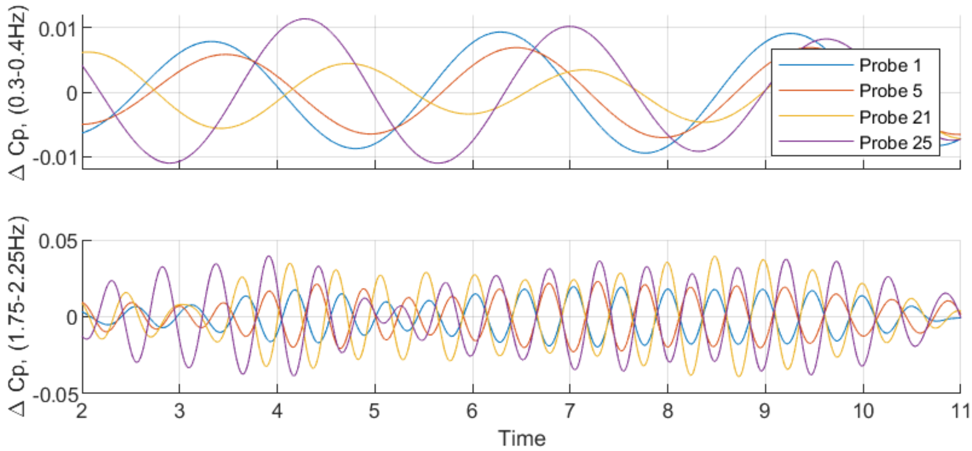

Figure 4.34: Band filtered pressure signal for the 4 rear end corner probes on the truck. Upper graph is the signal filtering between 0.3-0.4 Hz and the lower graph filter between 1.75-2.25 Hz.

4.5.4 CFL Number

According to theory, the CFL number should ideally be less than unity in the entire domain. This is not the case for the 1 ms simulations done. The CFL number in two planes, y=0 and z=2, are shown in Fig. 4.35 and Fig. 4.36. The scale goes from 0-4 where all the values above 4 are included in the colour representing 3-4. The CFL number exceeds one in quite a big part of the volume around the truck and especially in the region in front of the cab. Most of the cells around the trailer have a CFL number less than 2. Looking around the cab large regions are being limited by 3 instead, and for the corners of the front of the cab and around the rear mirrors the value goes up to 4 and above. This shows that the time step of 1 ms is already violating the CFL number in large regions of the domain.

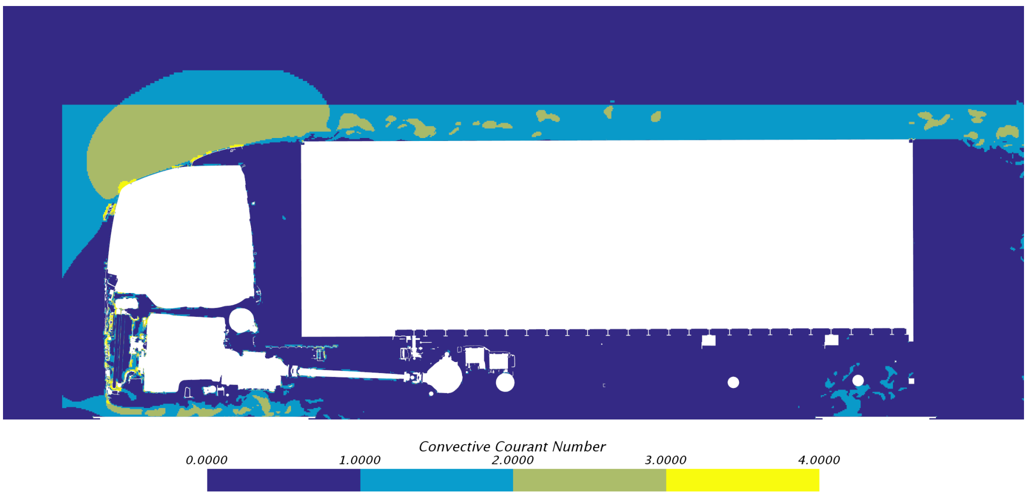

Figure 4.35: CFL number for 1 ms time step and 0 degree yaw in the y=0 plane. Limits from 0-4, where all above 4 is included in 4.

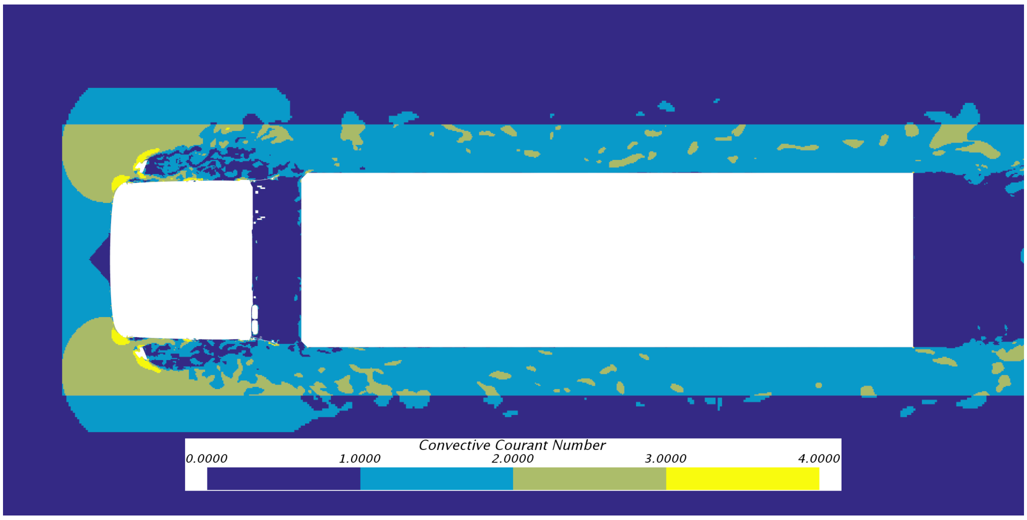

Figure 4.36: CFL number for 1 ms time step and 0 degree yaw in the z=2 plane. Limits from 0-4, where all above 4 is included in 4.

The CFL condition shows that the refinements in the mesh have been increased to a point where the temporal resolution is not sufficient. This is one of the main issues with spatial refinement; the temporal resolution must also be increased to fulfill the CFL condition. The impact of the high CFL numbers on the results of the base case will be investigated by comparison with simulations with a time step of 0.1 ms. These reference simulations will limit the number of cells that violate the CFL condition to below 0.05%, which is deemed sufficient. Only the 0 and -5 degrees yaw cases are investigated because of the enormous computational cost of such a small time step.

4.6 Temporal Resolution

The time step is of great interest to increase since the computational cost can be drastically reduced by taking longer time steps in DES. The result from Mocket [14] showed that the time step had a great influence on the physical properties for flow over a cylinder case but this is a very simple case. Ekman et al. [25] does a study on how the simulation gets affected by an increased time step for a car simulation. This study gives a very different result where the error is negligible for an increased time step. His study concludes that increasing the time step with a factor of 20 is still good for high accuracy and increasing it with a factor of 50 is acceptable in the perspective of drag and flow properties. Ekman et al. does not use DES modelling but instead uses stress blended Eddy simulation, which is based on the same principles as DES. Yet this indicates that there is still an interesting area to analyse since the simulations are so complex that the errors can be negligible from a decreased temporal resolution.

This chapter will cover the changes that occur when the time step of the implicit solver is increased. The simulations used in this section will be 0.1 ms, 1 ms, 2 ms, 4 ms, and 8 ms from Table 3.2. The simulations 1 ms, 2 ms, 4 ms, and 8 ms all use the same settings except time step. To note is that the 0.1 ms simulations use different URF settings, the number of inner iterations and is only run for 0 and -5 degree yaw. The comparison for the different time steps will not be compared to the wind tunnel results but instead as relative changes compared to the 1 ms simulations. This is because it is assumed that a finer discretization in time does give a more accurate solution. Therefore the 1 ms simulations should predict better than the 2 ms, 4 ms, and 8 ms simulations. The comparison for the finest time step of 0.1 ms will also be compared to the 1 ms in the same way as the other time steps. This is because these simulations were extremely expensive and were not sure to be run until late in the project. It should be noted that because of this most of the compared values will have a turning point at 1 ms, meaning that the delta values might be positive for the difference between 2 ms and 1 ms, this would then become negative for 0.1 ms and 1 ms.

4.6.1 CFL Number

Since the CFL condition is not satisfied for the base case of 1 ms time step a finer time step was tested of 0.1 ms. These refinements were only run for the yaw case of 0 and 5 degrees since they are extremely costly and do not fit in industrial use. The base case used a time step of 1 ms which left about 49% of the relevant cells exceeding CFL number equal to 1 but kept 99.5% of all the relevant cells below 4. The refined setting was run with a time step of 0.1 ms which reduced the percentage of cells down to 0.05% exceeding 1 in CFL number. This is considered to be temporally resolved to a sufficient degree. The CFL number distribution are shown in Fig. 4.37 and Fig. 4.38, for the two planes, y=0 and z=2. Those figures show how only a very few cells exceeds unity. Most of the cells exceeding unity are placed inside the RANS layer which is not that sensitive and hence can be excluded from the condition. Ekman et al. [25] used the transition factor from RANS to LES equal to 0.9 as the limit and this one is also used here. This limit makes only the LES cells and the late transition to be included. The cells that are not fulfilling the condition are based in small gaps, around the mirrors, by the wheels, and around the antennas on the roof. This is regions with very fine grid and high local velocities resulting in a very high CFL number.

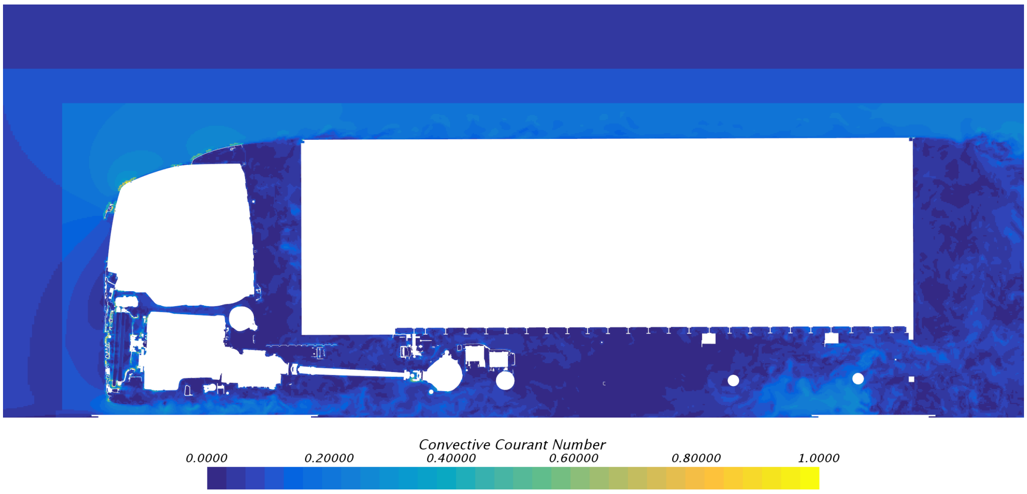

Figure 4.37: CFL number for 0.1 ms time step and 0 degree yaw in the y=0 plane. Limits from 0-1, were all above 1 is included in 1.

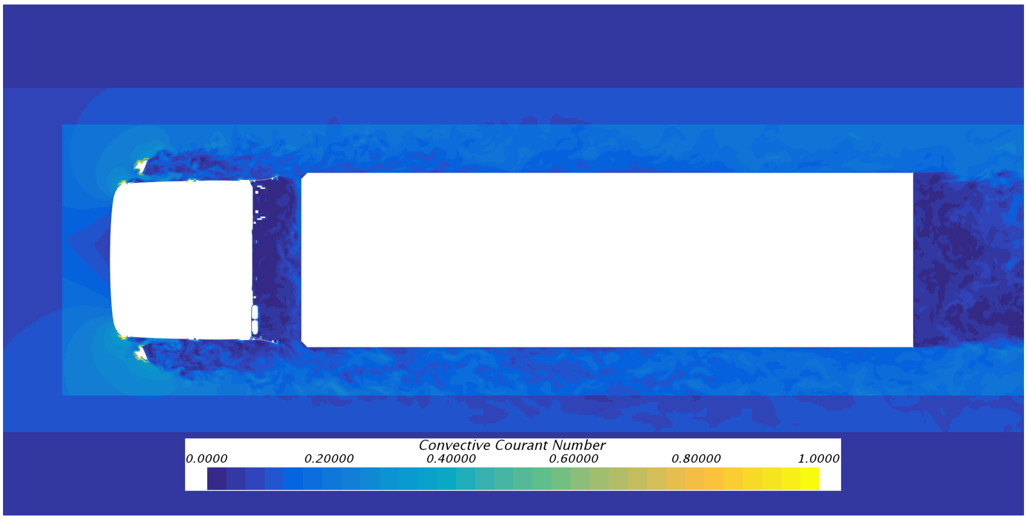

Figure 4.38: CFL number for 0.1 ms time step and 0 degree yaw in the z=2 plane. Limits from 0-1, were all above 1 is included in 1.

4.6.2 Comparison Between Time Steps

Since the parameters, C_d , C_s , and C_p were validated for wind tunnel tests those parameters are of great interest to start analysing for a different time step. The pressure will not only be compared probe by probe since the full surface pressure now is available. The pressure will also be compared on certain planes to give an overview of the pressure shift in the test section of the wind tunnel.

Comparison of C_d

The first parameter to be examined is the most crucial one, the C_d value. The ΔC_d values for the different time steps are listed in Table 4.6. In the table, the difference between 1 ms time step and the time steps of length 0.1, 2, 4, and 8 ms are stated. The confidence limits generated from the bandwidth-limited method is shown inside the parenthesis for each value. Using the difference and the confidential limits a t-test can be applied, according to the theory section 2.4, to each angle to see if there is a statistically significant difference between the mean values. Doing this assumes that the variance is equal for the two cases. The H_0 hypothesis is then that there is no significant difference in the mean value. Doing this it is found that the 2 ms time step does not give any significant difference in drag for any of the angles or the yaw weighted average at a 95% confidence level. Doing the same test for 0 and -5 degree yaw for 0.1 ms time steps gives a difference for the -5 degree yaw. This indicates that there is a significant difference between 1 and 0.1 ms time step when comparing according to the confidence of the convergence. These two simulations do have different URF settings and different amount of inner iterations, so there might be a difference introduced by this also.

Table 4.6: ΔC_d ((x) ms - 1 ms) between 1 ms time steps and 0.1, 2, 4, and 8 ms in drag counts. Values in parenthesis is corresponding confidential interval

Yaw	YWA	0.0	-2.5	-5.0	-7.5	-10.0
ΔC_d (0.1 ms)	N/A	-3 (11)	N/A	-10 (9)	N/A	N/A
ΔC_d (1 ms)	0 (7)	0 (10)	0 (6)	0 (4)	0 (4)	0 (6)
ΔC_d (2 ms)	6 (9)	6 (15)	5 (7)	8 (8)	1 (4)	7 (6)
ΔC_d (4 ms)	31 (8)	45 (12)	32 (7)	14 (4)	15 (5)	18 (4)
ΔC_d (8 ms)	54 (10)	78 (11)	60 (11)	22 (6)	18 (6)	25 (8)

Comparing the values from Table 4.6 it can be concluded that increasing the time step from 1 ms to 2 ms does not change the drag coefficient significantly at the confidence levels reached in this work. Looking at the results for 4 ms and 8 ms time steps the drag starts to increase significantly and they lie outside the 95% confidence level of the 1 ms steps. These numbers do not give any indication if too much information is lost in the simulations or if they could be used as settings for a "simplified" evaluation. This simplified evaluation could be a setting that is somewhere in between the steady-state and unsteady-state simulations where the accuracy from fully resolved IDDES is lost but the results still perform better than fully steady-state generated from RANS. But using C_d from only one type of geometry cannot validate the error term introduced from a larger time step so further analysis has to be made on the flow field properties.

Fig. 4.39 shows ΔC_d between the different time steps whereas the 0.1 ms time step is set as the reference instead of 1 ms. As seen in this figure the C_d value seems to converge nicely for the 0 degree yaw case as a clear diminishing difference is observed for the smaller time steps. For the -5 degree yaw, the convergence is less reduced per time step. The difference is about doubled when going from 0.1 to 2 ms compared to from 0.1 to 1 ms. The confidence intervals are quite large and make the changes hard to justify. For the 0 degree yaw case a big increase is seen for 4 ms and 8 ms time step but for -5 degree yaw, the change is less significant.

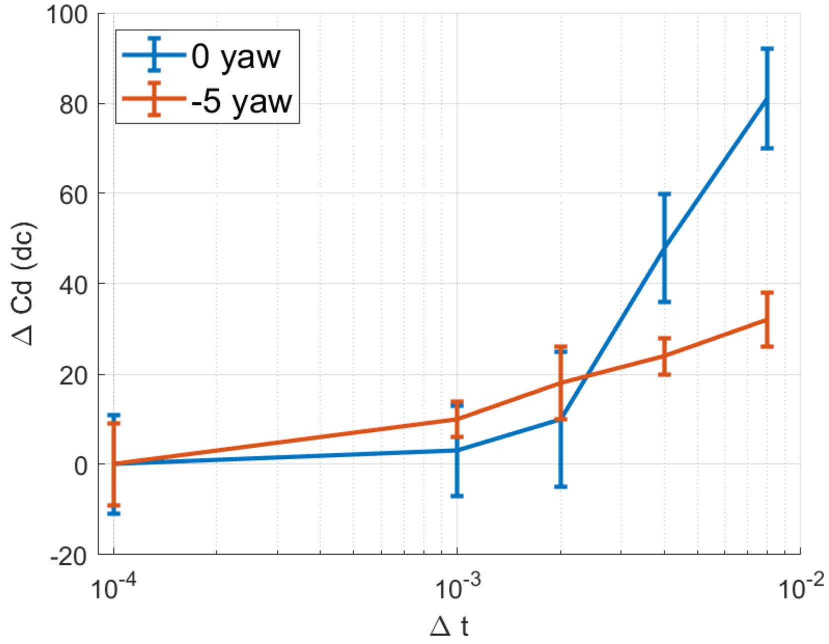

Figure 4.39: Difference between C_d for different time steps, ΔC_d ((x) ms - 0.1 ms) for 0 and -5 degree yaw, were (x) refers to 1, 2, 4, and 8 ms.

In Fig. 4.39 the relative distance between the time steps is shown. It is visualized with the log scale on the x-axis. The relative time step difference between 0.1 ms and 1 ms is 10 times. This is of a similar magnitude as between 1 ms and 8 ms, which is 8 times. By using the results for how the difference for C_d decays from 8 ms down to 0.1 ms for 0 degree yaw, it can be motivated that a finer time step than 0.1 ms, 0.01 ms for example, will not be significantly different from 0.1 ms. This is motivated by how the C_d starts to increase drastically in the regions of 1 to 8 ms. The refined reference of 0.1 ms time steps can from this be used as an initial error estimator for the 1 ms time steps. The error can be estimated to be in the order of 10 drag counts already in the base case, if comparing the difference between 0.1 and 1 ms time step in Table 4.6.

The data from Table 4.6 is visualized in Fig. 4.40. In this figure the difference for each yaw angle is visible. The reference, 1 ms, is the orange circles with a ΔC_d of 0. Comparing the 2 ms with the 1 ms simulations those are offset a bit for all simulations but this is in the same range as for the confidence intervals. For the 4 ms and 8 ms simulations, a trend of overpredicting C_d for the low angles is apparent. The evenly spread error for -5 degree seen in Fig. 4.39 is also seen here. The errors for -5 degree yaw are a lot more evenly spread compared to 0 degree yaw where 0.1, 1, and 2 ms are grouped and then 4 and 8 ms increase a lot.

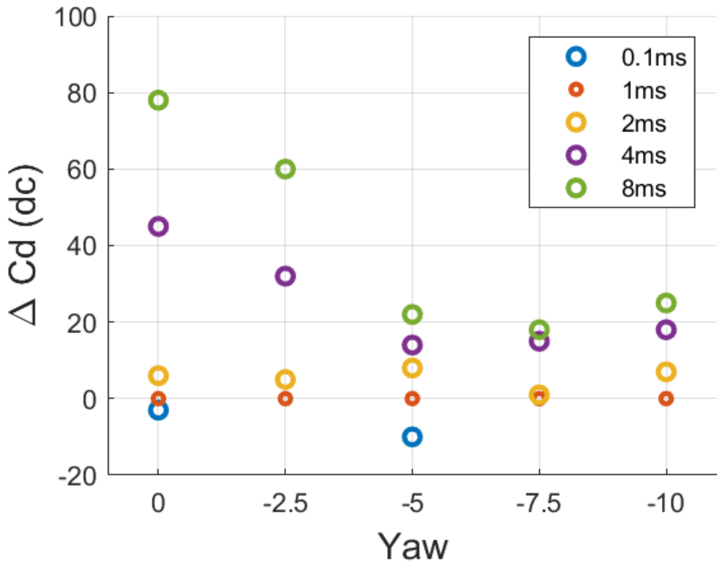

Figure 4.40: ΔC_d ((x) ms - 1 ms) between the different time steps for the different yaw angles.

Comparison of C_s

The second parameter to analyse for the different time steps is C_s . The difference, ΔC_s , between the time steps compared to 1 ms is tabulated in Table 4.7. The 0 degree yaw case shows no significant difference between any of the results. This is most likely because any error introduced would behave similarly on both sides of the truck. The difference for the 2 ms time step is in the range of 10 to 20 counts. This is outside the 95% confidence limit meaning that it is statistically different from 1 ms time step. However, looking at the -5 degree yaw an interesting result is seen for the 0.1, 1 and 2 ms simulations. both the 0.1 and 2 ms simulation underpredicts C_s compared to 1 ms, which means that there might be no significant difference between those three. Applying the t-test H_0 hypothesis testing does show that there is a difference between 1 and 2 ms but not between 0.1 and 2 ms.

Table 4.7: ΔC_s ((x) ms - 1 ms) between 1 ms time steps and 0.1, 2, 4, and 8 ms in side counts. Values in parenthesis is corresponding confidential interval

Yaw	YWA	0.0	-2.5	-5.0	-7.5	-10.0
ΔC_s (0.1 ms)	N/A	2 (5)	N/A	-5 (10)	N/A	N/A
ΔC_s (1 ms)	0 (10)	0 (5)	0 (12)	0 (10)	0 (10)	0 (12)
ΔC_s (2 ms)	-10 (9)	0 (6)	-11 (9)	-15 (11)	-20 (13)	-18 (8)
ΔC_s (4 ms)	-34 (7)	-1 (5)	-43 (7)	-40 (9)	-44 (8)	-51 (10)
ΔC_s (8 ms)	-58 (8)	-2 (6)	-68 (9)	-79 (9)	-91 (8)	-101 (11)

The data from Table 4.7 is visualized in Fig. 4.41. This figure show an increased error for increased yaw angle. It is interesting how the errors increase by similar size for all the angles, except for 8 ms were the higher angles gives a higher error.

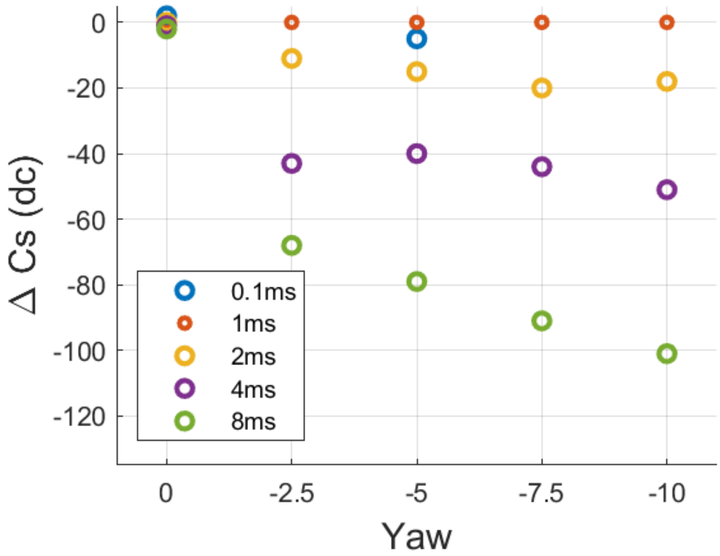

Figure 4.41: ΔC_s ((x) ms - 1 ms) between the different time steps for the different yaw angles.

Comparison of Surface C_p

The surface pressure on the truck is what contributes dominantly to the total drag, and most of this can be related to the base pressure. To analyze how this base pressure is affected by the time step the pressure coefficient, C_p , on the surface was compared between the time steps. The results are shown in Fig. 4.42. Fig. 4.42 show ΔC_p ((x) ms - 1 ms) for the 0.1, 2, 4, and 8 ms time step compared to the 1 ms time step. The scales means that if a region is red the pressure increase and if it is blue the pressure decrease. Note that the pressure "should" appear in the opposite way for the 0.1 ms simulations compared to 2, 4, and 8 ms if the trends are time-step dependent. From the figure, one can see that the difference increases for a larger time step and that it underpredicts the base pressure in the lower region of the trailer rear on the truck. The most negative part in the blue region in Fig. 4.42(d) correspond to a ΔC_p of about -0.15. For Fig. 4.42(a) and (b) almost no difference is seen but only minor changes in a few spots. This indicates that the difference in base pressure is very small for 0.1 and 2 ms compared to 1 ms. This is in agreement with the difference in C_d between the different time steps.

To further analyze the base pressure difference Fig. 4.43 shows the pressure difference for the -5 degree yaw. Fig. 4.43(a) shows a small overpredicted pressure in the lower corner towards the side facing the flow. This overprediction for 0.1 ms indicates that the pressure should be higher here according to the finer time step and this is one of the errors occurring due to the coarser temporal resolution. Fig. 4.43(b) has a more spread difference as it is lower in the upper and lower left region and higher in the lower right region. This difference in both directions show that the wake structures are not simulated correctly but in a global perspective looking on the drag signal those differences will cancel each other and give a wrong impression of the accuracy. Fig. 4.43(c) shows even larger differences that also seem to cancel

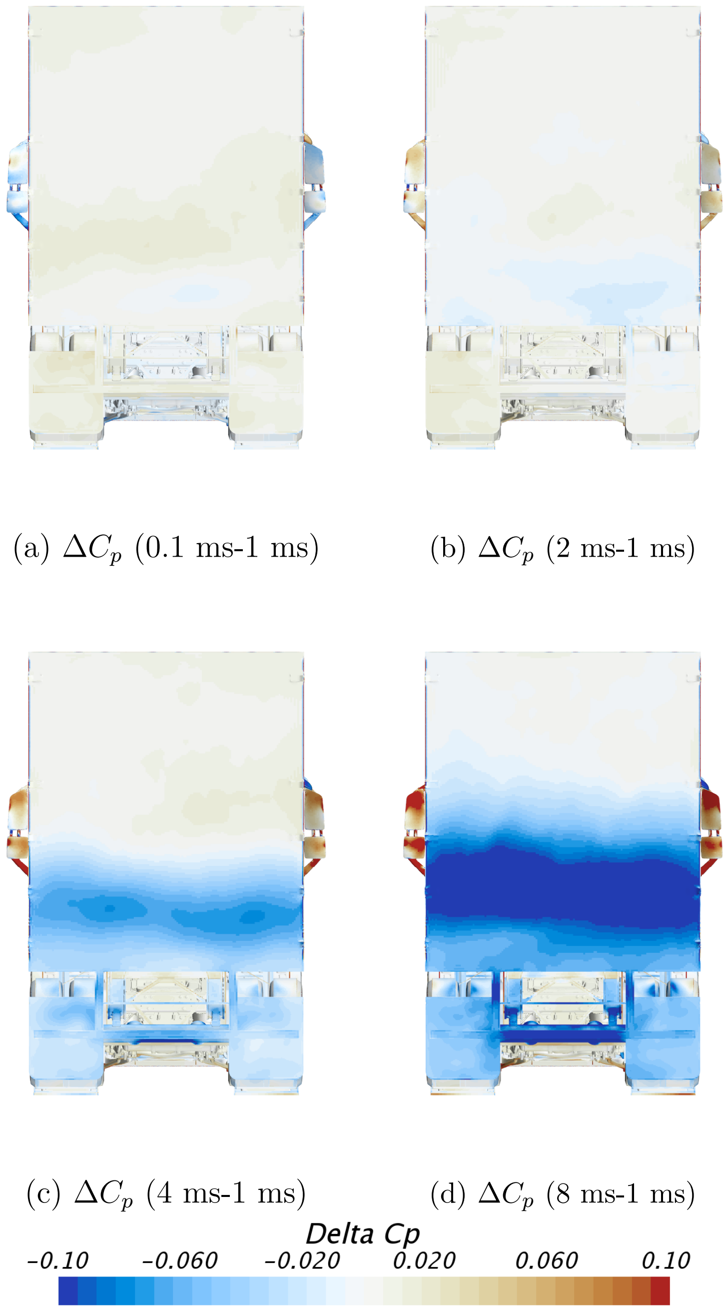

(a) ΔC_p (0.1 ms-1 ms)

(b) ΔC_p (2 ms-1 ms)

(c) ΔC_p (4 ms-1 ms)

(d) ΔC_p (8 ms-1 ms)

Figure 4.42: ΔC_p ((x) ms - 1 ms) on the rear end of the truck between 1 ms and 0.1, 2, 4, and 8 ms time steps for 0 degree yaw.

each other. This indicates why the drag prediction does not increase that much for an increased time step for the -5 degree yaw as for 0 degree yaw.

The pressure differences shown in Fig. 4.42 and Fig. 4.43 only show the average pressure difference. To show if the difference is significant with respect to averaging 25 probes on the rear surface will be used to create confidence intervals for the

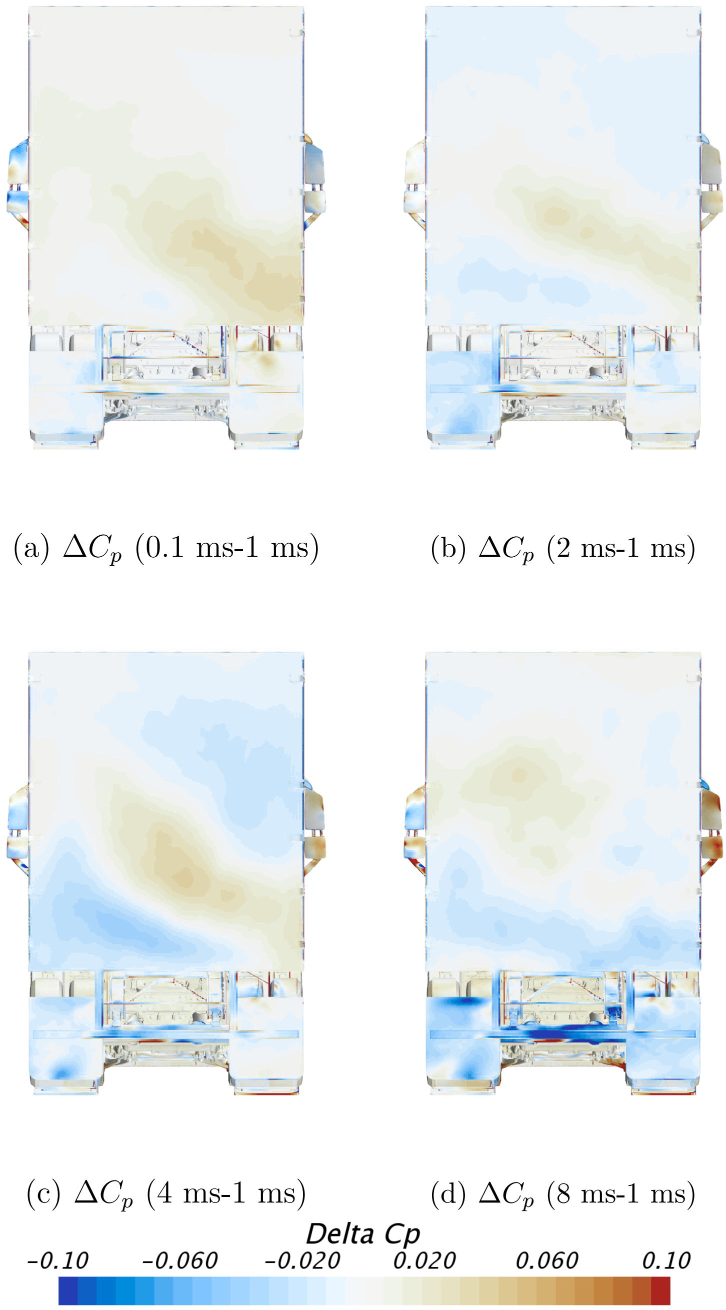

(a) ΔC_p (0.1 ms-1 ms)

(b) ΔC_p (2 ms-1 ms)

(c) ΔC_p (4 ms-1 ms)

(d) ΔC_p (8 ms-1 ms)

Figure 4.43: ΔC_p ((x) ms - 1 ms) on the rear end of the truck between 1 ms and 0.1, 2, 4, and 8 ms time steps for -5 degree yaw.

pressure. The 25 probes used are the same ones used in section 4.5.1 for the rear surface of the truck. The confidence intervals will be generated from the estimated bandwidth limited Gaussian white noise method from section 4.2. The confidence intervals for the probes for 2, 4, and 8 ms compared to 1 ms are shown in Fig. 4.44 for 0 and -5 degree yaw. The probes are split in 5 rows over the rear surface, and include five probes in each row. The first row on the top of the rear is 1-5 and then goes 6-10 and so on downwards. For 0 degree yaw it is seen that there is no significant difference between any of the time step for the two first rows of probes. For the third row, 11-15 the 8 ms time step has a significant difference but not the 2 or 4 ms. For the fourth and fifth row, 16-25, both the 4 and 8 ms time step significantly differs from 1 ms. 2 ms has no significant difference for any of the probes for 0 degree yaw. Looking at -5 degree yaw, the result is different. The pressure difference between the time steps here shows only significant difference for a few probes for 4 and 8 ms time step. This is in line with that the C_d value is not so different between the time steps for -5 degree yaw compared to 0 degree yaw.

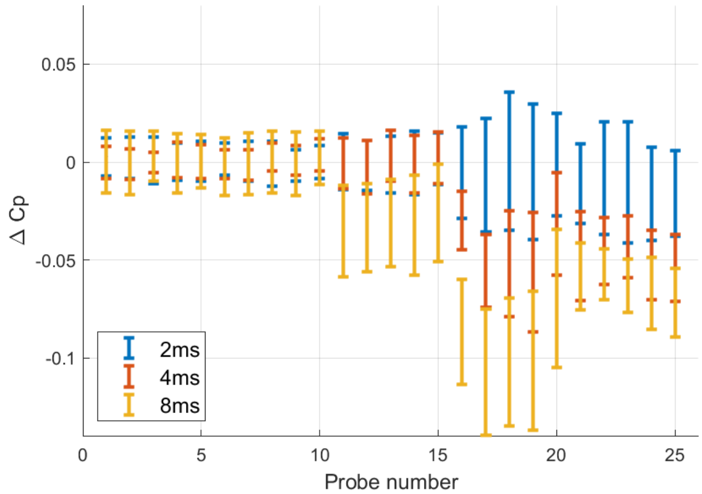

(a1) 0 degree yaw

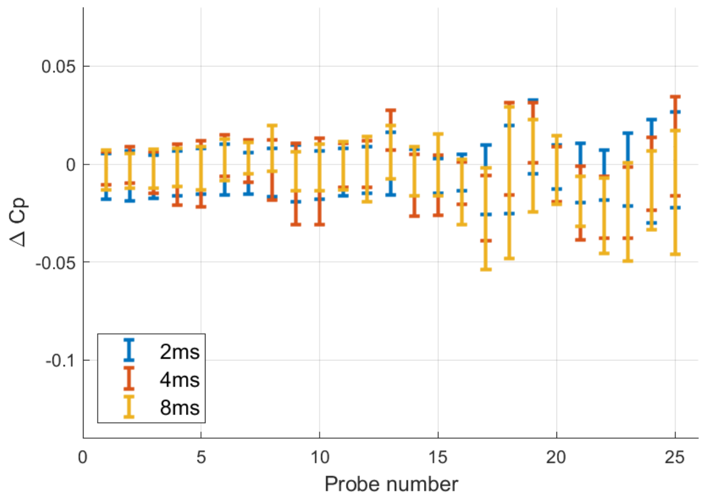

(a2) -5 degree yaw

Figure 4.44: ΔC_p ((x) ms - 1 ms) , presented as confidence intervals, between 1 ms time step and 2, 4, and 8 ms time step for the probes on the rear of the trailer for 0 and -5 degree yaw.

The surface pressure difference for the different time steps at 0 degrees yaw is shown in iso view in Fig. 4.45. From those figures, some crucial areas are found where the pressure differences are larger. The areas that get affected the most from 0.1 ms up to 1 ms time step is by the a-pillars, around the rear mirrors and the front wheel. There are also some changes on the side of the cab on the side windows and the front of the trailer. These areas are visible in Fig. 4.45 (a). The separation region behind the front corner underneath the rear mirror is affected very much. The pressure on the side window is also quite different. This shows that this region is highly sensitive to an increased time step. The different pressure distribution on the cab in the 0.1 ms comparison shows that there is flow structures changed in this region when the time step is set to 1 ms compared to 0.1 ms. This makes the 1 ms simulation not valid as a reference if the structures in the front region of the cab are the ones of interest. This is not necessarily an issue when the drag is the main factor of interest, but it should be noted. Looking on the 2 ms comparison, Fig. 4.45 (b), instead makes the changes smaller than for 0.1 ms, but the difference between the time steps are also lower when comparing the factor difference. In Fig. 4.45 (b) the biggest difference is observed by the front wheel instead. For the comparison with the time step of 4 and 8 ms in Fig. 4.45 (c) and (d), more differences are noticed over more areas of the truck. This shows that the pressure difference is altered quite heavily for those bigger time steps. From a general perspective the pressure on the cab is very sensitive to the different time steps and if the actual pressure fields are of interest in those areas the time step must be chosen with care.

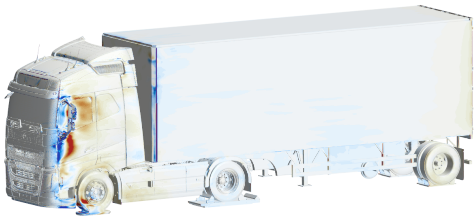

(a) ΔC_p (0.1 ms-1 ms)

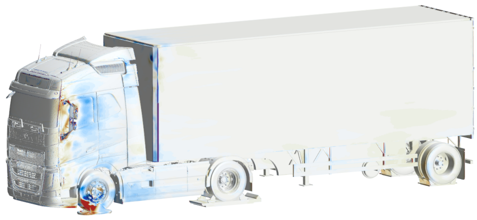

(b) ΔC_p (2 ms-1 ms)

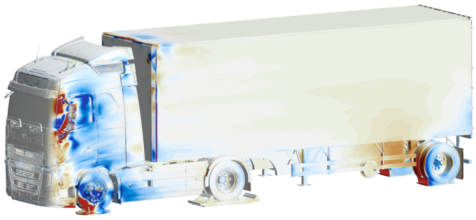

(c) ΔC_p (4 ms-1 ms)

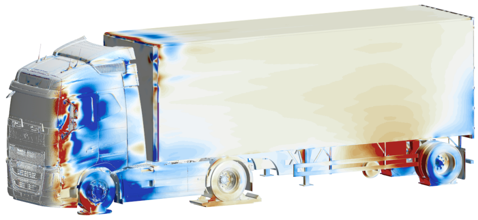

(d) ΔC_p (8 ms-1 ms)

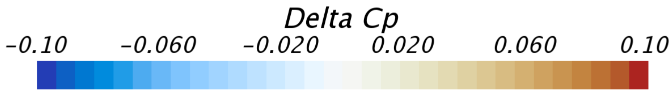

Figure 4.45: ΔC_p ((x) ms - 1 ms) on the truck between 1 ms and 0.1, 2, 4, and 8 ms time steps for 0 degree yaw.

Comparison of C_p Planes

To further evaluate the pressure difference observed between the different time steps, two crucial planes are observed. ΔC_p between 0.1, 2, 4, and 8 ms compared to 1 ms is visualised in the y=0 and z=2 plane in Fig. 4.46. Looking in the y=0 plane a trend of pressure shift is present about one cab length behind the trailer. The trend is that the pressure right behind the trailer is under-predicted and the pressure away from the trailer is overpredicted for an increased time step. A lower pressure region seems to roll up on the trailer from underneath and grow in magnitude for an enlarged time step, especially for 8 ms. Rolling up means that it is initialized underneath and expands into a larger region up behind the trailer. Looking at the z=2 plane the same pressure shift in the wake is present. Looking at the 8 ms comparison, Fig. 4.46(d2), the pressure difference seem to roll in from the sides. This means that the pressure difference is initialised on the edges of the trailer and then grows into the wake. The difference in the wake could come from how the separation and fluctuations in the wake flow are resolved for different time steps.

The pressure around the rear mirrors shows a difference that seems to scale strongly already from the 0.1 ms time step in Fig. 4.46(a2). Here the difference seems to be bigger in magnitude compared to the 2 ms time step in Fig. 4.46(b2). This indicates that the turbulent flow behind the mirrors is more sensitive to an enlarged time step than the wake structures when comparing to the 0.1 ms time step. This is in line with the pressure effects seen on the cab for Fig. 4.45. An interesting effect from the rear mirrors in the z=2 plane is how the pressure shift behind those are predicted oppositely compared to the pressure behind the trailer for an enlarged time step.

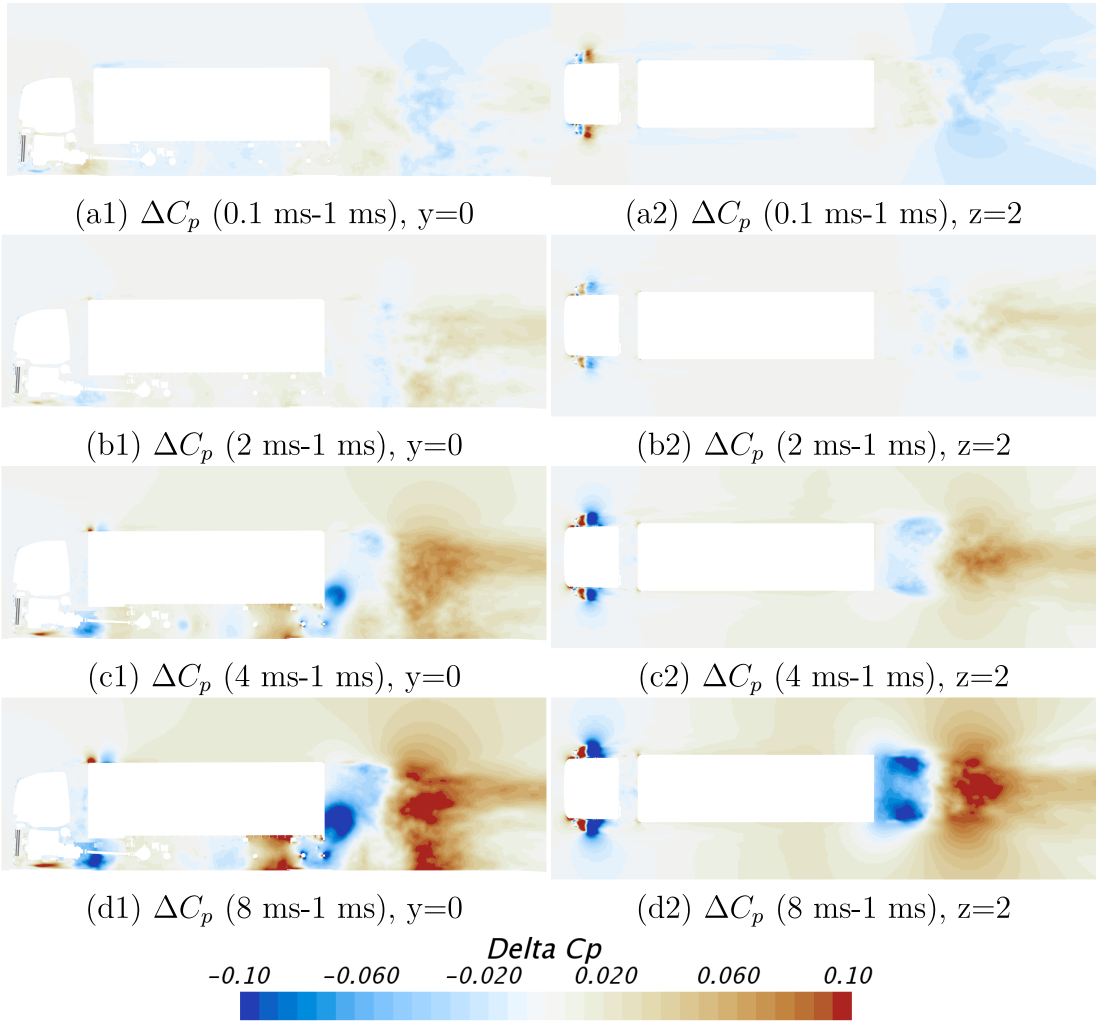

(a1) ΔC_p (0.1 ms-1 ms), y=0
(a2) ΔC_p (0.1 ms-1 ms), z=2
(b1) ΔC_p (2 ms-1 ms), y=0
(b2) ΔC_p (2 ms-1 ms), z=2
(c1) ΔC_p (4 ms-1 ms), y=0
(c2) ΔC_p (4 ms-1 ms), z=2
(d1) ΔC_p (8 ms-1 ms), y=0
(d2) ΔC_p (8 ms-1 ms), z=2

Figure 4.46: ΔC_p ((x) ms - 1 ms) in the y=0 and z=2 plane between 1 ms and 0.1, 2, 4, and 8 ms time steps for 0 degree yaw.

4.6.3 Frequency Content

The drag signal was windowed with the Hann window and transformed with fast Fourier transform to obtain the Power Spectral Density (PSD). This signal was compared for the different yaw angles for the different time steps, but no trend was found in the frequency content of the drag signals for the different time steps. Therefore, focus were put on the four corner probes on the rear end of the trailer. Those were analysed to see how they behave in the frequency domain. Those probes had for the 1 ms case two interesting peaks, one at about 0.3 Hz and one a bit higher at 2 Hz. The one at about 2 Hz was studied closer for the 0.1, 1, 2, 4, and 8 ms simulations. Fig. 4.47 show the time steps, 0.1, 1, 2, 4, and 8 ms, for each of the four probes. The interesting phenomenon is how the "2 Hz" peak moves in the frequency domain when the time step is changed. In the figure, there is an information box attached to the highest peak around 2 Hz for each time step. These boxes show how the peak is the lowest for 0.1 ms and then grows slightly for each of the time steps, 1, 2, and 4 ms. For the 8 ms time step, this peak has disappeared. This shows that the time step does change the temporal behaviour for the pressure even at low frequencies of about 2 Hz. The movement of the peak tells that the vortex shedding from the left to right side gets a higher frequency and thus a longer wave-length. This means that the slow transient movements gets faster for an enlarged time step and for the 8 ms time step it is gone. This could be an effect of how the wake structures gets averaged with a larger time step and starts to develop into a time averaged solution.

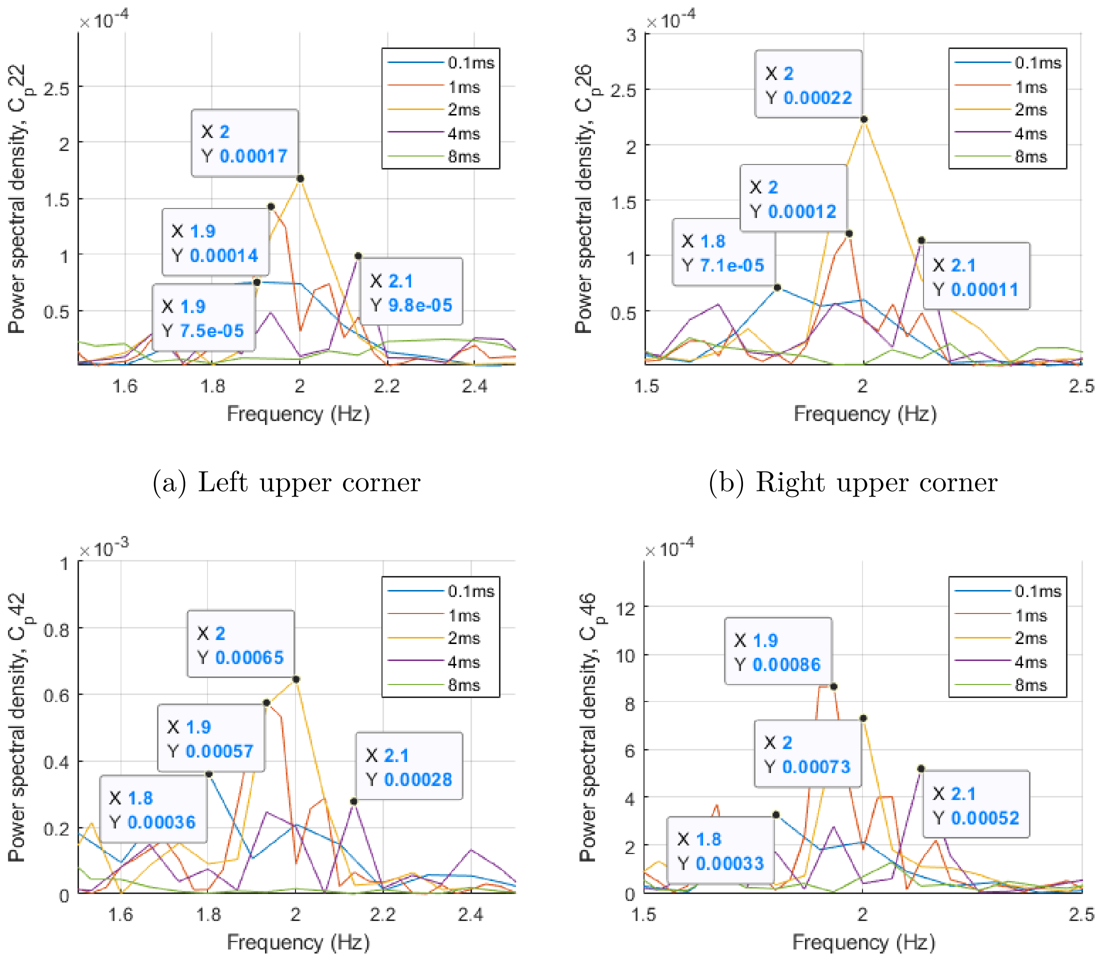

(a) Left upper corner

(b) Right upper corner

(c) Left lower corner

(d) Right lower corner

Figure 4.47: Frequency content from 1.5-2.5 Hz for the corner probes on the rear end of the truck. Notation boxes for all significant peaks in the region.

4.7 Inner Iterations

The effects from different time steps and different Under Relaxation Factors (URF) will be presented in this chapter. The simulations used in this study are the 0.1 ms, NURF (New URF), 1 ms, 2 ms, 4 ms, and 8 ms, all for 0 degree yaw, from Table 3.2. The different settings for the URF settings are Recommended (R) and Enhanced Stability (ES). The different time steps are 0.1, 1, 2, 4, and 8 ms. The simulations having the URF set with R is 0.1 ms and NURF and the rest uses ES. The time steps are according to the names and for the NURF simulation the time step is 1 ms. This study was conducted late in the project.

The initial settings for the simulations were to use 10 inner iterations and the URF set according to the enhanced stability. For the 0.1 ms simulation, the 10 inner iterations were considered excessive and the goal was to be able to reduce this to reduce the computational time. Together with the reduction of inner iterations for the 0.1 ms time step, it was decided to try the standard recommendations for the

URF values instead of the enhanced stability. The 0.1 ms simulations were run with 10 inner iterations and the R settings for the URF values for a while and the convergence was then controlled for the inner iterations. It was then found that 8 inner iterations were sufficient. The recommended URF settings gave no effect on the instability and thus they were kept as recommended. To see the effect on the convergence for the URF settings at R instead of ES the simulation NURF was tested to compare with the 1 ms simulation.

The result from the convergence study of the inner iterations are shown in Fig. 4.48. In the figure, one can read the result from the different time steps of 1, 2, 4, and 8 ms that all use the ES setting for the URF values. The magenta-coloured markers are for the New URF settings that are set with the R setting for the URF values for 1 and 0.1 ms time steps. All simulations use 10 inner iterations, except for the 0.1 ms time step, which uses 8 inner iterations. The axes in the figure show the residuals on the y-axis and the different type of residual on the x-axis. The abbreviations are Specific Dissipation Rate (SDR), Turbulent Kinetic Energy (TKE), Momentum (M), and New Under Relaxation Factors (NURF). The different residuals converge with a different order of magnitude, from only 10^0 down to 10^{-5}. The new recommended setting for URF proves to show a much better convergence when comparing 1 ms and "1 ms, NURF", as it reduces for all residuals. When comparing the different time steps with the ES settings there is a trend of a reduced convergence when increasing the time step. The difference is one order of magnitude at max for the different time steps, but smaller in most of them. The 0.1 ms time step shows a good convergence even when the number of inner iterations is reduced to 8. It is visible that the continuity and turbulent kinetic energy residuals are more sensitive to the time step then the momentum residuals. The specific dissipation rate residual is not converging very well.

The URF settings initially set in this project did not fit the simulations, as the enhanced stability was not needed. They were therefore heavily under relaxed to increase stability. This resulted in a slow convergence for the inner iterations for the 1 ms, 2 ms, 4 ms, and 8 ms simulations. Tuning the under relaxation factors to standard settings according to Ross and Herrmann [38], gave a significant change in convergence. The convergence phenomenon where studied late in the project and the initial ES settings were mainly focused on steady-state simulations and were set when there was a general problem of geometries that caused divergence issues. The settings were then adapted with minor changes to fit the unsteady DES settings. This study was however only applied to simulations that did not include any initial transient. Therefor there might be issues in the early stages of the simulations. In case there is issues in the early stages the URF could be changed when the initial transient has decayed and the solutions are only run to reduce the convergence limits.

The results here show that the longer time steps probably should use some extra inner iterations to converge to the same order as the 1 ms but this should also be tested together with the more suitable recommended under relaxation factors. The enhanced stability under relaxation factors come from a setting when there were

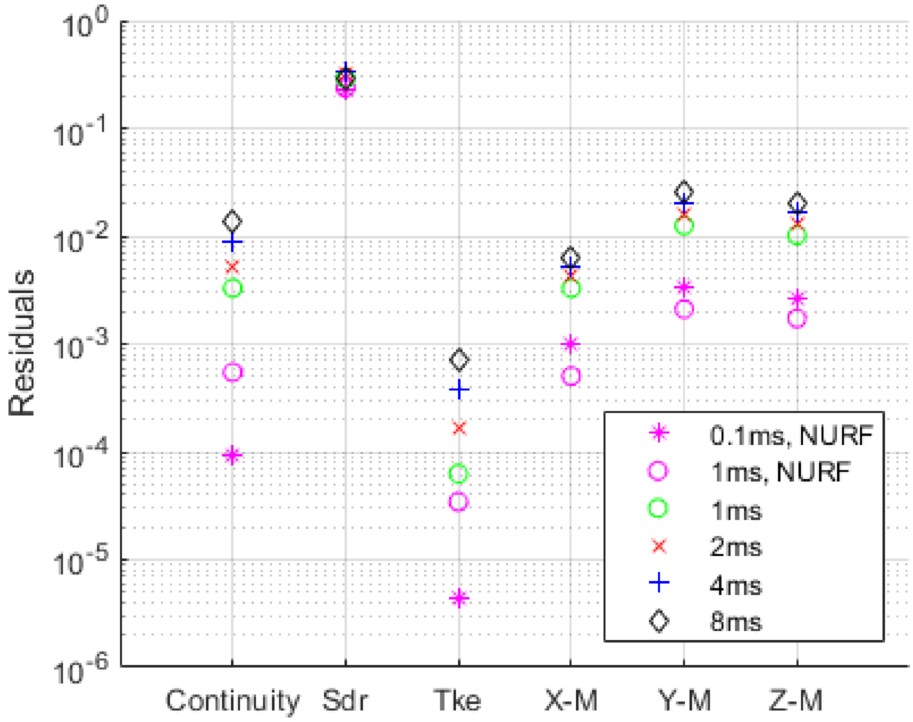

Figure 4.48: Residuals for different time steps and different under relaxation factor (URF) settings.

stability issues in the simulations because of geometric impurities. The geometries used now are pre-processed better and does not include these issues that earlier made the simulations diverge. Thus the recommended settings for the URF values are more preferable as they reduce the number of iterations needed for convergence. These results show that the time step used in the simulations affects the convergence, but it also shows that the convergence depends heavily on the under relaxation factors. Due to time limitation in this project, this was not studied further.

5

Discussion

The methods analysed in this work is mainly, wind tunnel modelling, averaging of unsteady properties, initial starting points for averaging of unsteady properties, spatial mesh, temporal discretization, and inner iterations. These six factors each contribute to the error presented in Eq. (3.1). Some of the errors can be quantified when a method for it has been established. Some errors are much harder to determine. This chapter will discuss the results and give suggestions for future work.

5.1 Discussion of Errors

The first error analysed is the error arising from the reference probes in the wind tunnel modelling. The method used in the current situation is rather insecure because of the lack of knowledge of those probes in the wind tunnel tests. If more data would have been available, such as the pressure and velocity measured in the reference probes, the scaling for the stagnation pressure could be omitted and the error in C_d , C_s , and C_p could maybe be reduced further.

A more well-defined error is the uncertainty from the averaging of instantaneous values and its convergence limits. Those are now set with conservative limits according to the bandwidth-limited Gaussian white noise method. This is very useful information in an industrial application. The downside of the method used is that it is quite sensitive in one aspect: the starting point can affect how the final confidence interval looks like. To combine the initial transient method with the band-width limited method does minimize the variance and can by doing so remove information that might should be included or excluded. To remove this insecurity, it is suggested to not use the methods blindly but study the behaviour for a set of representative simulations. As a general remark on the averaged values of the unsteady simulations of the truck geometry is that they oscillate very much. The truck generates large fluctuations take long physical time to resolve. The longest relevant time scales found are in the order of 10^1 and the shortest lays in the order of 10^{-3}. This makes the simulations very expensive to resolve.

Using the method evaluated for finding the initial transient is not recommended without manual input. The method can find very small t_0 which is not deemed appropriate to use as starting points since the signal most probably include an initial transient since it does so for other similar cases analysed. Therefore this method was not used to its full potential in this work but only as a guideline of where to set the commonly used initial time t_0. The reason for the poorly predicted initial transient can be because of the large oscillations in C_d and that the initialization from the RANS solution starts the simulation quite accurately.

The mesh analysis only gave significant differences worth the cost for the trailer refinement and not for the underbody and front cab refinement when only the drag coefficient was monitored. The drag coefficient might be a too coarse measurement to use to determine the spatial resolution. Instead, the two-point correlation method should be used to determine where the grid should be refined. This method was only tested for the base case due to lack of time. This method did give good indications of where the grid might need to be refined according to the turbulent length scales. To find out if refinement is needed in an industrial application, the method needs to be applied on multiple truck geometries to ensure that the requirements are similar for the majority of them. The resolution for the 1 ms case tested was very fine in most of the regions tested as the turbulent length scales was resolved by more than 16 cells. In a few regions, the resolution went down to 8 cells and should maybe be refined. For a very limited region, the resolution went down to 4 cells and should be refined for a better LES resolution.

The number of inner iterations was a factor that was considered late in the project. Preferably those should have been used to ensure the same convergence in-between time steps, but instead, only the difference in convergence was investigated. The difference in the residuals for the time step of 1, 2, 4, and 8 ms was within one order of magnitude for all the individual residuals. In this investigation the under relaxation factors were also investigated. Those were not set correctly in the initial state of the project, so the first simulations were heavily under relaxed and therefore converged slowly. This was not necessary and could have been changed earlier to make the simulations converge within fewer time steps.

5.2 Absolute Accuracy

The results from the base case, 1 ms simulations, compared to the wind tunnel show that there is an absolute error of -45 dc in C_d for the yaw weighted averaged value. This error includes a confidence interval of ± 7 dc from the convergence limit. This error in C_d is conceptually explainable by the surface pressure error, ΔC_p (Sim - WT) , on the rear end of the truck. This was compared by interpolating the pressure difference between the 25 probes used on the rear end of the trailer and then integrate the result to generate a difference in C_d . This showed that the pressure on the rear end explains a lot of the errors. By looking on the comparison in pressure to the wind tunnel it is found that the wake structures must be wrongly predicted and change with the yaw angle of the truck. This is seen in how the ΔC_p (Sim - WT) changes in appearance for different angles. Looking at the results from Fig. 4.30 the predictions for the higher yaw angles does not only overpredict the pressure as for 0 and -2.5 degree yaw. The -7.5 degree yaw angle include an underpredicted pressure region. This shows that the pressure field is not predicted as it should but when analysing only C_d this yaw angle seem to predict better than 0 degree yaw. This is an example of how multiple errors can cancel each other when they are added into one single value, C_d , to evaluate the results. This phenomenon highlights the importance of analysing the pressure distribution on the truck in a validation study and not only the C_d value. The confidence levels shows that there are limits in the current simulation method regarding how small changes are statistically significant from one setup to another. This has to be considered when using the CFD method for development analysis, that changes smaller than those limits can not be statistically proven to make a difference.

The pressure probes used to validate the CFD method seems to have a constant positive offset in the simulations. This could be an error in how the pressure coefficient is calculated, but it is not found where this error is introduced. The error for some of the probes are significantly larger than for others, for example the two most forward placed probes on both of the cab sides and the probe placed on the front of the trailer by the upper corner. The large error for those probes are speculated to arise because of the high pressure gradients in the regions. This would describe how the error is large if the flow is slightly miss-predicted in the regions as well as if the probe is slightly misplaced.

The simulation methodology used has an error compared to the wind tunnel that is not fully understood. This error is largest for 0 degree yaw, -58 dc, and smallest for -7.5 degree yaw, -22 dc. The error obtained is large when considering the unsteady IDDES method used. The CFL criterion is not less than 1 in the entire domain for this base case simulation. This is however not the entire source of the error, since when the two simulations with a finer time step is run those gives a difference of only 5-10 dc from the base case. The cause of the error could lie in how the flow in the wind tunnel is assumed. With the current setting, the inlet flow in the tunnel is assumed to be perpendicular to the inlet but this might not be the case because of the fan in the wind tunnel. The fan might leave rotational components in the flow even though it is supposed to have straightened up in the test section of the tunnel. This phenomenon was discussed by Josefsson but never validated [4]. The absolute reason is not found and remain a task for further development. A noticeable effect is however how a coarser and thus more inaccurate method can appear to better predict reality. Imperfections in measurements and methodologies can give new errors that cancel the previous ones. For this work, the results from the simulations with an increased time step have not been used to compare the results from the wind tunnel. This is because when comparing those to the wind tunnel the error decreases for an increased time step. This would mean that a coarser temporal resolution would generate a better result, which is counter-intuitive as the discretization errors should be larger.

5.3 Temporal Resolution

The different time steps tested was 1 ms as the base case and 2, 4, and 8 ms as the alternative time steps. 0.1 ms time step was also tested for 2 yaw angles, but those are very expensive so they are not feasible in an industrial application. The two 0.1 ms simulations cost 3.5 M CPU hours to run, this was done in-house at Volvo

GTT on their computational clusters. The reason those simulations were able to be tested was that the computational clusters were not occupied in the later part of the project because of the short-term lay-off due to the Covid-19 pandemic. This gave an invaluable opportunity to compare the results with a much finer time step. The comparison showed that there is a difference of 5-10dc between 0.1 and 1 ms time steps but the confidence intervals from the averaging are in the same order of $\pm 5-10$ dc. This shows that the violation of CFL number less than 1 could be done as long as it is done moderately. The limit of how long time steps that can be used is in the range from 0.1-2 ms time steps. This is based on the results from the increased time steps where the results start to diverge more and more from 1 ms. The difference between 1 and 2 ms time steps is not significant itself but the difference between 0.1 and 2 ms is. This means that if the thesis would not have included the 0.1 ms time step the new recommendation would have been 2 ms instead of the baseline of 1 ms to decide the C_d value. This because of the very small difference between the two and the great reduction in computational cost. Now as the results from the 0.1 ms time step is available it is seen that the drag is over predicted significantly for the 2 ms time step but it is still a valuable setting. Since it reduces the computational time very much the results can be used as long as the errors that come with it is included. Increasing the time step further to 4 or 8 ms should be done with care since the pressure field is significantly changed for those.

The time step of 0.1 ms had the CFL number limited in 99.95% in the domain, which might be more than necessary. Using the result from Fig. 4.35 and Fig. 4.36 for the CFL number with the 1 ms time step a new time step could be estimated to cover most of the regions of interest with a CFL number below 1. This could be done by assuming that the yellow regions, with CFL > 3, around corners and mirrors are allowed to exceed CFL number 1 but the rest should be under. This would then generate a new time step of 0.33 ms instead of 1 ms. This might work as a better baseline than 1 ms but still not as expensive as the 0.1 ms time step.

5.4 Further Development

To further develop the CFD method analysed in this work a few aspects should be considered. Firstly the baseline comparison to the wind tunnel tests should be used with a time step of somewhere around 0.33 ms with current mesh refinement to make sure the CFL condition is not violated in too large regions in the domain. When doing this it is recommended to set the under relaxation factors according to general guidelines that do not under relax the solutions if it is not necessary for stability. The number of inner iterations should also be studied and convergence criteria for the residuals should be set to apply for heavy-duty vehicle geometries. This could reduce the computational cost for the unsteady simulations significantly. Additionally, some mesh refinements should be done where the turbulent-length scales are smaller in the LES region and tailor the mesh more according to the IDDES solver. This should be done with the CFL number in mind to make the two discretizations operate together.

Considering the wind tunnel modelling more measurements from the actual tunnel flow would be beneficial. In the current state, there is a larger error than expected considering the solving method used, and the reason is unknown. Therefore it would be of interest to measure the actual flow in the tunnel to see if there is any rotational components or such that is not assumed in the current boundary condition. The same grid structure of pressure probes as for the rear end of the trailer would also be of interest on the sides of the trailer and cab. Having the probes in a grid makes the analysis easier to understand as it is possible to see shifts in pressure in different directions across the surface. To better understand the temporal behaviour of the wake of the truck it would also be of interest to measure the instantaneous pressure on the rear surface of the truck. This would require more advanced pressure probes that can capture those fluctuations but would help to understand what fluctuations are present in the actual wind tunnel pressure fields.

6
Conclusion

In this thesis, the CFD simulation modelling of a truck geometry inside a wind tunnel environment was investigated. A baseline simulation was created and validated to wind tunnel results from a test campaign in 2019. The baseline was used to identify errors in the method for the three parameters C_d , C_s , and C_p . The error in C_p was related to the error in C_d to understand where the error in C_d is originated. The CFD simulations were run in an unsteady state to capture the transient behaviour of the parameters and flow properties. Different methods were studied to evaluate the uncertainty of the averaging of the unsteady properties and the initial starting time for the averaging was inspected. The frequency content from the time-resolved signals was also studied to see how the signal behave in terms of frequency components. Different spacial discretizations were tested and the spatial resolution was evaluated by the difference of C_d and two-point correlation. To understand the temporal resolution the CFL number was used and identified in the domain. The results from the base case with 1 ms time step compared to the wind tunnel tests show that there is an error of -45 ± 7 dc in C_d for the yaw weighted averaged value. Additionally, a study on the temporal resolution was conducted. This study compared the 1 ms time step with longer and shorter time steps. The comparison used the same parameters as the wind tunnel validation. Those where compared to see how much a different time step affect a certain property. The frequency content of the time-resolved signals for the different time steps was also compared to see how a different temporal resolution affects it.

An important result from the study is how the C_d value is a highly complex property and includes a lot of information. This can make results that should be more accurate due to refinements seem more inaccurate instead. In this work this is considered to be an effect from how multiple errors can cancel each other and make the value appear more correct for a coarser solution. This was observed in both the spatial and temporal resolution. When they were refined the result differed more from the wind tunnel tests. The same phenomenon were present when the pressure difference between simulations and the wind tunnel tests were studied for the rear end of the trailer for different yaw angles. For the higher yaw angles the C_d value appeared more correct, but when the pressure over the rear end of the truck was analysed there were both over- and underpredicted regions present. Those regions canceled each other when studying ΔC_d and made the C_d value appear more correct compared to the 0 degree yaw case.

The confidence intervals for the averaged C_d values were estimated for the simulations. Those intervals gave limits for future comparison between simulations, limits of how small differences are significant. If the confidence interval covers the mean of a new simulation the value is not statistically different and thus there is no significant difference between the two simulations. This result is useful for future developing of the trucks when different concepts are simulated to reduce the C_d value. The confidence limits can then be used to justify new designs. Moreover, these intervals are useful when comparing different settings in the method, the time step for example. The time step can be increased in the simulations and let the CFL number exceed unity in the domain as long as it is done moderately. This is because the difference in the global force coefficients is not significant because of the averaging of the mean. The time steps can be set to 2 ms if only the global force coefficients are of primary interest. Although, if the details in the flow properties, such as the pressure fields, is the main interest, a finer time step is needed. The results from this study showed that with the current mesh used, a time step of about 0.33 ms should be sufficient to resolve the important features in the flow.

Bibliography

[1] European Commission. Paris Agreement, 2020. https://ec.europa.eu/clima/policies/international/negotiations/paris_en.

[2] European Commission. Reducing CO2 emissions from heavy-duty vehicles, 2020. https://ec.europa.eu/clima/policies/transport/vehicles/heavy_en#tab-0-0.

[3] W. H. Hucho. *Aerodynamics of Road Vehicles*. Society of Automotive Engineers, 1998.

[4] E. Josefsson. Examination of robustness and accuracy of CFD simulations for external aerodynamics of commercial vehicles. Master's thesis, Chalmers University of Technology, 2019.

[5] J. F. Wendt. *Computational Fluid Dynamics: An Introduction*. Springer-Verlag Berlin Heidelberg, 2009.

[6] H. K. Versteeg and W. Malalasekera. *An Introduction to Computational Fluid Dynamics: The Finite Volume Method*. Pearson Prentice Hall, 2007.

[7] F. R. Menter. Two-equation eddy-viscosity turbulence models for engineering applications. *AIAA Journal*, 32, 1994.

[8] L. Davidson. *Fluid mechanics, turbulent flow and turbulence modeling*. Chalmers University of Technology, 2019.

[9] F. R. Menter and M. Kuntz. Adaptation of eddy viscosity turbulence models to unsteady separated flows behind vehicles. In *The Aerodynamics of Heavy Vehicles: Trucks, Buses, and Trains*. Springer-Verlag Berlin Heidelberg, 2004.

[10] M. L. Shur, P. R. Spalart, M. Kh. Strelets, and A. K. Travin. A hybrid RANS-LES approach with delayed-DES and wall-modelled LES capabilities. *International Journal of Heat and Fluid Flow*, 29, 2008.

[11] Siemens. *Star-CCM+ Documentation*, 14th ed. edition.

[12] R. Courant, K. Friedrichs, and H. Lewy. On the Partial Difference Equations of Mathematical Physics. *Mathematische Annalen*, 100, 1928. P. Pox Translator, 1956.

[13] W. C. Reynolds. The Potential and Limitations of Direct and Large Eddy Simulations. In *Whither Turbulence? Turbulence at the Crossroads*. Springer Berlin Heidelberg, 1990.

[14] C. Mockett. *A comprehensive study of detached-eddy simulation.* PhD thesis, der Technischen Universität Berlin, 2009.

[15] S. Sagitov. *Statistical Inference.* Chalmers University of Technology, 2020.

[16] R. H. Shumway and D. S. Stoffer. *Time Series Analysis and Its Applications.* Springer International Publishing AG, 2017.

[17] The MathWorks. *MATLAB Documentation*, r2018b edition.

[18] National Instruments. *Understanding FFTs and Windowing*, 2019.

[19] W. L. Oberkampf and T. G. Trucano. Verification and validation in computational fluid dynamics. *Progress in Aerospace Sciences.*, 38, 2002.

[20] D. Flanagan. 9 m wind tunnel research facility, 2019. `https://nrc.canada.ca/en/research-development/nrc-facilities/9-m-wind-tunnel-research-facility`.

[21] D. Steen, F. J. Ross, J. Kiedaisch, and C. Czlapinski et al. Class 8 Truck Investigation Comparing Wind Tunnel Test to Simulated Open Road Performance Using CFD. *SAE Technical Paper*, 2018-01-5010, 2018.

[22] J. Forsgren and A. Tenstam. The NRC windrunnel FRI, 2019. Internal report AB Volvo, Unpublished.

[23] S. Cyr, K. Ih, and S. Park. Accurate Reproduction of Wind-Tunnel Results with CFD. *SAE Technical Paper*, 2011-01-0158, 2011.

[24] E. Ljungskog, S. Sebben, and A. Broniewicz. Inclusion of the physical wind tunnel in vehicle CFD simulations for improved prediction quality. *Journal of Wind Engineering and Industrial Aerodynamics*, 197, 2020.

[25] P. Ekman, T. Larsson, T. Virdung, and M. Karlsson. Accuracy and speed for scale-resolving simulations of the drivaer reference model. *SAE Technical Paper*, 2019-01-0639, 2019.

[26] M.Berglund. New wind average formulas for air resistance coefficient CD, corrected to European and USA wind and transportation conditions, have been calculated, 2007. Internal Report AB Volvo Gothenburg, Unpublished.

[27] P. Norman and K. Howard. Evaluating Statistical Error in Unsteady Automotive Computational Fluid Dynamics Simulations. *SAE Technical Paper*, 2020-01-0692, 2020.

[28] P. Elofsson, G. Mercier, B. D. Duncan, and S. Boissinot. Accurate Drag Prediction Using Transient Aerodynamics Simulations for a Heavy Truck in Yaw Flow. In *The Aerodynamics of Heavy Vehicles III Trucks, Buses and Trains.* Springer International Publishing, 2016.

[29] L. Sterken, S. Sebben, and L. Löfdahl. Numerical Implementation of Detached-Eddy Simulation on a Passenger Vehicle and Some Experimental Correlation. *Journal of Fluids Engineering*, 138, 2006.

[30] C. Mockett, T. Knacke, and F. Thiele. Detecton of initial transient and estimation of statistical error in time-resolved turbulent flow data. *International Symposium on Engineering Turbulence Modelling and Measurements*, 8, 2010.

[31] P. Heidelberger and P. D. Welch. A spectral method for confidence interval generation and run length control in simulations. *Communications of the ACM*, 24, 1981.

[32] M. Taboga. Lectures on probability and statistics, 2010. `https://www.statlect.com`.

[33] P. Heidelberger and P. D. Welch. Simulation run length control in the presence of an initial transient. *Operations Research*, 31, 1983.

[34] J. D. Chodera. A simple method for automated equibration detection in molecular simulations. *J Chem Theory Comput*, 12, 2006.

[35] J. Geweke. Evaluating the accuracy of sampling-based approaches to calculating posterior moments. Technical report, Federal Reserve Bank of Minneapolis, Research Department, 1991.

[36] L. Davidson. Large Eddy Simulations: how to evaluate resolution. *International Journal of Heat and Fluid Flow*, 30, 2009.

[37] E. Ljungskog. *Evaluation and modeling of the flow in a slotted wall wind tunnel*. PhD thesis, Chalmers University of Technology, 2019.

[38] F. J. Ross and S. Herrmann. Vehicle aerodynamics, 2017. Internal report Siemens, Unpublished.

[39] C. Windisch. What is a residual and how can i cut my energy bill?, 2017. `https://thesteveportal.plm.automation.siemens.com/articles/en_US/Video/What-is-a-residual-and-how-can-I-cut-my-energy-bill`.

A

Appendix

The integral-length scales in the least resolved direction for the under and side system.

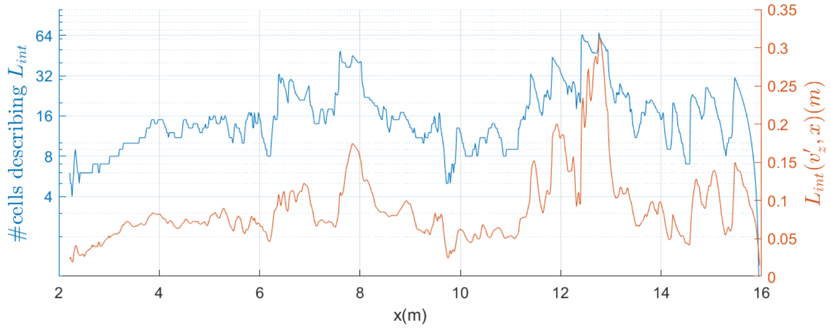

(a) $L_{int}(v'_z, x)$

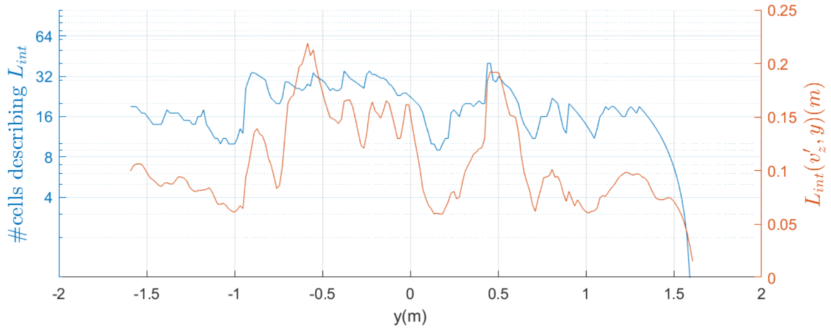

(b) $L_{int}(v'_z, y)$

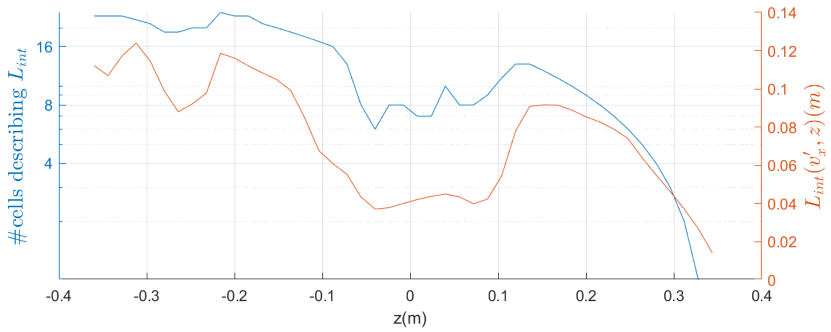

(c) $L_{int}(v'_x, z)$

Figure A.1: L_{int} and cells describing L_{int} for under system.

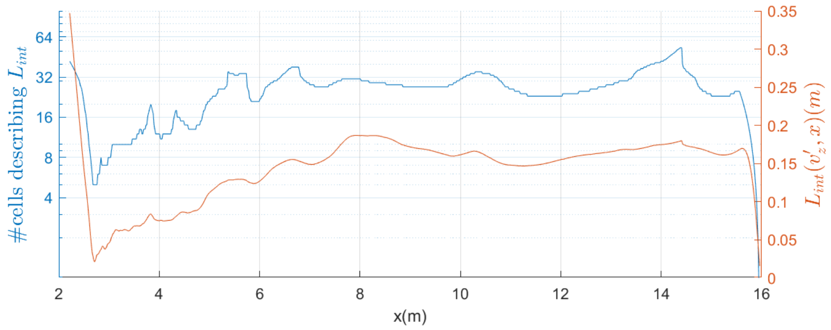

(a) $L_{int}(v'_z, x)$

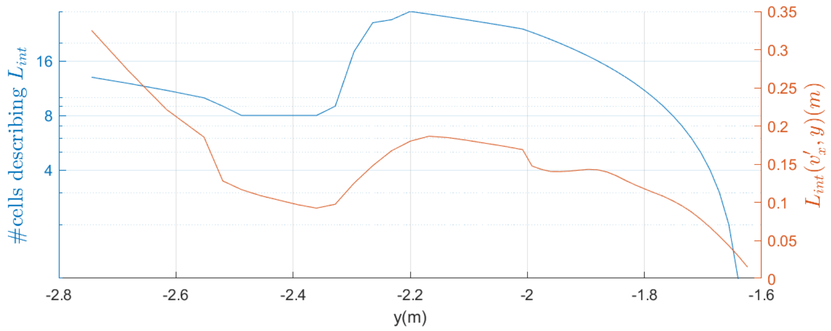

(b) $L_{int}(v'_x, y)$

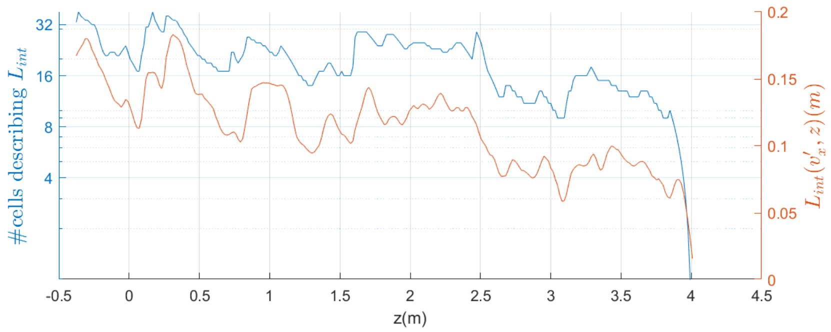

(c) $L_{int}(v'_x, z)$

Figure A.2: L_{int} and cells describing L_{int} for side system.